Proceedings of

The 4th International Conference on Mathematical Applications in Engineering 2017

International Islamic University Malaysia
8th - 9th of August 2017

Editors:
Faried Hasbullah
Suazlan Mt Aznam
Hanisah Manshor

Organized by

Faculty of Engineering
International Islamic University Malaysia

Co-organized by

MIMOS Berhad

Proceedings of the 4th International Conference of Mathematical Applications in Engineering 2017

This publication contains papers (extended abstracts) accepted for the 4th International Conference of Mathematical Applications in Engineering 2017 (ICMAE'17) which is held on the 8-9 August 2017 in the Kulliyyah of Engineering, International Islamic University Malaysia.

Published by:
Kulliyyah of Engineering
International Islamic University Malaysia (IIUM)
50728 Kuala Lumpur
Malaysia

First Edition, 2017

ISBN 978-983-42978-9-3

Preface

Mastery and perfection in mathematics is a mandatory pre-requisite in advancing the frontiers of science. Mathematics provides the methodology and framework of rigorous thoughts in understanding and unveiling the beauty of the physical universe bestowed upon us by the grace of Allah Almighty, Him alone the Owner and Master of all the worlds. It is often astonished how simple mathematical expressions are sufficed in describing complex physical phenomena.

Today, the rapid development in science and technology poses new challenges to mathematicians and scientists that requires innovative approach and methodology or eventually new mathematical theories. As such, the Kulliyyah of Engineering, International Islamic University Malaysia (IIUM) in collaboration with MIMOS Bhd. are therefore proud to present the 4th International Conference on Mathematical Modelling in Engineering 2017 (ICMAE4). We aspire ICMAE to serve as an effective platform for academicians and researchers internationally to share ideas, state-of-the-art innovations and future developments of mathematical methods in diverse field of studies. The specific conference topics include:

- Mathematical physics and differential equations
- Algebra & analysis
- Mathematical modelling & simulation
- Probability & mathematical statistics
- Analytical & numerical methods

All technical papers presented during the conference shall be peer reviewed and accepted papers will appear in the **Open Access** *Journal of Physics: Conference Series (JPCS)*.

Table of Contents

Extended Abstract of the 4th International Conference on Mathematical Applications in Engineering (ICMAE2017), 8-9th August 2017

Equiconvergence in Summation Associated with Elliptic Polynomial

A. Fargana[1], A. A. Rakhimov[2], A. A. Khan[3], and T. B. H. Hasan[4]

[1,2,4]Department of Science in Engineering, International Islamic University Malaysia (IIUM), Kuala Lumpur, Malaysia.

[3]Department of Manufacturing and Material Engineering, International Islamic University Malaysia (IIUM), Kuala Lumpur, Malaysia.

[1]nipafarjana94@gmail.com, [2]abdumalik@iium.edu.my, [3]aakhan@iium.edu.my ,[4]torla@iium.edu.my

Introduction. In this paper we prove a precise equiconvergence relation between index of the Bochner-Riesz means of the expansions and power of the singularity of the distributions with compact support in summation associated with the elliptic operator.

Localization principle for the Fourier series at certain point means dependence of the **c**onvergence or divergence only from the behaviour of the function in the small neighbourhood of that point [1]. Equiconvergence of the Fourier series and the Fouer integral means convergence of both at the same and at the same term. The same for equisummmability when summation of the Fourier series and the Fourier integral is going by regular method. Here in this paper we consider the Reisz method of summation.

Note that, in N dimensional case, when N > 1, equiconvergence and localization principles for the Fourier series and the integral is not valid by the Pringsheim convergence [2]. Equiconvergence of a spectral expansion corresponding to the Schrodinger operator with the summable potential, with Fourier integral is studied in [3]. A comparison theorem on equiconvergence of the Fourier Jacobi series with certain trigonometric Fourier series is proved in [4]. In [5] it is showed that uniform equiconvergence of the expansions of the integrable functions in eigenfunctions of the Sturm-Liouville operator. And the more general expanded expansions of distributions is studied in [6]-[12].

In this paper we discussed about equiconvergence in summation of the Fourier series and the Fourier integral of the linear continuous functional which associated with an elliptic polynomial.

Preliminaries

Let the space of infinitely differentiable function $\varphi: T^N \rightarrow C$ is denoted by $\varepsilon(T^N)$. The locally convex topology formed from the system of semi norms

$$P_{k,\gamma}(\phi) = \sup_{x \in k} \left| D^{\gamma} \phi(x) \right| ,$$

where, K is a compact subset of $T^N = [-\pi, \pi]^N$, $\gamma = (\gamma_1, \gamma_{2,} ..... \gamma_N)$ is N dimensional vector with the non-negative integer components γ_j (j = 1, 2 ...., N). By $|\gamma| = (\gamma_1 + \gamma_2 + ... + \gamma_N)$ we

denote a length of the multi-index γ. For instance, $D^{\gamma} = D_1^{\gamma_1} D_2^{\gamma_2} .....D_N^{\gamma_N}$, where $D_j = \frac{1}{i}\frac{\partial}{\partial x_j}, j = 1,2,.....N$.

The conjugate space $\varepsilon'(T^N)$ to the local convex topological space $\varepsilon(T^N)$ is the set of all distributions with the compact support in T^N. Any functional $f \in \varepsilon'(T^N)$ can be written as

$$f = (2\pi)^{-\frac{N}{2}} \sum_{n \in Z^N} f_n e^{inx}, \tag{1}$$

where Z^N is the set of all vectors with integer components, f_n is the Fourier coefficient which is defined as the value of f on the test function on $f = (2\pi)^{-N/2} e^{-inx}$ and $x \in T^N$. Consider the following elliptic polynomial:

$$A(n) = \left(\sum_{j=1}^{r+1} n_j^{\ 2} \right)^{m+1} + \left(\sum_{j=r+2}^{N} n_j^{\ 2} \right)^{m} \left(\sum_{j=1}^{N} n_j^{\ 2} \right),$$

where $n = (n_1, n_2, ...n_N) \in Z^N$. m is a positive integer number, and *r= 0, 1, 2, ……, N-1*. The Riesz means of order *s* (*s* is non-negative real number) of the Fourier series (1) is define as

$$\sigma_\lambda^s f(x) = (2\pi)^{-\frac{N}{2}} \sum_{A(n)<\lambda} \left(1 - \frac{A(n)}{\lambda} \right)^s f_n e^{inx}. \tag{2}$$

Now, we extend a distribution *f* from *N* - dimensional torus T^N to the whole space R^N by zero. For the extended distribution use again symbol f. Then the Bochner-Riesz means of order *s* of the Fourier integral of f is,

$$R_\lambda^s f(x) = (2\pi)^{-\frac{N}{2}} \int_{A(\xi)<\lambda} \left(1 - \frac{A(\xi)}{\lambda} \right)^s \hat{f}(y) e^{iA(\xi)x} d\xi, \tag{3}$$

where, $\hat{f}(y) =< f, (2\pi)^{-N/2} e^{-iA(\xi)x} >$ is the Fourier transformation of the extended functional *f* and it acts on , $(2\pi)^{-N/2} e^{-iA(\xi)x}$ via x.

Main Theorem

Let *l* be any real number and $L_2^l(T^N)$ denote the Liouville space of distributions

$$L_2^l(T^N) = \{ f \in \varepsilon' : \sum_{n \in Z^N} (1 + A(n))^l \} f_n^2 < \infty \}.$$

Theorem 1. Let $l>0$ and ε is any positive number.

If $s = \varepsilon + \max\{\frac{(N-r-1)(1-1/2m)}{2} + \frac{r}{2}, \frac{N-1}{2}\} + l$, then for any $f \in L_2^{-l}(T^N)$

$$\sigma_\lambda^s f(x) = R_\lambda^s f(x) + O(1)\|f\|_{-l},$$

where $\|\cdot\|_{-l}$ is a norm in $L_2^{-l}(T^N)$:

$$\|f\|_{-l} = (2\pi)^{-\frac{N}{2}} \sqrt{\sum_{n\in Z^N} (1+A(n))^{-l} f_n^{\,2}}\,.$$

References

[1] Khavin VP, Nikol'skiı NK. Commutative Harmonic Analysis. IV, Encyclopaedia of Mathematical 1992; Sciences, vol. 42.

[2] Alimov ShA, Il'in VA, Nikishin EM. Problems of Convergence of Multiple Trigonometric Series and Spectral Decompositions. Russian Mathematical Surveys 32 (1977) 115-139.

[3] Denisov SA. Equiconvergence of a Spectral Expansion Corresponding to a Schrodinger Operator with Summable Potential, with Fourier Integral. Differential Equations. 34 (1998) 1043-1048.

[4] Marcokova M. Equiconvergence of Two Fourier Series. Journal of Approximation Theory. 80 ((1995) 151-163. http://dx.doi.org/10.1006/jath.1995.1012

[5] Sadovnichaya V. Equiconvergence of Eigenfunction Expansions for Sturm-Liouville Operators with a Distributional Potential. Sbornik: Mathematics. 201 (2010) 61-76.

[6] Alimov ShA. On the Spectral Decompositions of Distributions. Doklady Mathematics. 331 (1993) 661-662.

[7] Alimov ShA, Rakhimov AA. Localization of Spectral Expansions of Distributions. Difference Equations. (1996) 32, 798-802.

[8] Alimov ShA, Rakhimov AA. Localization of Spectral Expansions of Distributions in a Closed Domain. Difference Equations. 33 (1997) 80-82.

[9] Rakhimov AA. On the Localization of Multiple Trigonometric Series of Distributions. Dokl. Math. 62 (2000) 163-165. (translation from Dokl. Akad. Nauk, Ross. Akad. Nauk, 374, 20-22).

[10] Rakhimov A.A. Localization Conditions for Spectral Decompositions Related to Elliptic Operators from Class Ar. Mathematical Notes. 59 (1996) 298-302. (translation from Mat. Zametki, 59, 421-427).

[11] Rakhimov A, Ahmedov A. Zainuddin H. On the Spectral Expansions of Distributions Connected with Schrodinger Operator. Applied Mathematics Letters. 25 (2012) 921-924.

[12] Rakhimov AA. Spectral Decompositions of Distributions from Negative Sobolev Classes. Difference Equations. 32 (1996) 1011-1013. https://zbmath.org/?q=an:0890.47031.

Parametric Model Based On Imputations Techniques for Partly Interval Censored Data

Faiz A. M. Elfaki
Department of Mathematics, Statistics and Physics, College of Arts and Science, Qatar University, IIUM, P.O. Box 2713, Doha, Qatar

felfaki@qu.edu.qa

Introduction

One of the main objectives in the survival studies is that the comparison of survival functions. In this paper, we will discuss the comparison problem for several imputation techniques in the existence of part interval censored (PIC) failure time data. PIC data often occurs in medical and health studies that are followed by periodic follow-up, and also in others fields. By PIC data we means, for some subjects, the exact failure times are observed, but for the remaining subjects, the survival time of interest is observed only to belong to an interval instead of being exactly ([1], [2], [3]). An example of this kind of data is provided by the Framingham Heart Disease Study ([4]). Another example reported by [5] about Fatigue Failure (Crack size data) which may be considered as PIC data. In this article several imputation techniques used to estimate the survival function and compared with the one that obtained by Turnbull based on interval censored and PIC failure time data. In the next two sections we will discuss the parametric model and imputation techniques.

Parametric Model

The nonparametric methods outlined in the previous section have become the standard approach to the analysis of simple homogeneous survival data without covariate information. However, parametric survival time distributions are sometimes used for inference. Assume that the true survival times $X_1, X_2, ..., X_n$ are independent and identically distributed with survival function $S(t;\beta)$ and hazard function $h(t;\beta)$ but that only a right censored sample $(\tilde{X}_i, D_i)$, $i = 1,...,n$ is observed. Under independent censoring, the likelihood function for the parameter is

$$L(\beta) = \prod_{i=1}^{n} (h(\tilde{X}_i, \beta))^{D_i} S(\tilde{X}_i, \beta) \qquad (1)$$

where β is parameter needed to be estimated. The function (1) may be analyzed using standard large sample theory. Thus, standard test, that is, Wad test, Score test, and likelihood test are used as inferential tools. Two frequently used parametric survival models are the Weibull distribution and exponential distribution. Both of these distributions contain the very simplest model.

Imputation Methods

We used several imputation techniques and compared them with Turnbull's model and with each other's. The imputation techniques are based on Kaplan-Meir estimator.
The imputation techniques used in this thesis can be classified into two different categories:

1. ***Simple imputation methods***
   There are three main types of simple imputation methods, that is; right-point, left-point and mid-point imputations.

2. ***Probability-based imputation methods***
   The most common probability-based imputation methods, that is; conditional mean imputation, conditional median imputation and random Imputation.

An Example

We applied the proposed method to the modified breast cancer data that was presented by ([6] and [7]). The data consist of 46 patient treated by Radiation (R) only and 48 patients treated by Radiation plus adjuvant Chemotherapy (R+C). This study was implemented to compare the cosmetic effects of Radiation alone against R+C on women with early breast cancer and the event of interest was the time to first occurrence of breast retraction and the patients were observed at clinic visits every 4 to 6 months, where the actual dates of the event were recorded exactly if available. If not the interval of events were noted. The modified data set is shown in Table 4.1 in order to set up the data as the partly interval censored data, for instant we set up for radiation 25 observation as right censored, 21 as interval censored and 20 as exact. Likewise, for R+C the set up to be 13 observation as right censored, 35 as interval censored and 20 as exact. The result of this data set will be analysis as interval censored and PIC as show in the next section.

Based on parametric analysis for cancer PIC data. Fig 1 and 2 show the results obtained by random imputation and median imputation, respectively. The Figures look similar to Turnbull method. The likelihood ratio test shows better result in the case of midpoint, right point, mean and random imputations as shown in Table 1.

Table 1: Likelihood Ratio Test and their P-value based on parametric model from cancer PIC data

Imputation Techniques	Likelihood Ratio Test	P-value
Midpoint	4.6	0.032
Left-point	3.03	0.082
Right-point	4.74	0.029
Mean	4.49	0.034
Median	4.22	0.04
Random	5.13	0.023

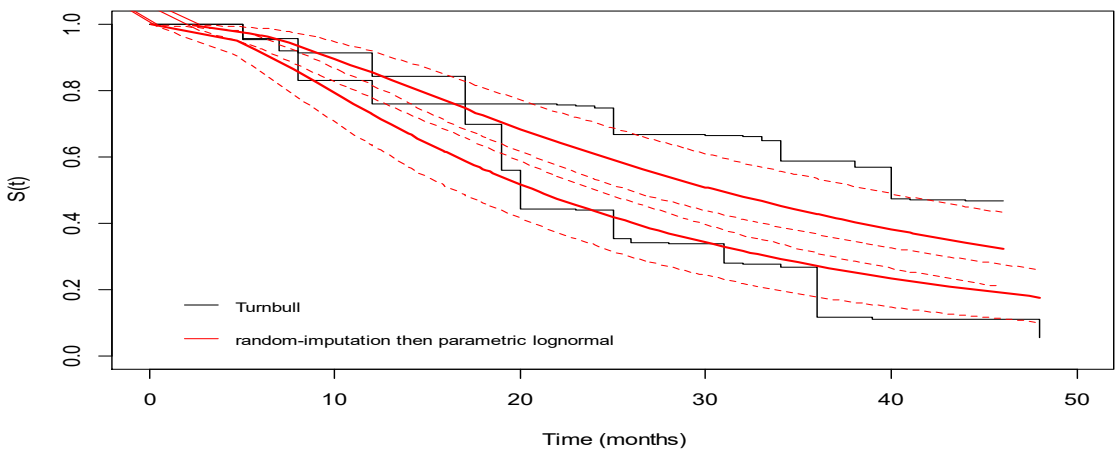

Fig 1: Estimated survival function obtained by random imputation vs Turnbull based on

parametric model from cancer PIC data.

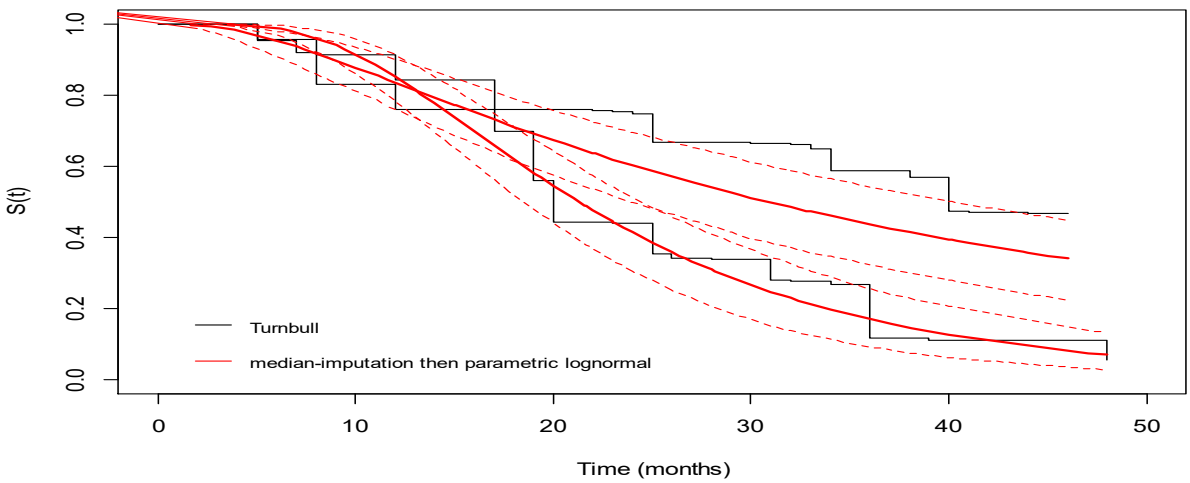

Fig 2: Estimated survival function obtained by median imputation vs Turnbull based on parametric model from cancer PIC data.

Conclusion

In summary, we have proposed a simple modification of estimating survival function for partly-interval censored data using parametric model based on imputation techniques. Modification of breast cancer data is used and R software also used to obtain the results. Our results are fund to be similar to the one obtained by Turnbull. However, based on partly interval censored data, the random imputation and mean & median imputation show better results compared with others imputation techniques as well as Turnbull with respect to their the smallest P-value (Table 1).

References

[1] Huang, J. Asymptotic properties of nonparametric estimation based on partly interval-censored data. *Statistica Sinia*, (1999): 9; 501 – 519.

[2] Kim, J. S.. Maximum likelihood estimation for the proportional hazards model with partly interval-censored data. Journal of the Royal Statistical Society, (2003): 65; 489- 502.

[3] Zhao, X. Zhao, Q.J. Sun. Generalized log-rank test for partly interval-censored failure time data. Biometrical Journal. (2008):3;375-385.

[4] Odell, P. M., Anderson, K. M. and D'Agostino, R. B. Maximum likelihood estimation for interval-censored data using a Weibull-based accelerated failure time model. Biometrics. (1992):48;951-959.

[5] Kumar, P. Modeling and analysis of degradation data. Indian Institute Technology Bombay, Available:http://www.academia.edu/266427/Modelling_and_Analysis_of_Degradation_Data [Accessed: 5/1/2013]. (2010).

[6] Abdallah Zyoud. Imputation Techniques for Reliability Analysis Based ON Partly Interval Censored Data. M.Sc., thesis. International Islamic University Malaysia. (2017).

[7] Finkelstein, D. M., and Wolfe, R. A. A semi parametric model for regression analysis of interval-censored failure time data. Biometrics. (1985): 41;933-945.

Some Effects of Perturbed Flight Schedules to the Performance of Aircraft Routings

Khusnul Novianingsih
Department of Mathematics Education, Universitas Pendidikan Indonesia
Jl. Dr. Setiabudhi No. 229 Bandung 40154, INDONESIA.

k_novianingsih@upi.edu

Introduction. Airline schedules are operated under uncertain conditions. Some factors such as bad weather and airport congestion can cause some flight schedule can be delayed or canceled. These affect to airline on-time performance which it is related to passenger satisfaction. To reduce the number of flight delays, airlines need to construct robust aircraft routings. Robust aircraft routings are aircraft route schedules that are arranged to minimize a specific robustness measure, as the expectation of departure delay, arrival delay, or propagated delay. Recently, some researchers have shown that improving the robustness of aircraft routings can be done by perturbed flights. They improve the robustness of aircraft routing through optimization models to determine the optimal perturbations [2,3,4,5]. This research characterize the influence of perturbed flights analytically. Unlike Schaefer et al. [1] who investigate the perturbation of the original flight schedule to improve the operational performance of a given crew schedule, this paper observes the effect of perturbed flight schedules to the aircraft routing operations.

Flight Delay on an Aircraft Schedule. Let F and R be a set of flights and a set of aircraft routings, respectively. Given an aircraft route r which consists a sequence of flights $f_1,\ldots, f_n$. Assume that in flight schedule operations we use a push-back recovery and we divide sources of a delay for flight f_i into two categories: ground delay and block-time delay. A ground delay is a delay before an aircraft take-off, and it does not include propagated delay caused by the previous flight in the same routing. A block-time delay is delay in the air, and we can view as the difference between the planned block-time of a flight with its actual block-time. For aircraft routing r, let $\alpha_1,\ldots, \alpha_n$ and $\beta_1,\ldots, \beta_n$ be nonnegative random variables where α_i indicates departure delay of flight f_i and β_i indicates arrival delay of flight f_i, respectively. Let $\lambda_1,\ldots, \lambda_n$ be nonnegative random variables, where λ_i represents ground delay of flight f_i in r. Let $\mu_1,\ldots, \mu_n$ be nonnegative random variables, where μ_i indicates the block-time delay of flight f_i relative to its planned block-time. Assume that the distributions of ground-time delay and block-time delay are independent of the time of day. Let $pd_{i,i+1}$ be the propagated delay to flight f_{i+1} caused by flight f_i.

Proposition 1. The departure delay of flight f_i in routing r is given by

$$\alpha_1 = \lambda_1, \quad \alpha_i = \lambda_i + \max\{\alpha_{i-1} + \delta_{i-1} - s_{i-1,i}, 0\} \qquad (1)$$

for $i = 2,\ldots,n$, where $s_{i-1,i} = tt_{i-1,i} - mt_i$ is the planned slack to connect flight f_{i-1} and f_i.

For each f_i in r, we obtain the bound of departure delay and arrival delay in the following propositions.

Proposition 2. For each f_i in r,

$$\lambda_1 \le \alpha_i \le \sum_{k=1}^{i} \lambda_k + \sum_{k=2}^{i} \left| \mu_{k-1} - s_{k-1,k} \right| \tag{2}$$

Corollary 3. For each f_i in r,

$$\lambda_1 \le \beta_i \le \sum_{k=1}^{i} \lambda_k + \mu_i + \sum_{k=2}^{i} \left| \mu_{k-1} - s_{k-1,k} \right| \tag{3}$$

The Perturbed Schedule. Let **x** and **y** be a nonnegative vector in $\mathbf{R}^{|F|}$. The *perturbed schedules* F + (**x**,**y**) is defined as the new flight schedules which obtain from F where the departure time and the arrival time of each flight i in F are changed by ($dept_i - x_i$) and ($arrt_i + y_i$), respectively. Perturbed schedules F + (**x**,**y**) is called as feasible perturbed schedules if the planned aircraft routings in F remain feasible under perturbed schedules F + (**x**,**y**). Let $S'_{i-1,i}$ be the slack to connect flight f_{i-1} and f_i in r'. Let bt'_i be the block time of flight f_i in r'. Let α'_i be the departurte time of flight f_i in r'.

Proposition 4. If we have $\alpha'_i \le \alpha_i$, *then the arrival delay of flight* f_i *in* r'

$$\beta'_i \le \beta_i \tag{4}$$

for i = 1,...,n.

Proposition 5. If $S_{i-1,i} \le S'_{i-1,i}$ and $bt_i = bt'_i$ *for i = 2,...,n, then*

$$\alpha'_i \le \alpha_i, \tag{5}$$

Proposition 6. If $bt_i \le bt'_i$ *for i = 1,...,n, and* $S_{i-1,i} = S'_{i-1,i}$ *for i = 2,...,n, then the departure delay of flight* f_i *in* r'

$$\alpha'_i \le \alpha_i \tag{6}$$

for i = 1,...,n.

Proposition 7. For $\lambda_1,..., \lambda_n$ *of arbitrary ground delays and* $\delta_1,..., \delta_n$ *of arbitrary block-time delays for flights in r,* if $x_i = y_i = c$, *where c is a positive number then*

$$\alpha'_i = \alpha_i \tag{7}$$

for i = 1,...,*n*.

Computational Results. We consider one-day flight schedules of an airline in Indonesia for computational study. The schedules consist of 287 flights which are covered by 92 aircraft routings. We construct a simulation for measuring the performance of flight schedules. To perturbate schedules, we allow departure times and arrival times of planned flight schedules to be moved earlier or later no more than 15 minutes in order to preserve passenger projection in flight schedule design. To observe the effect of additional slack to the performance of aircraft routing in operations, we modify the departure times and the arrival

times of the original flight schedules such that the new flight schedules will produce the aircraft routings with more slack then the original aircraft routings, but the original block-times do not change. The same technique is also applied to obtain the new flight schedules that will produce aircraft routings with more lenght of block-times than the original block-times and the same length of slacks with the original slacks. For both cases, we record total departure delay, total arrival delay, and 15-minute on time performance (15-OTP). According 15-OTP, a flight is delay if depart on a gate in more than 15 minutes after its schedule departure time. The computational results show that the larger slack will result to the better aircraft routing performance. The same condition also occurs for the additional of block-time. The increasing block-time in aircraft routings will affect to the increasing of the aircraft routing performance. We also simulate four cases of perturbations for each aircraft routing. In the first case, we set $x_1 = 15$, $x_i = x_{i-1}$, and y_i = 5 minutes. In Case 2, we set $x_1 = 15$, $x_i = \frac{1}{3} x_{i-1}$, and y_i = 5 minutes. In Case 3, we set $x_1 = 15$, $x_i = \frac{1}{2} x_{i-1}$, and y_i = 5 minutes. We set $x_1 = 15$, $x_i = \frac{2}{3} x_{i-1}$, and y_i = 5 minutes for the last case. We perform the same flight delay simulation for all cases. we can see that all cases give better performance rather than the original. The simulation results show that the performance will continue to increase if the additional of block-times of each flight in the aircraft routings is large than the reducing slack in its connection. More block-times are the better performance.

Summary

The flight schedule perturbations can improve the aircraft routing operations. We can perturbate the planned flight schedules for adding slacks or adding block-times of aircraft routings. By simulation, we show that the performance of aircraft routing will increase if we move the departure times of each flight in an aircraft routing no longer than the departure-time changes of the previous flights.

References

[1] A. J. Schaefer, G. L. Nemhauser, Improving airline operational performance through schedule perturbation, Ann. Oper. Res. 114 (2006) 3-16.

[2] M. Sohoni, Y. Lee, D. Klabjan, Robust airline scheduling under block time uncertainty, Transport. Sci. 45 (2013), 451-464.

[3] S. AhmadBeygi, A. Cohn, M. Lapp, Decreasing Airline Delay Propagation by Re-allocating Schedule Slack, Technical Report, University of Mechigan, 2008.

[4] S. Lan, J. P. Carke, C. Bernhart, Planning for robust airline operations: Optimizing aircraft routings and flight departure times to minimize passenger disruptions, Transport. Sci. 40 (2006) 15-28.

[5] V. Chiraphadanakul, C. Bernhard, Robust flight schedules through slack re-allocation, Euro J. Transport. Log. 2 (2013) 277-306.

Extended Abstract of the 4th International Conference on Mathematical Applications in Engineering (ICMAE2017),
8-9th August 2017

A note on a separating system of rational invariants for finite dimensional generic algebras

U.Bekbaev

Department of Science in Engineering, KOE, International Islamic University of Malaysia 50728 Kuala Lumpur, Malaysia.

Introduction. In [1] we have offered an approach to classification problem of finite dimensional algebras with respect to basis changes. It has been shown that if one has a special map with some properties then he is able to classify all algebras who's set of structural constants do not nullify a certain polynomial. In this case he is also able to provide a separating system of rational invariants for those algebras. It was successfully applied in [2] to get a complete classification of all 2-dimensional algebras over algebraically closed fields.

Unfortunately, so far we have no example of such a map in 3-dimensional case. Therefore in the current paper we deal with a weaker problem, namely with a construction of separating system of rational invariants for finite dimensional generic algebras. The theoretical existence of such system of invariants is known [3]. By generic algebras we mean the set of all algebras who's system of structural constants does not nullify a fixed nonzero polynomial in structural variables, over the basic field F. In process of dealing with the problem we show a way for a rough classification of finite dimensional algebras by attaching them some quadratic forms.

Main results. Further whenever $A = (a_{ij}) \in Mat(p \times q, F)$, $B \in Mat(p' \times q', F)$ we use $A \otimes B$ for the matrix

$$\begin{pmatrix} a_{11}B & a_{12}B & ... & a_{1q}B \\ a_{21}B & a_{22}B & ... & a_{2q}B \\ . & . & \vdots & . \\ a_{p1}B & a_{p2}B & ... & a_{pq}B \end{pmatrix}, \text{ where } F - \text{ is a field of characteristic not 2.}$$

Let us consider any m-dimensional algebra $\mathbf{A}$ with multiplication $\cdot$ given by a bilinear map $(\mathbf{u}, \mathbf{v}) \mapsto \mathbf{u} \cdot \mathbf{v}$. If $e = (e_1, e_2, ..., e_m)$ is a basis for $\mathbf{A}$ then one can represent the bilinear map by a matrix

$$A_e = (A^i_{ejk})_{i,j,k=1,2,...,m} \in Mat(m \times m^2; F),$$

where $e_j \cdot e_k = e_1 A^1_{ejk} + e_2 A^2_{ejk} + ... + e_m A^m_{ejk}$, $j, k = 1, 2, ..., m$, such that

$$\mathbf{u} \cdot \mathbf{v} = eA_e(u \otimes v)$$

for any $\mathbf{u} = eu, \mathbf{v} = ev$, where $u = (u_1, u_2, ..., u_m), v = (v_1, v_2, ..., v_m)$ are column vectors. So the algebra $\mathbf{A}$ (binary operation, bilinear map, tensor) is presented by the matrix $A_e \in Mat(m \times m^2; F)$- the matrix of structure constants (MSC) of $\mathbf{A}$ with respect to the basis e.

If $e' = (e'_1, e'_2, ..., e'_m)$ is also a basis for $\mathbf{A}$, $g \in GL(m, F)$, $e'g = e$ then it is well known that

$$A_{e'} = gA_e(g^{-1})^{\otimes 2}$$

is valid. Further a basis e is fixed and therefore instead of A_e we use A, we do not make difference between $\mathbf{A}$ and its matrix A. Let $X = (X^i_{jk})_{i,j,k=1,2,...,m}$ stand for a variable matrix and $Tr_1(X)$,

$Tr_2(X)$ stand for the row vectors

$$(\sum_{i=1}^{m} X^i_{i1}, \sum_{i=1}^{m} X^i_{i2}, ..., \sum_{i=1}^{m} X^i_{im}), \quad (\sum_{i=1}^{m} X^i_{1i}, \sum_{i=1}^{m} X^i_{2i}, ..., \sum_{i=1}^{m} X^i_{mi}),$$

respectively.

We use τ for the representation of $GL(m, F)$ on the $n = m^3$ dimensional vector space $V = Mat(m \times m^2; F)$ defined by

$$\tau : (g, A) \mapsto B = gA(g^{-1} \otimes g^{-1}).$$

For simplicity instead of "τ-equivalent", "τ-invariant" we use "equivalent" and "invariant".

We represent each MSC A as a row vector with entries from $Mat(m, F)$ by parting it consequently into elements of $Mat(m, F)$:

$$A = (A_1, A_2, ..., A_m), \ A_1, A_2, ..., A_m \in Mat(m, F).$$

If C is a block matrix with blocks from $Mat(m, F)$ we use notation $C^{\overline{*}}$, where $*$ is the tensor product or transpose operation, to mean that the operation $*$ with C is done "over $Mat(m, F)$" (not over F), for example for the above presented matrix A

$$A^{\overline{t}} = \begin{pmatrix} A_1 \\ A_2 \\ \vdots \\ A_m \end{pmatrix} - \text{ column vector over } Mat(m, F),$$

$$A^{\overline{\otimes}2} = (A_1^2, A_1A_2, ..., A_1A_m, A_2A_1, A_2^2, ..., A_2A_m, ..., A_mA_1, A_mA_2, ..., A_m^2).$$

It is shown that equality $B = gA(g^{-1} \otimes g^{-1})$ implies the equality

$$\tilde{Tr}(\begin{pmatrix} B_1^2 & B_1B_2 & \cdots & B_1B_m \\ B_2B_1 & B_2^2 & \cdots & B_2B_m \\ \vdots & \vdots & \cdots & \vdots \\ B_mB_1 & B_mB_2 & \cdots & B_m^2 \end{pmatrix}^{\overline{\otimes}k}) =$$

$$((g^{-1})^{\otimes k})^t \tilde{Tr}(\begin{pmatrix} A_1^2 & A_1A_2 & \cdots & A_1A_m \\ A_2A_1 & A_2^2 & \cdots & A_2A_m \\ \vdots & \vdots & \cdots & \vdots \\ A_mA_1 & A_mA_2 & \cdots & A_m^2 \end{pmatrix}^{\overline{\otimes}k})(g^{-1})^{\otimes k},$$

where $\tilde{Tr}$ means the component-wise application of trace to the blocks of the corresponding block matrix. One can represent the above obtained matrix equality in the following compact form

$$\tilde{Tr}((B^{\overline{t}}B)^{\overline{\otimes}k}) = ((g^{-1})^{\otimes k})^t \tilde{Tr}((A^{\overline{t}}A)^{\overline{\otimes}k})(g^{-1})^{\otimes k}.$$

Note that $\tilde{Tr}((A^{\overline{t}}A)^{\overline{\otimes}k})$ is a symmetric matrix. The obtained equality allows formulation of the following theorem.

Theorem 1. *Invariants of the quadratic forms given by the matrix $\tilde{Tr}((X^{\overline{t}}X)^{\overline{\otimes}k})$ are invariants of the m-dimensional algebras.*

This result can be used for a rough classification of finite dimensional algebras: Two m-dimensional algebras A, B are rough equivalent if the quadratic forms given by matrices

$$\begin{pmatrix} Tr(A_1^2) & Tr(A_1A_2) & \cdots & Tr(A_1A_m) \\ Tr(A_2A_1) & Tr(A_2^2) & \cdots & Tr(A_2A_m) \\ \vdots & \vdots & \cdots & \vdots \\ Tr(A_mA_1) & Tr(A_mA_2) & \cdots & Tr(A_m^2) \end{pmatrix}, \begin{pmatrix} Tr(B_1^2) & Tr(B_1B_2) & \cdots & Tr(B_1B_m) \\ Tr(B_2B_1) & Tr(B_2^2) & \cdots & Tr(B_2B_m) \\ \vdots & \vdots & \cdots & \vdots \\ Tr(B_mB_1) & Tr(B_mB_2) & \cdots & Tr(B_m^2) \end{pmatrix}$$

are equivalent.

It is clear that entries of $\tilde{Tr}(X^{\bar{t}}X)$ are polynomials in components of X and there exists nonsingular matrix $Q(X^{\bar{t}}X)$ with rational entries in X such that the matrix

$$\tilde{Tr}(\overline{X}^{\bar{t}}\overline{X}) = (Q(X^{\bar{t}}X)^{-1})^t\tilde{Tr}(X^{\bar{t}}X)Q(X^{\bar{t}}X)^{-1} = D(X)$$

is a diagonal matrix and $Q(g) = I$ whenever g is a nonsingular diagonal matrix, where $\overline{X} = \tau(Q(X^{\bar{t}}X), X)$.

In algebraically closed field F case it means that one can define a nonempty invariant open subset $V_0 \subset V$ such that $\tilde{Tr}(\overline{A}^{\bar{t}}\overline{A}) = D(A)$ and $D(A)$ is nonsingular whenever $A \in V_0$.

Theorem 2. *Two algebras $A, B \in V_0$ are equivalent(isomorphic) if and only if $\overline{B} = \tau(g_0, \overline{A})$ for some $g_0 \in GL(m, F)$ for which $g_0^tD(B)g_0 = D(A)$.*

Assume that there exists matrix $P(X)$, with rational entries with respect to components of X, such that $P(\overline{A})$ is nonsingular for any $A \in V_0$ and the equality

$$P(\tau(g, \overline{A})) = P(\overline{A})g^{-1} \text{ holds true whenever } g^tD(\tau(g, A))g = D(A) \qquad (1)$$

Theorem 3. *For A,B $\in V_0$ there exists $g_0 \in GL(m, F)$ such that $g_0^tD(B)g_0 = D(A)$ and $\overline{B} = \tau(g_0, \overline{A})$ if and only if*

$$\tau(P(\overline{B}), \overline{B}) = \tau(P(\overline{A}), \overline{A}),\ (P(\overline{B})^{-1})^tD(B)P(\overline{B})^{-1} = (P(\overline{A})^{-1})^tD(A)P(\overline{A})^{-1}.$$

So Theorems 2 and 3 imply that the system of entries of matrices

$$\tau(P(\overline{X}), \overline{X}), \quad (P(\overline{X})^{-1})^t\tilde{Tr}(\overline{X}^{\bar{t}}\overline{X})P(\overline{X})^{-1}$$

is a separating system of rational invariants for algebras from V_0.

The above presented results show importance of construction of matrix $P(X)$ with properties (1). In the paper a construction of such matrix will be discussed.

Acknowledgments. The author acknowledges MOHE for a support by grant FRGS14-153-0394.

References

[1]. U. Bekbaev, On classification of m-dimensional algebras, IOP Conf. Series: Journal of Physics: Conf. Series, **819**, 2017, pp. 2-9.

[2]. H. Ahmed, U. Bekbaev, I. Rakhimov, Complete Classification of Two-Dimensional Algebras, AIP Conference Proceedings 1830, 070016 (2017); doi: 10.1063/1.4980965.

[3]. V. Popov, Generic Algebras: Rational Parametrization and Normal Forms, arXiv: 1411.6570v2 [math.AG], 2014, pp. 1-20.

Extended Abstract of the 4th International Conference on Mathematical Applications in Engineering (ICMAE2017), 8-9th August 2017

The Multistage Homotopy Perturbation Method for solving Hyperchaotic Chen System

Nur Isnida Razali [1], **M. S. H Chowdhury [1]**, and Zanariah Abdul Majid [2]

[1]*Department of Science in Engineering, Faculty of Engineering International Islamic University Malaysia, Jalan Gombak, 53100 Kuala Lumpur, Malaysia. E-mail: sazzadbd@iium.edu.my*

[2] *Department of Mathematics, Faculty of Science, Universiti Putra Malaysia, 43400 Selangor, Malaysia*

sazzadbd@iium.edu.my

Introduction

Since decades, chaos nonlinear phenomena have drawn attention of many researchers all over the world. Chaotic behaviour found in various systems such as electrical system, population growth, weather, molecular vibrations mechanical devices and many more. Dynamical systems that exhibit chaotic behavior are very sensitive to the initial conditions. Because of its higher unpredictability and extreme sensitivity to initial conditions, chaos is widely used in field like secure communication and encryption [1]. But it is not secured enough [2] until in 1996 when Pecora found that it can be overcome by choosing higher-dimensional hyperchaotic systems as secret key encryption, which has an increasing randomness and higher predictability [3]. Hyperchaotic system was first discovered by O.E. Rossler in 1979 [4]. Details of other hyperchaotic systems can be found in many references [5-13].

The Homotopy technique [14,15] has been applied in many nonlinear problems in engineering field for the reason that homotopy method deforms continuously from a difficult into a simpler problem which can be easily solved. Inspired from the previous works done by others, in this present paper, we are interested to solve hyperchaotic Chen systems using multistage homotopy perturbation method (MHPM). The hyperchaotic Chen system [16, 17] is given by

$$\begin{aligned} \dot{x} &= a(y-x)+w, \\ \dot{y} &= dx - xz + cy, \\ \dot{z} &= xy - bz, \\ \dot{w} &= yz + rw. \end{aligned} \tag{1}$$

The above system is hyperchaotic for the parameters of $a = 35$, $b = 3$, $c = 12$, $d = 7$, and $r = 0.5$ with the initial conditions as $x(0) = -20, y(0) = 0, z(0) = 0$ and $w(0) = 15$.

Results and Discussion

The series solutions for 15-term HPM for hyperchaotic Chen system (2) are obtained as :

$$x(t) = -20.0 + 715.0t - 14958.75000\,t^2 + 193915.2083\,t^3 - 1862311.641\,t^4 + 11648014.04\,t^5 - 782382.0271\,t^6 - 1397601846\,t^7 + 27028163520\,t^8 - 334919921200\,t^9 + 2586282504000\,t^{10} + + 3406869902000\,t^{11} - 581768028700000\,t^{12} + 13372041570000000\,t^{13} - 212029685400000000\,t^{14}$$

$y(t) =$ $-140.0\,t + 1662.500000\,t^2 - 18920.41667\,t^3 - 196909.6354\,t^4 + 11464051.41\,t^5 - 279184644\,t^6 + 4764117419\,t^7 - 58999397170\,t^8 + 406793603700\,t^9 + 3539842879000\,t^{10} - 193395949000000\,t^{11} + 4341484559000000\,t^{12} - 70942516200000000\,t^{13} + 898449650500000000\,t^{14}$

$z(t) =$ $1400.0\,t^2 - 45850.00000\,t^3 + 949717.7083\,t^4 - 12891221.88\,t^5 + 89122615.75\,t^6 + 1151838885\,t^7 - 56664558560\,t^8 + 1277368685000\,t^9 - 20929183260000\,t^{10} + 260102072300000\,t^{11} - 2099638152000000\,t^{12} - 2959658978000000\,t^{13} + 533351445800000000\,t^{14}$

$w(t) =$ $15.0 + 7.5\,t + 1.875000000\,t^2 + 0.3125000000\,t^3 - 48999.96092\,t^4 + 1744400.004\,t^5 - 39133747.92\,t^6 + 565133927.6\,t^7 - 3314666453\,t^8 - 97148329530\,t^9 + 4100955790000\,t^{10} - 93117682730000\,t^{11} + 1522699888000000\,t^{12} - 17406073610000000\,t^{13} + 73528243810000000\,t^{14}$

There are 3 methods used in this study to solve the hyperchaotic Chen which are HPM, MHPM and the well-established RK4 as the reference. The algorithm discussed is coded in the computer algebra package Maple together with the Maple's built-in fourth-order Runge-Kutta. From the results presented in Table 1 for hyperchaotic Chen, the absolute errors between Δt=0.01 with Δt=0.001 are still large comparing to Δt=0.001 with Δt=0.0001 which the minimum difference recorded is to the value of 10^{-5}. Therefore, the step size of Δt=0.001 is chosen for this study because it gives small error and computationally costly as the time taken is reasonable. The time range in this work is taken to be from $t=0$ *to* $t=10$.

Table 1: Hyperchaotic Chen system, differences between RK4 solutions on Δt=0.01, Δt=0.001and Δt=0.0001

$\Delta = \lvert RK4_{0.01} - RK4_{0.001} \rvert$					$\Delta = \lvert RK4_{0.001} - RK4_{0.0001} \rvert$				
t	Δx	Δy	Δz	Δw	t	Δx	Δy	Δz	Δw
1	0.0004482	5.998E-06	0.00132	0.0003517	1	6.956E-09	1.711E-08	6.184E-08	2.865E-08
2	0.003455	0.002203	0.006475	0.01659	2	2.405E-07	1.553E-07	4.548E-07	1.061E-06
3	0.002024	0.003053	0.0005701	0.01326	3	1.228E-07	1.982E-07	7.074E-09	9.202E-07
4	7.054E-05	0.0007172	0.003162	0.02676	4	1.373E-08	3.838E-08	2.089E-07	1.836E-06
5	0.005558	0.007073	0.001747	0.007351	5	3.710E-07	4.749E-07	1.235E-07	5.514E-07
6	0.04084	0.08134	0.0463	0.2095	6	2.770E-06	5.468E-06	3.047E-06	1.400E-05
7	0.044	0.05512	0.004727	0.05878	7	2.962E-06	3.717E-06	3.362E-07	3.859E-06
8	0.01109	0.02319	0.05064	0.02173	8	7.865E-07	1.589E-06	3.354E-06	1.205E-06
9	0.0128	0.003577	0.1543	0.3116	9	8.382E-07	2.363E-07	1.016E-05	2.041E-05
10	0.1429	0.1313	0.1916	0.7805	10	8.919E-06	8.120E-06	1.256E-05	5.031E-05

In table 1, we compare the solutions of HPM and MHPM to the RK4. Obviously, we can see that MHPM solves the hyper chaotic system accurately based on the differences between MHPM and RK4. As for HPM, it diverges rapidly thus far from the RK4 solution even at t=1.

Table 2: Differences between 15-term HPM and 15-term MHPM with RK4 solutions on Δt=0.001.

$\Delta = \lvert HPM - RK4_{0.001} \rvert$					$\Delta = \lvert MHPM_{0.001} - RK4_{0.001} \rvert$				
t	Δx	Δy	Δz	Δw	t	Δx	Δy	Δz	Δw
1	1.992E+17	8.317E+17	5.285E+17	5.756E+16	1	6.956E-09	1.711E-08	6.184E-08	2.866E-08
2	3.367E+21	1.416E+22	8.706E+21	1.068E+21	2	2.405E-07	1.553E-07	4.549E-07	1.061E-06
3	9.931E+23	4.186E+24	2.545E+24	3.247E+23	3	1.228E-07	1.982E-07	7.073E-09	9.203E-07
4	5.603E+25	2.365E+26	1.429E+26	1.859E+25	4	1.374E-08	3.838E-08	2.090E-07	1.836E-06
5	1.278E+27	5.398E+27	3.251E+27	4.279E+26	5	3.710E-07	4.750E-07	1.235E-07	5.515E-07
6	1.644E+28	6.949E+28	4.175E+28	5.538E+27	6	2.770E-06	5.468E-06	3.048E-06	1.400E-05
7	1.425E+29	6.025E+29	3.614E+29	4.820E+28	7	2.962E-06	3.717E-06	3.363E-07	3.860E-06
8	9.252E+29	3.913E+30	2.344E+30	3.139E+29	8	7.866E-07	1.590E-06	3.354E-06	1.205E-06
9	4.817E+30	2.037E+31	1.219E+31	1.638E+30	9	8.382E-07	2.363E-07	1.016E-05	2.042E-05
10	2.107E+31	8.914E+31	5.330E+31	7.180E+30	10	8.920E-06	8.121E-06	1.256E-05	5.032E-05

Conclusion

According to the data in table 2 for hyperchaotic Chen system, we see that the 15-term MHPM solutions at $\Delta t=0.001$ highly agree with the solutions of RK4 to at least 5 decimal places while HPM solutions are not valid even at t=1. This demonstrates that the hyperchaotic Chen is solved accurately by MHPM. The method has the advantage of giving an analytical form of the solution within each time interval which is not possible in purely numerical techniques like RK4. The present technique offers an explicit time-marching algorithm that works accurately over such a bigger time step than the RK4. The results presented in this paper suggest that MHPM is also readily applicable to the hyperchaotic systems involving more complex dynamical behaviors.

References

[1] Chen G, Dong X. From chaos to order: methodologies, perspectives and applications. Singapore: World Scientific; 1998.

[2] Perez G, Cerdeira H. Extracting messages masked by chaos. Phys Rev Lett 1995; 74 (11):1970.

[3] Pecora L. Hyperchaos harnessed. Phys World 1996; 9:17.

[4] Rossler O. An equation for hyperchaos. Phys Lett A 1979; 71(2-3):155.

[5] Li C, Chen G, Chaos and hyperchaos in the fractional-order Rossler equations. Physica A 2004; 341-55.

[6] Wang G, Zhang X, Zheng Y, Li Y. A new modified hyperchaotic Lu system. Physica A 2006; 371: 260.

[7] Li Y, Tang KS, Chen G. Hyperchaotic Chen system and its generation. Dyn Contin Discret Impul Syst, Ser B: Appl Algorithms 2007; 14:97.

[8] Thamilmaran K, Lakshmanan M, Venkatesan A. A hyperchaos in modified canonical Chua's circuit. Int J Bifurc Chaos 2004; 14 (1):221.

[9] Jia Q. Hyperchaos generated from the Lorenz chaotic system and its control. Phys Lett A 2007; 366:217.

[10] Yuxia L, Wallace K, Chen G. Generating hyperchaos via state feedback control. Int J Bifurcat Chaos 2005; 15:3367-75.

[11] Park J. Adaptive synchronization of hypechaotic Chen system with uncertain parameters. Chaos Solitons Fractals 2005; 26:959-64.

[12] Chen A, Lu J, Yu S. Generating hyperchaotic Lu attractor via state feedback control. Physica A 2006;364:103-10.

[13] Qiang Jia. Projective synchronization of a new hyperchaotic Lorenz system. Physics Letters A 370 (2007) 40–45.

[14] J.-H He. A coupling method of homotopy technique and perturbation technique for nonlinear problems, Int. J. Nonlinear Mech. 35 (1) (2000) 37-43.

[15] J.-H He. Homotopy perturbation technique. Comput. Methods Appl. Mech. Engrg. 178(3/4) (1999) 257-262.

[16] Yuxia L, Wallace K, Chen G. Generating hyperchaos via state feedback control. Int J Bifurcat Chaos 2005; 15:3367-75.

[17] Park J. Adaptive synchronization of hypechaotic Chen system with uncertain parameters. Chaos Solitons Fractals 2005; 26:959-64

Extended Abstract of the 4th International Conference on Mathematical Applications in Engineering (ICMAE2017), 8-9th August 2017

Analytical Approximations for The Oscillators with Anti-Symmetric Quadratic Nonlinearity

Md. Alal Hosen[1,4*], **M. S. H. Chowdhury[2]**, Mohammad Yeakub Ali[3], Ahmad Faris Ismail[4]

[1]Department of Manufacturing and Material Engineering, Faculty of Engineering, International Islamic University Malaysia, Jalan Gombak, 53100 Kuala Lumpur, Malaysia.

[2]Department of Science in Engineering, Faculty of Engineering, International Islamic University Malaysia, Jalan Gombak, 53100 Kuala Lumpur, Malaysia.

[3]Department of Mechanical Engineering, Faculty of Engineering, International Islamic University Malaysia, Jalan Gombak, 53100 Kuala Lumpur, Malaysia.

[4]Department of Mathematics, Rajshahi University of Engineering and Technology (RUET), Rajshahi-6204, Bangladesh.

[1]alal_ruet@yahoo.com, [2]sazzadbd@iium.edu.my, [3]mmyali@iium.edu.my, [4]faris@iium.edu.my

Abstract

A second-order ordinary differential equation involving anti-symmetric quadratic nonlinearity changes sign. In this reason, Harmonic Balance Method (HBM) cannot be directly applied. The main purpose of the present paper is to propose an analytical approximation technique based on the HBM for obtaining approximate angular frequencies and the corresponding periodic solutions of the oscillators with anti-symmetric quadratic nonlinearity. The presented technique gives excellent results as compared with the corresponding numerical.

Introduction

The mathematical model of oscillation of the human eardrum is the quadratic nonlinear oscillator [1]. Researchers have been investigated many analytical approaches to solve nonlinear differential equations. Perturbation technique [2] is the versatile technique, whereby the solution is expanded in powers of a small parameter. Several authors employed many other powerful analytical methods (non-perturb) to drive approximate periodic solutions especially for strongly nonlinear oscillators, namely, the Max-Min Approach [3], Energy Balance Method [4] and so on. Investigating Homotopy Perturbation Method and Modified Homotopy Perturbation Method [5] to solve the oscillators with anti-symmetric quadratic nonlinearity. Solving strongly nonlinear systems, the method of harmonic balance [6,7] is another efficient method. In this paper, an analytical technique has been established based on the HBM to obtain approximate solutions of the oscillators with anti-symmetric quadratic nonlinearity. The approximated results have compared with the corresponding numerical solutions (Runge-Kutta fourth order method).

Solution Procedure

Let us consider a second-order nonlinear differential equation is in the following form as

$$y'' + \omega_0^2 y = -\varepsilon\, f(y, y') \text{ and the initial condition } [y(0) = a_0,\ y'(0) = 0], \tag{1}$$

where $f(y, y')$ is a nonlinear function such that $f(-y, -y') = f(y, y')$, $\omega_0 \geq 0$ and ε is a constant.

A n-th order periodic solution of Eq. (1), can be supposed as

$$y = a_0(\rho\cos(\omega t) + u\cos(3\omega t) + v\cos(5\omega t) + w\cos(7\omega t) + \cdots), \tag{2}$$

where a_0, ρ and ω are constants. If $\rho = 1 - u - v - \cdots$, solution Eq. (2) readily satisfies the initial conditions Eq. (1).

Substituting Eq. (2) into Eq. (1) and expanding $f(y, y')$ in a Fourier series, it can be transformed into

$$\begin{aligned} a_0[\rho(\omega_0^2 - \omega^2)\cos(\omega t) + u(\omega_0^2 - 9\omega^2)\cos(3\omega t) + \cdots] = -\varepsilon[F_1(a_0, u, \cdots)\cos(\omega t) \\ + F_3(a_0, u, \cdots)\cos(3\omega t) + \cdots] \end{aligned} \tag{3}$$

Equating the coefficients of equal harmonic terms of Eq. (3), the following nonlinear algebraic equations can be found as

$$\rho(\omega_0^2 - \omega^2) = -\varepsilon F_1, \quad u(\omega_0^2 - 9\omega^2) = -\varepsilon F_3, \quad v(\omega_0^2 - 25\omega^2) = -\varepsilon F_5, \cdots \tag{4}$$

With help of the first equation, ω is eliminated from all the rest of Eq. (4). Thus Eq. (4), can be expressed as in the following form

$$\rho\omega^2 = \rho\omega_0^2 + \varepsilon F_1, \quad 8\omega_0^2 u\rho = \varepsilon(\rho F_3 - 9uF_1), \quad 24\omega_0^2 v\rho = \varepsilon(\rho F_5 - 25vF_1), \cdots \tag{5}$$

Substitution $\rho = 1 - u - v - \cdots$, and simplification, second-, third- equations of Eq. (5), can be transformed into

$$u = G_1(\omega_0, \varepsilon, a_0, u, v, \cdots, \lambda_0), \quad v = G_2(\omega_0, \varepsilon, a_0, u, v, \cdots, \lambda_0), \cdots, \tag{6}$$

where $G_1, G_2, \cdots$ exclude respectively the linear terms of $u, v, \cdots$.

Whatever the values of ω_0 and a_0, there exists a parameter $\lambda_0(\omega_0, \varepsilon, a_0) << 1$, such that $u, v, \cdots$ are expandable in following series

$$u = U_1\lambda_0 + U_2\lambda_0^2 + \cdots, \quad v = V_1\lambda_0 + V_2\lambda_0^2 + \cdots, \quad \cdots \tag{7}$$

where $U_1, U_2, \cdots, V_1, V_2, \cdots$ are constants.

Finally, substituting the values of $u, v, \cdots$ from Eq. (7) into the first equation of Eq. (5), the unknown angular frequency ω is determined.

Example: Differential equation with anti-symmetric quadratic nonlinearity

Let us consider the following equation which has investigated in Momani et. al. [18] is

$$y'' + 2y + y^2 = 0 \text{ and the initial conditions } [y(0) = a_0,\ y'(0) = 0]. \tag{8}$$

As we know, an asymmetric behavior of the nonlinear oscillator is different in positive and negative directions.

Results and discussions

The approximate solution is shown Fig. 1 for initial amplitude $a_0 = 0.2$ together with corresponding numerical solutions. It is noted that the presented technique is simpler than several existing procedures, namely, the Homotopy Perturbation Method and the Modified Homotopy Perturbation Method et. al. [5].

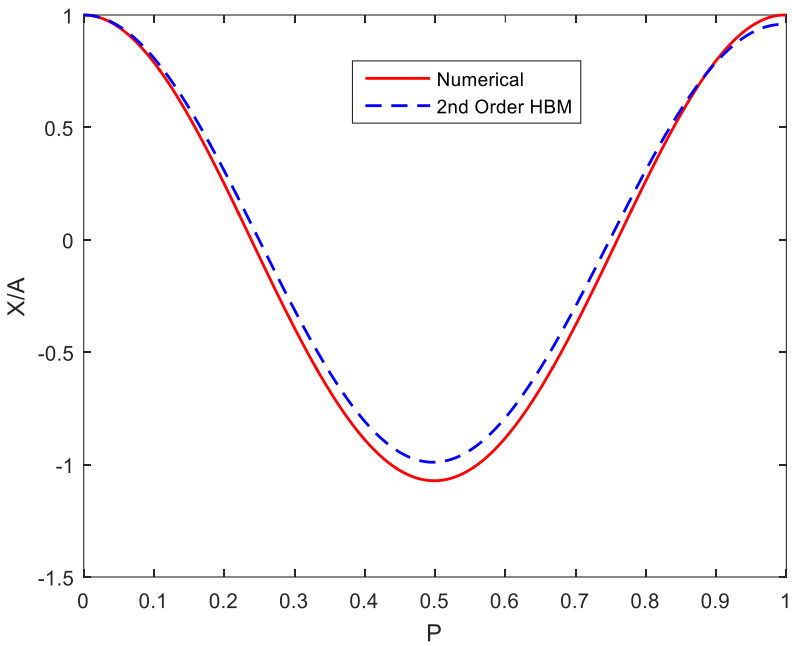

Fig. 1: Comparison the obtained results (represented by blue dashed line) with the corresponding numerical solutions (represented by red solid line) for the initial amplitude $a_0 = 0.2$.

Conclusion

In this paper, an analytical approximate technique based on the Harmonic Balance Method has been presented to determine approximate angular frequencies and the corresponding periodic solutions of the oscillators with anti-symmetric quadratic nonlinearity. The solution procedure is straightforward and simple as compared with the previously existing methods. The approximated solutions show a good agreement with its exact ones and much better than the existing results.

References

[1] R. Porwal, N.S. Vyas, Damped quadratic and mixed-parity oscillator response using Krylov-Bogoliubov method and energy balance, J. Sound Vib. 309 (2008) 877-886.

[2] J.B. Marion, Classical Dynamics of Particles and System, San Diego, CA: Harcourt Brace Jovanovich, (1970).

[3] D.D Ganji, M. Azimi, Application of max min approach and amplitude frequency formulation to nonlinear oscillation systems. UPB Scientific Bulletin, Series A: App. Math. Phy. 74(3) (2012) 131-140.

[4] M. Akbarzade, A. Farshidianfar, Nonlinear transversely vibrating beams by the improved energy balance method and the global residue harmonic balance method, Appl. Math. Modelling 45 (2017) 393-404.

[5] S. Momani, G.H. Erjaee, M.H. Alnasr, The modified homotopy perturbation method for solving strongly nonlinear oscillators, Computers and Mathematics with Applications 58 (2009) 2209-2220.

[6] R.E. Mickens, Oscillation in Planar Dynamic Systems, World Scientific, Singapore, 1996.

[7] M.A. Razzak, A simple harmonic balance method for solving strongly nonlinear oscillators, Journal of the Association of Arab Universities for Basic and Applied Sciences, 21 (2016) 68-76.

Extended Abstract of the 4th International Conference on Mathematical Applications in Engineering (ICMAE2017), 8-9th August 2017

Impact of Donor-Acceptor Morphology On the Charge Carrier Generation in Organic Photovoltaic Devices

M. L. Inche Ibrahim[1]

[1] Department of Science in Engineering, Faculty of Engineering,
International Islamic University Malaysia
Jalan Gombak, 53100 Kuala Lumpur, MALAYSIA.

[1] *mlukmanibrahim@gmail.com*

Introduction. Organic photovoltaic (OPV) devices (a term used here to refer both organic solar cells and photodiodes) have distinctive and interesting properties that could lead to various applications. They are also relatively cheap to fabricate, which mean that organic solar cells have the potential to be a viable energy source.

When light is absorbed by the organic photoactive layer (PL), excitons (strongly bound electron-hole pairs) are produced. How free charge carriers are generated is a fundamental step in the working operation of OPV devices. At the donor-acceptor (DA) interface, excitons are generally transformed into charge-transfer (CT) states. Since CT states are produced with excess energies, it has been suggested that the energy required to overcome the binding energy is provided by the excess energies [1,2]. Another situation is that CT states with excess energies relax to the ground CT states before dissociating into free charge carriers. The dissociation via the relaxed CT states has been supported experimentally [3–7]. The Onsager–Braun (OB) model [8] is widely used to describe the dissociation of relaxed CT states. However, the OB model has several fundamental issues [9].

Very recently, Ref. [9] has made an improvement to the OB model by including the effect of DA morphology and by employing the correct charge carrier mobilities. The impacts of the PLs properties such as the carrier mobilities and the permittivity on the performance of OPV devices have been investigated by many studies (for example by Refs. [10-12]) and well understood. However, the impact of the DA morphology of the PL on the charge carrier generation is still unclear. The aim of this paper is to investigate how the DA morphology impacts the generation of charge carriers based on the new model proposed by Ref. [9].

Model and procedures. The dissociation probability of a CT state is defined as [8]

$$P_d = \frac{k_d}{k_d + k_f} \tag{1}$$

where k_d is the CT state dissociation rate coefficient, and k_f is the CT state decay rate coefficient. According to the modified OB model proposed by Ref. [9], k_d is given by

$$k_d = \frac{3q\left(\mu_{n,i} + \mu_{p,i}\right)}{4\pi\varepsilon a^3} \exp\left(\frac{-E_b}{k_B T}\right) \frac{J_1\left(2\sqrt{-2b_{\text{eff}}}\right)}{\sqrt{-2b_{\text{eff}}}} \tag{2}$$

where q is the elementary charge, $\mu_{n,i}$ is the actual electron mobility at DA interface, $\mu_{p,i}$ is the actual hole mobility at DA interface, ε is the effective permittivity of the photoactive layer (PL), a is the separation distance between the electron and the hole of the CT state, $E_b = q^2/(4\pi a)$ is the binding energy of the CT state, k_B is the Boltzmann constant, T is the absolute temperature, J_1 is the Bessel function of the first kind of order 1, and $b_{\text{eff}} = q^3\lambda|F|/(8\pi\varepsilon k_B{}^2T^2)$. Here, $|F|$ is the magnitude of the electric field, and λ is a parameter that describes how the DA morphology influences the CT state dissociation.

Note that $\mu_{n,i}$ and $\mu_{p,i}$ are generally not the same as (can be higher than) the conventional carrier mobilities that are used to calculate the electric current [9]. $\mu_{n,i}$ and $\mu_{p,i}$ are fixed for any given DA mixture (independent of the DA morphology and device architecture) unlike the conventional carrier mobilities [9]. The detailed explanation on the actual carrier mobilities can be obtained in Ref. [9].

A CT state's direction is defined as the direction from the electron to the hole of the CT state. A more positive value of λ means the effective direction of the CT states inside the PL is more aligned in the direction of the electric field inside the PL, while a more negative value of λ means the effective direction of the CT states inside the PL is more aligned in the direction opposite to the direction of the electric field. $\lambda = 1$ (the maximum value) means that all the CT states inside the PL are in the same direction as the direction of the electric field. $\lambda = -1$ (the minimum value) means that all the CT states inside the PL are exactly opposite to the direction of the electric field. $\lambda = 0$ means the effective direction of the CT states is perpendicular to the direction of the electric field. In other words, $\lambda = 0$ means that the electric field basically does not contribute to the CT state dissociation. However, since $\lambda = 0$ gives an undefined value of k_d according to Eq. (2), we simply neglect the term $J_1\left(2\sqrt{-2b_{\text{eff}}}\right)/\sqrt{-2b_{\text{eff}}}$ in Eq. (2) in order to represent k_d (and thus P_d) when $\lambda = 0$.

The CT state dissociation probability may also be called the charge carrier generation probability, which will be used from here on. In order to achieve a comprehensive understanding on how the charge carrier generation is influenced by the DA morphology, we calculate and analyze the charge carrier generation probabilities P_d with respect to λ (which represents the DA morphology) together with other relevant parameters, which are the effective permittivity, the actual mobilities, and the electric field.

Results

In the calculations, we use $k_f = 1\times10^8\,\text{s}^{-1}$, $a = 1.3\times10^{-9}$ m, and $T = 300$ K. The range of $|F|$ used here is from 0 Vm^{-1} to $6\times10^7\,\text{Vm}^{-1}$, and this should cover the possible operating $|F|$ in various OPV devices.

We find that for devices with $\varepsilon_r = 3.5$ and $\mu_{n,i} = \mu_{p,i} = 2\times10^{-6}\,\text{m}^2\text{V}^{-1}\text{s}^{-1}$ (which are typical values for organic PLs), the value of λ (and thus the DA morphology) plays an important role in the charge carrier generation, practically at the whole range of the studied $|F|$. Note that $\varepsilon_r = \varepsilon/\varepsilon_0$, where ε_0 is the vacuum permittivity.

As we increase ε_r to higher values using the same values of $\mu_{n,i}$ and $\mu_{p,i}$, the charge carrier generation increases and the role of DA morphology on the charge carrier generation

becomes less important. Similarly, as the values of $\mu_{n,i}$ and $\mu_{p,i}$ are increased but with the same value of ε_r, the charge carrier generation increases and the role of DA morphology on the charge carrier generation becomes less important.

In summary, for devices with typical values of ε_r and $\mu_{n,i} + \mu_{p,i}$, the DA morphology plays an important role in order to maximize the charge carrier generation, practically at all possible operating electric fields. Devices with relatively very high ε_r and/or $\mu_{n,i} + \mu_{p,i}$, the role of DA morphology on the charge carrier generation can be said to be insignificant. In order to maximize the charge carrier generation, devices with relatively poorly-designed donor-acceptor morphology (low λ) but having ε_r and/or $\mu_{n,i} + \mu_{p,i}$ that are significantly higher than the (current) typical values are more desirable than devices with excellently-designed donor-acceptor morphology (very high λ) but having typical values of ε_r and $\mu_{n,i} + \mu_{p,i}$.

References

[1] Ohkita H et al 2008 J. Am. Chem. Soc. **130** 3030

[2] Grancini G, Maiuri M, Fazzi D, Petrozza A, Egelhaaf H J, Brida D, Cerullo G and Lanzani 2013 Nat. Mater. **12** 29

[3] Howard I A, Mauer R, Meister M and Laquai F 2010 J. Am. Chem. Soc. **132** 14866

[4] Lee J, Vandewal K, Yost S R, Bahlke M E, Goris L, Baldo M A, Manca J V and Voorhis T V 2010 J. Am. Chem. Soc. **132** 11878

[5] Van der Hofstad T G J, Di Nuzzo D, van den Berg M, Janssen R A J and Meskers S C J 2012 Adv. Energy Mater. **2** 1095

[6] Vandewal K et al 2014 Nat. Mater. **13** 63

[7] Devizis A, De Jonghe-Risse J, Hany R, Nuesch F, Jenatsch S, Gulbinas V and Moser J E 2015 J. Am. Chem. Soc. **137** 8192

[8] Braun C L 1984 J. Chem. Phys. **80** 4157

[9] Inche Ibrahim M L 2017 J. Phys. D: Appl. Phys. **50** 065103

[10] Inche Ibrahim M L, Ahmad Z, K Sulaiman K, and Muniandy S V 2014 AIP Adv. **4** 057133

[11] A Koster L J A, Shaheen S E, and Hummelen J C 2012 Adv. Energy Mater. **2** 1246.

[12] Shieh J T, Liu C H, Meng H F, Tseng S R, Chao Y C, and Horng S F 2010 J. Appl. Phys. **107** 084503

Extended Abstract of the 4th International Conference on Mathematical Applications in Engineering (ICMAE2017), 8-9th August 2017

Insertion Algorithms for Network Model Database Management Systems

Abdurashid Mamadolimov[1], Khikmat Saburov[2]

[1,2]Applied Mathematics Laboratory, MIMOS,
Technology Park Malaysia, 57000, Kuala Lumpur, Malaysia

[1]rashid.mdolimov@mimos.my, [2]khikmat.saburov@mimos.my

Introduction. The network model is a database model conceived as a flexible way of representing objects and their relationships. Its distinguishing feature is that the schema, viewed as a graph in which object types are nodes and relationship types are arcs, forms partial order, is not restricted to being a tree or lattice. When a database is large and a query comparison is expensive then the efficiency requirement of managing algorithms is minimizing the number of query comparisons i.e., the efficiency is measured by query complexity of an algorithm. For example, conceptual graphs form a network model structure and query comparison will be a graph homomorphism checking which a very expensive operation is [1]-[9].

In this paper we consider updating operation for network model database management systems. We develop a new sequential algorithm for updating operation. Also we suggest a distributed version of the algorithm.

One of the important components of updating operation is a searching. In [10], Mozes, Onak, and Weimann present a linear-time algorithm that finds the optimal strategy for searching a tree-like partially ordered set. Dereniowski [11] proves that finding an optimal search strategy for general posets is hard and gives a polynomial-time approximation algorithm with sub-logarithmic approximation ratio. In [12] [13] we proposed new sequential and distributed algorithms for searching operation. Another component of updating operation is a finding parents. For finding parents operation Levinson [14] and Ellis [15] have proposed several modifications of breadth/depth first search technique using some simple properties of partially ordered sets. In this paper we used height of elements of poset for a good ordering of a dataset.

Partially ordered set (poset). Definition. A *chain* from an element a to an element b $(\neq a)$ in a poset D is a sequence of different elements $a = x_0, x_1, \dots, x_l = b$ of a poset D such that each of its elements, except last one, is a parent for the next element in the sequence; l is called a *length* of the chain; A chain from element a to element b with maximum length is called *maximum chain* from *a* to *b*.

Definition. A length of maximum chain from top element $\top$ to an element x is called *height* of x in a poset D and denoted as $Height(x, D)$. Height of bottom element is called *height of poset* i.e., $Height(D) = Height(\perp, D)$.

Proposition 1. For any two elements x and y of a poset D, if $x > y$ then $Height(x, D) < Height(y, D)$.

Proposition 2. For any element x of a poset D,

$$Height(x, D) = \max_{y \in Parents(x,D)} Height(y, D) + 1.$$

Proposition 3. Let x, y, z be elements of some poset. If $x \geq y$ is false then for any z such that $z \leq x$, we have that $z \geq y$ is also false.

Also we use the next proposition in our algorithms.
Proposition 4. Let $(P, \leq)$ be a poset and D be any non-empty, finite subset of P. Let $q \in P \backslash D$. Let L_h be a set of elements of D with fixed height h i.e., $L_h = \{x \in D | \ Height(x, D) = h\}$. Let L_h^+ be a set of elements of D with height more than h i.e., $L_h^+ = \{x \in D | \ Height(x, D) > h\}$. If $\forall x \in L_h$, $x > q$ is false, then $\forall y \in L_h^+$, $y > q$ is also false.

Representation of a poset: the extended descendants list data structure. For representation of a poset we use list of descendants or list of ancestors in special form. Let $c_1, \dots, c_n$ be elements of poset D and let c_1 be top element, i.e., $c_1 = \top$. We define partial order over integers $D' = \{1,2, \dots, n\}$ in the following way: for any $x, y \in D'$, $x \leq y$ if and only if $c_x \leq c_y$. Two lists are associated with an element $c_i \in D$, $i = 1..n$: *list of descendants* $\mathbf{D}(i)$ and *list of ancestors* $\mathbf{A}(i)$. The list of descendants includes $Height(i, D)$ as a first component of the list, second component is $Outdeg(i, D')$, and first $Outdeg(i, D')$ descendants are $Children(i, D')$, and other descendants:

$$\mathbf{D}(i) = [Height(i, D'); \ Outdeg(i, D'); Child_1(i, D'), \dots, Child_{Outdeg(i,D')}(i, D'); \\ Descendant_{Outdeg(i,D')+1}(i, D'), \dots, \bot], \quad i = 1..n.$$

We assume that elements $c_1, \dots, c_n$ of poset D are ordered such that $Height(i, D')$ is a non-decreasing function of *i*. Also we denote the number of elements of dataset D' with $Height(x, D') = h$ as n_h, $h = 0,..Height(\ D') = H$. It is clear that $\sum_{h=0}^{H} n_h = n$. The list of ancestors is dually defined.

Updating operation. *Updating* can be done using *Inserting* and *Deleting* of a query element. The *Deleting* first uses *Searching* of a query element then deletes it and its links to parents and children. *Deleting* and *Searching* have the same query complexity. These two operations are almost same. Since in early works [12], [13] we developed algorithms for *Searching* operation, in this paper we do not consider the *Deleting* operation. *Inserting* can be done using *Finding Parents* and *Finding Children* operations. *Finding Parents* and *Finding Children* are dual operations, i.e., an algorithm for *Finding Parents* can be very easily adapted to *Finding Children* operation and vice versa. Thereby we consider *Finding Parents* operation in this paper. We assume that a query element is not in a database; otherwise again we have an operation which is equivalent to *Searching*. Since our original operation is *Inserting* this assumption is inartificial.

Algorithm for finding parents operation. Let $(P, \leq)$ be a poset and D be any dataset i.e., non-empty, finite subset of P: $D \subseteq P$, $|D| = n$, where n is a positive integer. Let a query element $q \in P$ be not in D i.e., $q \notin D$. Although the query element *q* is not in the dataset *D*, it has parents, children and ancestors, descendants in *D* i.e., query element has a virtual address in the dataset. The proposed algorithm takes list of descendants **D**(i), $i = 1..n$ of a given poset *D*, the numbers n_h, $h = 0,..Height(D') = H$ of elements of dataset D' with $Height(x, D') = h$ and a query element q $(\notin D)$ as input and finds $Parents(q, D)$.
Data representation way described in section III allows us to distribute the elements of dataset in the table. The height of the table is $H + 1$, where H is height of dataset. Width of the table is equal to $\max\{n_0, n_1, \dots, n_H\}$. The top element $\top$ is only element on the 0-th row of the table, for $h = 1,\dots, H$, *h*-th row of the table contains elements of dataset from $\sum_{i=0}^{h-1} n_i + 1$ to $\sum_{i=0}^{h} n_i$. Proposed algorithm scans elements of this table from up to down and from left to right. Scanning is a comparison of current element *c* and query element *q*: if $c > q$ then YES

status will be assigned to the element *c*, else NO. Regarding Proposition 3 if NO status is assigned to the element *c* then NO status will be assigned to all its descendants also.

Algorithm scans not only current element *c* but all its children also. If all children of *c* have NO status then *c* is a parent of query element *q*. Regarding Proposition 4 algorithm ends if all elements of some row of the table have NO status.

Distributed algorithm. Proposed algorithm can be adapted for distributed computing. For distributed algorithm we use parallel random-access machine (PRAM) model of computation with $P_1, P_2, \dots, P_m,\ m \geq 2$ processors. In PRAM model of computation all processors can access common RAM in a single algorithm-step.
In the distributed algorithm one of the processors starts and ends to compute following sequential algorithm. Scanning of elements in each row will be done parallelly by *m* processors.

$$\{\sum_{i=0}^{h-1} n_i + 1 + (s-1)\left\lceil \frac{n_h}{m} \right\rceil,\ \sum_{i=0}^{h-1} n_i + s\left\lceil \frac{n_h}{m} \right\rceil\},$$
$$s = 1..m,$$

here $\lceil a \rceil$ is the smallest integer not less than *a*.
Each interval is scanned by one processor. In the proposed distributed algorithm two or more processors do not check the same query comparison if they do not come to common child of two elements with same height and from different intervals at exactly the same time. In other words, there is no overlapping of partition of scanning space up to query comparisons. We also note that the processors are almost uniformly tasked.

Summary. A *query complexity* of an algorithm is the number of query comparisons that is used in the algorithm. Our goal was to develop an updating algorithm(s) with a query complexity as less as possible.
We first analyzed an updating operation and picked out an operation *Finding Parents* as a most considerable sub-operation. We proposed an algorithm for *Finding Parents* operation. We used a new data structure for posets: it is an extended descendant list of a poset. The main extra parameter of this representation is a height/level of an element of a database. The extended descendant list of
poset allows us to distribute the elements of a database in a rectangular table. Then algorithm starts to scan cells of the table. For minimizing of query complexity we have also used the properties of posets.
We also proposed a distributed version of the algorithm. Proposed distributed algorithm responds two main requirements for distributed algorithms: uniform distribution of computation among processors and no overlapping computation.

References.

[1] Sowa J.F., *Conceptual Graphs*, IBM Journal of Research and Development, 20(4), 1976, pp336 - 357.

[2] Sowa J.F., *Conceptual Structures: Information Processing in Mind and Machine*. 1984, Addison- Wesley.

[3] Chein M., Mugnier M.-L., *Graph-based Knowledge Representation. Computational Foundations of Conceptual Graphs*. 2009, Springer.

[4] Chein M., Mugnier M.-L., *Conceptual Graphs: Fundamental Notions*, Revue d'Intelligence Artificielle, 6(4), 1992, pp365-406.

[5] Willems M., *Projection and unification for conceptual graphs*, In Proc. of ICCS'95, Vol. 954 of LNCS, pp 278-292, 1995, Springer.

[6] Mugnier M.-L, *On Generalization / Specialization for Conceptual Graphs*, Journal of Experimental and Theoretical Artificial Intelligence, 7, 1995, pp325-344.

[7] Baget J.-F., *Representer des connaissances et raisonner avec des hypergraphes: de la projection a la derivation sous contraintes*. PhD Thesis, 2001, University Montpellier II.

[8] Baget J.-F., *Simple Conceptual Graphs Revisited: Hypergraphs and Conjuctive Types for Efficient Projection Algorithms*, In Proc. of ICCS'03, vol. 2746 of LNAI. 2003, Springer.

[9] Croitoru M. and Compatangelo E., *A tree decomposition algorithm for conceptual graph Projection*, In Proc. of KR'06, pp271-276. 2006, AAAI Press.

[10] Mozes S., Onak K., Weimann O., *Finding an optimal tree searching strategy in linear time*, In: SODA'08: Proceedings of the nineteenth annual ACM-SIAM symposium on Discrete algorithms, Philadelphia, PA, USA, Society for Industrial and Applied Mathematics, 2008, pp1096-1105.

[11] Dereniowski D., *Edge ranking and searching in partial orders*, Discrete Appl. Math. 156(13), 2008, pp2493-2500.

[12] Mamadolimov A., *Search algorithms for conceptual graph databases*, International Journal of database Management Systems (IJDMS), Vol.5, No.1, 2013, pp 35-44.

[13] Mamadolimov A., *Searching Algorithms in Partially Ordered Set*, SIAM Conference on Discreet Mathematics, June 18- 21, 2012, Dalhosie University, Halifax, Nova Scotia, Canada.

[14] Levinson R.A., *A self-organizing retrieval system for graphs*, In The 3rd National Conference of the American Association for Artificial Intelligence, 1984, pp 203-206, Austin, Texas, AAAI Press, Menlo Park.

[15] Ellis G.R., *Managing Complex Objects*. PhD Thesis. University of Queensland, 1995.

Multicollinearity and Regression Analysis

Jamal I. Daoud

Department of Science in Engineering
IIUM, 53100, Jalan Gombak, Selangor Darul Ehsan, Malaysia

jamal58@iium.edu.my

Introduction

In regression analysis there are many assumptions about the model, namely, multicollinearity, nonconsistant variance (non-homogeneity), linearity, and autocorrelation. If one or more assumption is violated, then the model in hand is no more reliable and also is not acceptable in estimating the population parameters.

In this study we focus on multicollinearity as a violation of one of basic assumption for successful regression model assumptions of successful regression model. Multicollinearity appears when two or more independent variables in the regression model are correlated. a little bit of multicollinearity sometimes will cause big problem but when it is moderate of high then it will be a problem to be solved.

Correlation of predictors and the impact on regression model

What impact does the correlation (strong) between predictors have on the regression model and subsequent conclusions? To do that we demonstrate the impact on two sets of data. The analysis of regression for the first set yielded the following regression information

For first set of data where the correlation is quite low we start by finding a model containing x1 alone then including x2 alone then finding the model including both predictors as in the following table:

Table 1: Coefficients of models for first set of data

Term	Coef	SECoef	T-value	P-value	VIF
X1	2.20	3.3	0.67	0.524	1.00
X2	0.354	0.638	0.55	0.594	1.00
X1	2.27	3.46	0.66	0.532	1.00
X2	0.371	0.662	0.56	0.593	1.00

Comparing results in the table above showing that the standard error of coefficients has been changed slightly for x1 increased from 3.3. to 3.46, while for x2 changed from 0.638 to 0.662, and this is due to a very low correlation between predictors for first set of data.

For second set of data with a very high correlation between predictors (0.996) the results are shown in Table 2.

Table 2: Coefficients of models for second set of data

Term	Coef	SECoef	T-value	P-value	VIF
X11	-0.309	0.279	-1.11	0.299	1.00
X21	-0.704	0.579	-1.22	0.258	1.00
X11	2.71	2.96	0.92	0.390	1.00
X21	-6.39	6.24	-1.02	0.340	1.00

For Table 2 we have many types of comparisons. First we see that standard deviation of coefficients have been changed, for x11 from 3.46 in separate model to 2.96 which is still acceptable but the dramatic change occurred to standard error for x12 it has been increase from 0.579 for separate model to 6.24 for multiple model. The consequence of this increment will lead to a problem that is highlighted in the next point.

Diagnostic of Multicollinearity and VIF

There are many signs in the analysis for the multicollinearity among which

(i) The correlation among predictors is large

(ii) In case if the correlation is not calculated the following are signs of having the multicollinearity:

(1) When the predictors coefficients vary from one to another model

(2) When applying t-test, the coefficient is not significant but put all together (Ftest) for the whole model it is significant.

Relying only on correlation between pairs of predictors has limitation, the small or large value of correlation is something subjective depends on individual and also on the field of research that is why most of the time to detect the multicollinearity we use some indicator called variance inflation factors (VIF).

When correlation exists among predictor's the standard error of predictors coefficients will increase and consequently the variance of predictor's coefficients are inflated. The VIF is a tool to measure and quantify how much the variance is inflated. VIFs are usually calculated by the software as part of regression analysis and will appear in VIF column as part of the output. To interpret the value of VIF the flowing rule is used

- VIF=1 not correlated
- 1<VIF<5 moderately correlated
- VIF>5 highly correlated

Back to results of our data analysis it is evident that for the first set of data we obtained for both variables x1 and x2 similar VIF=1.00, means the correlation is zero which is perfect condition to apply regression analysis and this is due to very low correlation coefficient, while in the second case when the data has very high correlation (0.996) we found that for both variable the VIF was 113.67 which is evidence of a very high correlation between x11 and x12. In the latter case we cannot commence with regression unless this problem is solved

Problem solving

When two or more predictors are highly correlated, the relationship between the independent variables and the dependent variables is distorted by the very strong relationship between the independent variables, leading to the likelihood that our interpretation of relationships will be incorrect. In the worst case, if the variables are perfectly correlated, the regression cannot be computed. Multicollinearity can be resolved by combining the highly correlated variables through principal component analysis, or omitting a variable from the analysis that associated with other variable(s) highly.

Conclusions

1- Multicollinearity is one of serious problems that should be resolved before starting the process of modelling the data
2- It is highly recommended that all regression analysis assumption should be met as they are contributing to accurate conclusion and helps to make inference on the population.
3- Ignore and dismiss the model if the multicollinearity discovered after finding the model specially with high correlation as the model cannot be interpreted

References

[1] Carl F. Mela* and Praveen K. Kopalle. The impact of collinearity on regression analysis: the asymmetric effect of negative and positive correlations. J. of Applied Economics, 2002, 43,667-677.

[2] D. R. Jensen and D.E. Ramirez. Variance Inflation in Regression, Advances in Decision Sciences, 2012, 2013, 1-15.

[3] Debbie J. Dupuis1 and Maria-Pia Victoria-Feser. Robust VIF regression with application to variable selection in large data sets, The Annals of Applied Statistics, 2013, 7,319-341.

[4] Golberg, M. Introduction to regression analysis, Billerica, MA: Computational Mechanics Publications, 2004, 436.

[5] Kleinbaum, David G. Applied regression analysis and other multivariable methods, Australia; Belmont, CA: Brooks/Cole, 2008,906.

[6] McClendon, McKee J. Multiple regression and causal analysis, Prospects Heights, Ill.: Waveland Press 2002,358.

[7] Seber, G. A. F. (George Arthur Frederick). Linear regression analysis, Hoboken, N.J.: Wiley-Interscience, 2003,557.

Extended Abstract of the 4th International Conference on Mathematical Applications in Engineering (ICMAE2017), 8th—9th August 2017

Mechanism of the Free Charge Carrier Generation in the Dielectric Breakdown

N A A Rahim[1], R Ranom[2], and H Zainuddin[3]

[1,2,3]Department of Electrical Engineering, Universiti Teknikal Malaysia Melaka
76100 UTeM Durian Tunggal, Melaka Bandaraya Bersejarah, MALAYSIA.

[1]m*011520012@student utem.edu.my*, [2]rahifa@utem.edu.my, [3]hidayat@utem.edu.my

Abstract. The long-life performance of an insulator is depended on the result of continuous stresses like electrical, environmental, mechanical and thermal. Thereby, many studies that were conducted to investigate the effect of this stress on the insulator and their solution to prevent the insulator from degradation and breakdown. However, study on the physical process of discharge phenomenon that lead to the conductive path and breakdown on the insulator surface is not well concerned and understood. Therefore, this paper was focuses on the charge carrier generation and transport mechanism that causing the electric discharge and breakdown of the dielectric in the high voltage application system. This charge carrier generation and transport mechanism are accounted with the Nernst Planck theory to model the behavior of the charge carriers while Poisson's equation is used to determine the distribution of electric field on the insulator. A mathematical model of a surface discharge on an insulator based on the Nernst Planck Theory is then discussed.

Introduction. The insulation is the most important part in the high voltage application to resist some stresses like mechanical, thermal, electrical and environmental stress that acts permanently or temporary on the insulators [1]. Thus, precaution action must be taken to reduce the failure factor of insulation by the presence of the stresses. The good insulator must be able to avoid the flow of current to the undesired path.

The outdoor insulators are often exposed to the pollution especially in the polluted area. This condition does not affect the performance of the insulator until the surface of the insulator become moist due to the dew, rain or fog [2]. Due to the surface discharge activities, a conducting path due to the drying out process will be formed on the surface of the insulator and it will allow the flow of leakage current from the high voltage electrode to the ground electrode [3]. Although the leakage current flow is quite small, the long term of leakage current flow due to the discharge may lead to the insulator breakdown. Thus, study on the physical discharge activities on the insulator are quite important to decrease the system failure.

To understand the propagation of the surface discharge on the insulator, the mechanism for the charge carrier generation and transportation must be known. There are several types of mechanisms for the charge carrier generation and transportation that can lead to the breakdown of the insulators. Apart of the mechanism that involve in the charge carrier generation are the impact ionization [4], field emission [5], secondary electron emission [6], ionic dissociation [7] and molecular ionization [8]. Besides that, recombination of free charge carriers like electrons, positive ions, and negative ions with each other and the surrounding

media also can give the contribution in the charge carrier generation of the insulation. In addition to the recombination of the free charge, electrons also combine with neutral molecules to form negative ion in the process of electron attachment [5].

For the transportation mechanism of the charge carrier, charge transport continuity equation accounted the Nernst Planck theory can be used to understand the charge carrier behavior on the insulator [9] and this equation will be coupled with Poisson's equation for the field distribution equation. Therefore, study on the mechanisms that can lead to the breakdown of the insulators are very important to prevent some failure in the high voltage system. Thus, this paper is focuses on the charge generation and transportation mechanism for the dielectric breakdown in the high voltage application system.

Governing Equation. The charge continuity equation accounted the Nernst Planck theory was used to model the behavior of the charge carriers like positive ions, negative ions and electrons in the insulator system. The Nernst-Planck theory has been used to model the ion transport in many physical and biological system such as protein channel of biological membranes [10], neuron cell membranes [11], and electrolytic solutions [12]. Generally, the charge continuity equation can be written as:

$$\frac{\partial N_i}{\partial t} + \nabla . J_i = G_i - R_i \tag{1}$$

where i indicate the species of the charge; positive ion, negative ion and electron in the dielectric system. $J_i\ [mol.m^{-2}.s^{-1}]$ is a total flux density for species i at distance $x\ [m]$ between the electrode, $N_i\ [mol.m^{-3}]$ is the concentration of each charge carrier, $G_i [mol.m^{-3}.s^{-1}]$ is the generation rate and $R_i [mol.m^{-3}.s^{-1}]$ is the recombination rate of the ions species.

The charge transport mechanism continuity equations are coupled with Poisson's equation to determine the electric field distribution. The equation of Poisson's equation can be expressed as follows:

$$\nabla.\left(-\varepsilon_0 \varepsilon_r \vec{E}\right) = \left(N_p - N_n - N_e\right) q N_A \quad where\ \vec{E} = -\nabla V \tag{2}$$

where $\vec{E}\ [V.m^{-1}]$ is the electric field vector, $\varepsilon_0\ [F.m^{-1}]$ is permittivity of free space charge, ε_r is relative permittivity of material, $N_p, N_n, and\ N_e$ are the concentration of each charge carrier determined from the charge continuity equations (1), $q\ [C]$ is the elementary charge and $N_A\ [mol^{-1}]$ is the Avogadro's number.

Findings. Thus, electric field dependent molecular ionization will be chosen in the modelling of surface discharge on the outdoor insulator. This is due to the surface discharge activities that occurred through the insulator surface when there is a flow of contaminant electrolyte. This phenomenon will lead to the flow of leakage current and propagation of electric field on the insulator surface. For the development of surface discharge modelling, charge transport continuity equation accounted the Nernst Planck theory and coupled with Poisson's equation were used to model the behavior of the charge carriers and to determine the electric field distribution. For the equation of total flux density, only diffusion and migration term will be considered. This is because in the surface discharge development there are involved the influence of high electric field and there are been expected that it will included the diffusion of charge carrier from high concentration to the low concentration in the electrolyte. Thus, the diffusion and migration term will be taken as a dominant role and the convection term will be neglected in the surface discharge formation.

Summary

It can be concluded that the study on the mechanism of the charge carrier generation in the dielectric system is important to prevent the system failure and losses. This paper is focuses the charge carrier generation and transport mechanism that causing the electric discharge and lead to the breakdown of the dielectric in the high voltage application system. From the previous studies, it has been known that there are several types of mechanism of charge carrier generation and transportation in the dielectric. In the case of development of surface discharge on the outdoor insulator, electric field dependent molecular ionization will be chosen as the charge generation mechanism. The charge transport continuity equation will involve the diffusion-migration equation that accounted the Nernst Planck theory and coupled with Poisson's equation for determine the electric field distribution. In the modelling of surface discharge on the insulator surface, the correct parameters of each elements that involved must be known and the mathematical equation can be solved by using finite difference method.

References

[1] C. Rusu-Zagar, P. V. Notingher, and C. Stancu, "Ageing and Degradation of Electrical Machines Insulation," *J. Int. Sci. Publ. Mater. Methods Technol.*, vol. 8, pp. 526–546, 2007.

[2] Y. Li, H. Yang, Q. Zhang, X. Yang, X. Yu, and J. Zhou, "Pollution flashover calculation model based on characteristics of AC partial arc on top and bottom wet-polluted dielectric surfaces," *IEEE Trans. Dielectr. Electr. Insul.*, vol. 21, no. 4, pp. 1735–1746, 2014.

[3] A. Syakur, H. Berahim, Tumiran, and Rochmadi, "Hydrophobic Contact Angle and Surface Degradation of Epoxy Resin Compound with Silicon Rubber and Silica," *Electr. Electron. Eng.*, vol. 2, no. 5, pp. 284–291, 2012.

[4] P. Solomon and N. Klein, "Impact Ionization in Silicon Dioxide at Fields in the Breakdown Range," *Solid State Commun.*, vol. 17, pp. 1397–1400, 1975.

[5] F. M. O. Sullivan, "A Model for the Initiation and Propagation of Electrical Streamers in Transformer Oil and Transformer Oil Based Nanofluids by," 2007.

[6] E. M. J. Niessen, "Numerical simulation of secondary electron emission charging at insulator surfaces," *Int. Symp. Discharges Electr. Insul. Vacuum-Eindhove*, no. 18, pp. 162–165, 1998.

[7] L. Onsager, "Deviations from Ohm's Law in Weak Electrolytes," *J. Chem. Phys.*, vol. 2, pp. 599–615.

[8] C. Zener, "A Theory of the Electrical Breakdown of Solid Dielectrics," *Proc. R. Soc.*, vol. Volume 109, no. Society, The Royal Society, Royal Sciences, Physical, pp. 523–529, 1926.

[9] H. Zainuddin and P.L. Lewin, "Modeling of Degradation Mechanism at the Oil-Pressboard Interface due to Surface Discharge," *COMSOL Confference*, pp. 1–22, 2015.

[10] A. Singer, "A poisson-nernst-planck model for biological ion channels — an asymptotic analysis in a 3-d narrow funnel," pp. 27–29.

[11] P. M. Nanninga, "A computational neuron model based on Poisson – Nernst – Planck theory," *ANZIAM J. 50*, vol. 50, pp. 46–59, 2008.

[12] E. Samson and J. Marchand, "Numerical Solution of the Extended Nernst-Planck Model," *J. Colloid Interface Sci.*, vol. 8, pp. 1–8, 1999.

Extended Abstract of the 4th International Conference on Mathematical Applications in Engineering (ICMAE2017), 8-9th August 2017

Numerical Computation of Underground Thermal Performance for Malaysian Climate

Azfarizal Mukhtar[1], Mohd Zamri Yusoff[2], and Ng Khai Ching[3]

(azfarizal.mukhtar@gmail.com)
Center for Fluid Dynamics, College of Engineering,
Universiti Tenaga Nasional (UNITEN)
Jalan IKRAM-UNITEN 43000 Kajang
Selangor

[1] azfarizal.mukhtar@gmail.com, [2] Zamri@uniten.edu.my, [3] nkching@uniten.edu.my

Abstract. In this study, the soil temperature profile was computed in MATLAB based on the harmonic heat transfer equations at various depths. The meteorological data ranging from January, 1st 2016 to December, 31st 2016 measured by local weather stations were employed. The findings indicted that as the soil depth increases, the temperature changes are negligible and the soil temperature is nearly equal to the mean annual air temperature. Likewise, the results have been compared with those reported by other researchers. Overall, the predicted soil temperature can be readily adopted in various engineering applications in Malaysia.

***Keywords*.** Passive energy, Mathematical model, Hot and humid climate, Soil temperature.

Introduction. Soil is not a good insulator for underground structure: the resistance of heat flow of dry earth is less than 15% of that of moisture and decreases rapidly when the moisture content increases. However, the soil is a terrific moderator for temperature fluctuations [1] in which it does not responds to daily temperature variations and only reacts gradually to seasonal changes. Due to the high thermal inertia (51% of the energy from the sun absorbed by the soil as shown in Fig.1) and the great heat capacity of the soil structure, it allows a damping of surface temperature fluctuations at a rate that varies exponentially with respect to the soil depth [2]. In other words, at a sufficient depth, the soil temperature is lower than the surface air temperature during daytime (the trend is opposite during nigth-time). Therefore, soil temperature is seemingly a key factor in affecting the heat transfer of an underground building and the thermal storage for new sources of renewable energy [3–6]. Therefore, the investigation of soil temperature at different depths is necessary to calculate the heat flux through the building surface. Meanwhile, the soil temperature data can be used for designing underground building in Malaysia.

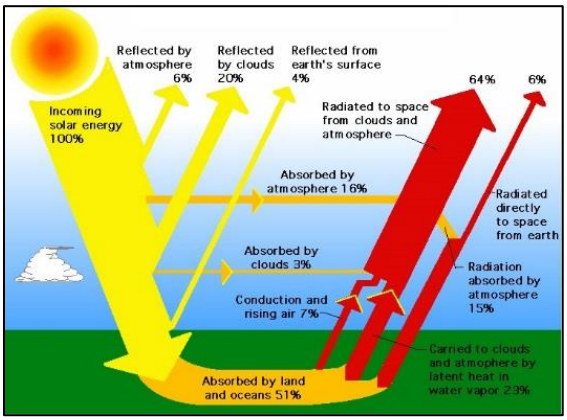

Fig. 1. Earth energy balance

Thus, in response to this need, an equation was established to determine the soil temperature for Malaysian climate. The analysis included the investigations of high and low dry bulb temperatures, average dry bulb temperature, amplitude of surface temperature and mean annual air temperature. In addition, the phase constant (the minimum surface temperature throughout the year) was investigated as well. All analyses were performed by using the climate data provided by the Malaysian Meteorological Department for station 48684. It is worth to mention here that our proposed correlation considered the soil depth of up to 15m. Table 1 shows the monthly average temperature (derived from the hourly temperature).

Table 1: Climate Data for Petaling Jaya.

Month	Jan	Feb	Mar	Apr	May	June	Jul	Aug	Sept	Oct	Nov	Dec	Yearly
Record High Dry Bulb Temp (°C)	35.90	35.70	36.20	36.90	36.20	35.70	35.80	34.80	34.80	34.20	34.10	35.10	36.90
Record Low Dry Bulb Temp (°C)	23.80	25.00	23.70	24.60	23.40	23.40	27.41	23.80	28.01	23.60	23.30	22.50	22.50
Ave Dry Bulb Temp (°C)	29.13	29.19	29.99	30.13	29.23	28.96	28.59	29.51	28.84	28.70	27.51	27.67	28.95
Amplitude of Surface Temp (°C)	5.99	6.18	5.82	7.20	6.39	7.49	7.92	4.92	6.56	6.10	5.64	7.50	6.48

Mathematical Description. The soil temperature can be affected by variables such as topography, meteorology and sub-surface. Basically, the energies from meteorology elements such as solar, atmospheric agents and air are continuously transmitted to the soil surface (see Fig. 1). Solar energy is the most dominant factor. In addition, daily and seasonal changes in solar energy will inflict a cyclical variation in air and soil temperatures. Other factors such as wind and rain could cause local variations as well. The typical annual temperature variation at the surface (or close to the soil surface) follows the pattern of simple harmonic equation. This harmonic equation can be modelled based on the Kasuda model [7], where the soil temperature is a function of time (day), soil depth and air temperature:

$$T\,(z,t) = T_{mean} - \left[\left(T_{amp} e^{-z\left(\frac{\pi}{365\alpha}\right)^{1/2}}\right)\cos\left\{\left(\frac{2\pi}{365}\right)\left(\left(t - t_0\right) - \left(\frac{z}{2}\right)\left(\frac{365}{2\alpha}\right)^{1/2}\right)\right\}\right] \quad (1)$$

Here, $T\,(z,t)$ is the undisturbed soil temperature at time t(day) and depth z(m), T_{mean} is the mean surface temperature, T_{amp} is the amplitude of surface temperature, α is the thermal diffusivity of the soil (m^2/day) and t_0 is the day of the year with minimum surface temperature. T_{mean}, T_{amp} and t_0 can be determined from the meteorology data. However, α should be determined based on the physical soil characteristic such as soil type and moisture content. From Table 1, the lowest and highest temperatures are 22.50°C and 36.90°C, respectively. The temperature amplitude is 6.48°C and t_0 is taken from the basis of daily average temperature as shown in Fig. 2. Meanwhile, the mean annual air temperature is 28.95°C. The thermal diffusivity, α is 0.06 m^2/day with R^2 value of 0.9999 [4]. Substituting the above-mentioned values into Eq. (1), the soil temperature can be predicted as:

$$T\,(z,t) = 28.95 - 6.48\, e^{\left(-z \times \left[\frac{\pi}{366\alpha}\right]^{0.5}\right)}\, cos\left[\frac{2\pi}{366}\,(t - 169) - z \times \left[\frac{\pi}{366\alpha}\right]^{0.5}\right] \quad (2)$$

The soil temperature, which is generated from MATLAB software, is applicable up to soil depth of 15m. The results are shown in Fig. 3.

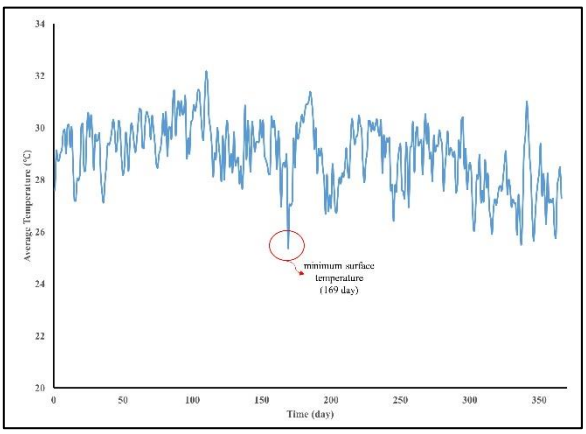

Fig. 2: Daily average temperature of 2016

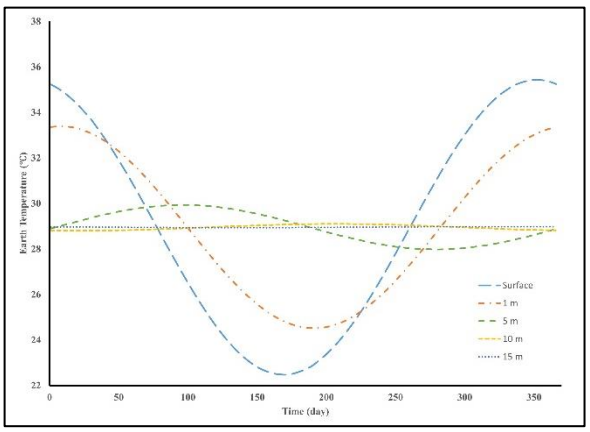

Fig. 3: Soil temperature distribution at various depths throughout the year

Results. As Fig. 3 shows the time history of temperature distribution for various depths calculated from Eq. (2). With the increasing the depth, the temperature changes are negligible as the temperature is almost constant starting at 10 m depth and so on, which is nearly equal to the mean annual air temperature, 28.95℃. These findings are consistent with those reported by previous researchers [4,5].

Summary. In this study, the soil temperature has been determined from the Malaysia meteorology data. An empirical equation has been proposed. At a depth of 10 m and beyond, the soil temperature is constant which is equal to the mean annual air temperature. The present results can then be used to calculate the heat flux through the underground building structure in Malaysia. Subsequently, the thermal performance in an underground building can then be determined accurately.

References

[1] Anselm AJ. Earth Shelters; A Review of Energy Conservation Properties in Earth Sheltered Housing. 2012.

[2] Porras-amores C, Mazarron FR, Cid-falceto J, Cañas I. Energy efficient underground construction: natural ventilation during hot periods. Int. Conf. Pet. Sustain. Dev. IACSIT Press, vol. 26, 2011, p. 32–6.

[3] Márquez JMA, Bohórquez MÁM, Melgar SG. Ground Thermal Diffusivity Calculation by Direct Soil Temperature Measurement. Application to very Low Enthalpy Geothermal Energy Systems. Sensors 2016;16.

[4] Yusof TM, Anuar S, Ibrahim H. Numerical Investigation of Ground Cooling Potential for Malaysian Climate. Int J Automot Mech Eng 2014;10:2081–90.

[5] Hazbei M, Nematollahi O, Behnia M, Adib Z. Reduction of Energy Consumption using Passive Architecture in Hot and Humid Climates. Tunn Undergr Sp Technol 2015;47:16–27.

[6] Moradi H, Eskandari H. An experimental and numerical investigation of Shovadan heating and cooling operation. Renew Energy 2012;48:364–8.

[7] Kusuda T, Achenbach PR. Earth Temperatures and Thermal Diffusivity at Selected Stations in the United States. ASHRAE Trans 1965:61–74.

Extended Abstract of the 4th International Conference on Mathematical Applications in Engineering (ICMAE2017), 8-9th August 2017

A Response Surface Methodology for Mitigating Hot Gasses in Enclosed Car Park

Ahmad Faiz Tharima[1], Mohd Zamri Yusoff[2], Md Mujibur Rahman[3]

College of Engineering, Universiti Tenaga Nasional (UNITEN), Putrajaya Campus, Jalan IKRAM-UNITEN, 43000 Kajang, Selangor, Malaysia.

[1]pait.afz@gmail.com, [2]Zamri@uniten.edu.my,[3]Mujibur@uniten.edu.my

Abstract. A hot gas rise towards ceiling due to buoyancy by fire will cause severe damage to the building structure. The temperature rises need to be controlled as among the element of compliance in performance-based design. The channel flow between beams has used in this study to mitigate hot gases out of the enclosure by mean of response surface methodology. Fire Dynamic Simulator was employed as a simulation tool while the result was statistically examined using analysis of variance via Minitab application. It was found that the result was linear with predicted R^2 (93.25%) and within the permissible R^2 (98.13%). The ceiling height has been identified not affect in controlling hot gases while four control parameters which are beam spacing, transversal beam, extraction rate and longitudinal beam with p-values of 0.00, 0.000, 0.023 and 0.000 respectively, have been found to have the significant effect on the smoke temperature control. In providing design of enclosed car park with better condition, the engineers afterward could only have considered the high significant factors mentioned above in their design as compared to others factors studied in previous study.

Introduction. The temperatures rise need to be controlled as among the elements of compliance in performance-based design as well as in perceptive code. A hot gas rise towards ceiling due to fire buoyancy will reduce oxygen concentration eventually create harmful to an occupants [1] and cause severe damage to the building structure such as enclosed car park [2], subway station [3] corridor -like structures [4], tunnel-like corridor [5] and underground shelter [6] as well as others building.

The fire temperatures measurement is essential to predict ignition of the object, the onset of flashover and structure damage [7]. Apart of that, it is also beneficial for predict smoke layer descent towards the floor [8] and arranges for a smoke detection [9–11] as well as sprinkler activation [12]. Following that, previous researchers had developed various ratio from experimental and numerical simulation such as beam depth to the ceiling height [13–15], radial distance to the ceiling height [16], beam spacing to ceiling clearance [15].

However, according to the literature [11–15], most studies were conducted by means of trial and error based. These arrangements have not yet statistically proofed and which parameters show the significant effect of the temperature. In addition, the parameters that were investigated such as heat release rate (HRR) and the wind were categorized as non-control factors. Indeed, a few research papers related to the hot smoke control with the presence of the beam has been reported by [13–15,19,22–27] but still lacking regarding cost operational reducing (i.e in term of horizontal ventilation numbers and volume flow rate). Therefore, this

study aims to channel the hot gasses by means statistical analysis based on established control parameters and resulting in the optimum operational cost of the ventilation fan.

Method. The research work was planned to be carried out as similar to ref [29]:

(a) determine the important controllable factors
(b) determine the Design of Experiment (DOE)
(c) perform computational fluid dynamics (CFD) simulation
(d) conduct reliability test of DOE
(e) conduct statistical analysis with polynomial regression model and analysis of variance (ANOVA)

Mathematical Model. The form of mathematical model is as follows:

$$y = \propto_0 + \sum_{i=1}^{3} \propto_i x_i + \sum_{i=1}^{3} \propto_{ii} x_i^2 + \sum_{i=1}^{2} \sum_{j=i+1}^{3} \propto_{ij} x_i x_j \qquad (1)$$

Where y is the predicted response (hot gases temperature); x_i and x_j are the uncoded independent variables and $\propto_0, \propto_i, \propto_{ii}$ *and* $\propto_{ij}$ are intercept, linear, quadratic and interaction constant coefficient respectively.

Results

Polynomial regression model. The relationship between temperature and five controllable factors (namely ceiling height X, beam span length X_1, transversal beam depth X_2, longitudinal beam depth X_3 and extraction rate X_4) was studied. The simulation result based on CCD model has developed a full quadratic equation as follows:

$$y = 360.9 - 265X - 365.0X_1 - 8401X_2 + 81.7X_3 + 8032X_4 + 31285X_2^2 + 710XX_1 + 9598XX_2 - 11194XX_4 + 2436X_1X_2 - 3584X_1X_4 - 16229X_2X_4 \qquad (2)$$

Based on statistical analysis, the result was linear with predicted R^2 (93.25%) and within the permissible R^2 (98.13%). It was found that the result was linear and good agreement can be seen between actual and predicted values.

Analysis of variance (ANOVA)

Table 1 shows the linear, interaction and quadratic variables for the coded coefficient. In ANOVA analysis, the terms that found statistically significant only will be included in the model. Each variable with P-value less than 0.01 is considered highly significant, and between 0.01 and 0.05 is significant. The variable with P-value more than 0.05 is considered non-significant [30]. In the present work, it is observed that most of the variables have a highly significant on the linear effect, interaction and second order form. Only the ceiling height term in the linear effect was not significant. This illustrates the importance of employing the significant variables in design lower temperature in the enclosed car park.

Table 1. Coded Coefficients for Transformed Response

Coded Factor	Effect	Coef	SE Coef	T-Value	P-Value	Degree of Importance
X	-8.01	-4.00	2.15	-1.87	0.078	Non- significant
X_1	-57.17	-28.59	2.15	-13.32	0.000	High significant
X_2	-81.63	-40.81	2.15	-19.01	0.000	High significant

X_3	10.62	5.31	2.15	2.47	0.023	significant
X_4	70.58	35.29	2.15	16.44	0.000	High significant
X_2^2	25.03	12.51	3.25	3.86	0.001	Significant
XX_1	18.00	9.00	2.28	3.95	0.001	High significant
XX_2	27.26	13.63	2.28	5.99	0.000	High significant
XX_4	-32.58	-16.29	2.28	-7.16	0.000	High significant
X_1X_2	17.40	8.70	2.28	3.82	0.001	High significant
X_1X_4	-28.20	-14.10	2.28	-6.19	0.000	High significant
X_2X_4	-13.31	-6.65	2.28	- 2.92	0.009	High significant

Finally, based on P-value discussed above and significant effect, one term could be removed, and the model was summarized as the following equation with little error.

$$y = 360.9 - 365.0X_1 - 8401X_2 + 81.7X_3 + 8032X_4 + 31285X_2^2 + 710XX_1 + 9598XX_2 - 11194XX_4 + 2436X_1X_2 - 3584X_1X_4 - 16229X_2X_4 \quad (3)$$

Conclusion. In this research, the influence hot gasses temperature is investigated with identified factors such as ceiling height, beam span length, transversal and longitudinal beam depth, as well as extraction rate via Response Surface Methodology (RSM), integrated with Fire Dynamic Simulator (FDS). In this model, as for reliability test result, RSM can be used to investigate the controllable probability factors that influenced the response. In accordance to that, four factors have confirmed effecting temperature in enclosed car park. With only important parameters included in this study, it is considered novelty in yielding lower temperature for the overall of car park geometry. The engineers afterward could only have considered the high significant factors mentioned above in their design as compared to others factors studied in previous study.

References

[1] X.G. Zhang, Y.C. Guo, C.K. Chan, W.Y. Lin, Numerical simulations on fire spread and smoke movement in an underground car park, Build. Environ. 42 (2007) 3466–3475. doi:10.1016/j.buildenv.2006.11.002.

[2] M. Zahirasri, Multiple Vehicle Design Fire Scenarios in Car Parking Buildings by, (2015).

[3] N. Meng, L. Hu, S. Zhu, L. Yang, Effect of smoke screen height on smoke flow temperature profile beneath platform ceiling of subway station: An experimental investigation and scaling correlation, Tunn. Undergr. Sp. Technol. 43 (2014) 204–212. doi:10.1016/j.tust.2014.05.008.

[4] J. Ji, Y.Y. Fu, C.G. Fan, Z.H. Gao, K.Y. Li, An experimental investigation on thermal characteristics of sidewall fires in corridor-like structures with varying width, Int. J. Heat Mass Transf. 84 (2015) 562–570. doi:10.1016/j.ijheatmasstransfer.2015.01.020.

[5] T. Beji, S. Ukleja, J. Zhang., M.A. Delichatsios, Fire behaviour and external flames in corridor and tunnel-like enclosures, FIRE Mater. (2012). doi:10.1002/fam.

[6] A. Mukhtar, N.K. Ching, M.Z. Yusoff, Optimal Design of Opening Ventilation Shaft by Kriging Metamodel Assisted Multi-objective Genetic Algorithm, 7 (2017). doi:10.7763/IJMO.2017.V7.565.

[7] W.D.W. and P.H. Thomas, Estimating Temperatures in Compartment Fires, in: SFPE Handb. Fire Prot. Eng., 2nd ed., 1995.

[8] E.K. Budnick, D.D. Evans, H.E. Nelson, Simplified Fire Growth Calculations, in: Fire Prot. Handb.,

19th ed., 2003.

[9] M. He, Y. Jiang, J. Vythoulkas, T. AI-Farra, Smoke Detector Performance FOr Level Ceiling With Deep Beams and Deep Beam Pocket Configuration, Igarss 2014. (2014) 1–5. doi:10.1007/s13398-014-0173-7.2.

[10] F. J, R. S, G. D, Evaluating Smoke Detector Spacing Requirements for Parallel Beamed Hallways and Sloped Ceilings, Igarss 2014. (2014) 1–5. doi:10.1007/s13398-014-0173-7.2.

[11] F. G.P, D. W.D, K. J.H, Simulating the Effect of Beamed Ceilings on Smoke Flow , Part I . Comparison of Numerical and Experimental Results, (1992).

[12] R. Vettori, Effect of a Beamed, Sloped, and Sloped Beamed Ceilings on the Activation Time of a Residential Sprinkler, (2003).

[13] C.C. Koslowski, V. Motevalli, Effect of Beams on Ceiling Jet Behavior and Heat Detector Operation, J. Fire Prot. Eng. 5 (1993) 97–111. doi:10.1177/104239159300500302.

[14] C. Koslowski, V. Motevalli, Behavior of a 2-Dimensional Ceiling Jet Flow : A Beamed Ceiling Configuration, (1994) 469–480.

[15] Delichatsios, The Flow of Fire Gases Under a Beamed Ceiling, 10 (1981).

[16] N. Johansson, J. Wahlqvist, P. Van Hees, Numerical experiments in fire science : a study of ceiling jets, (2014). doi:10.1002/fam.

[17] N. Johansson, Numerical experiments and compartment fires, Fire Sci. Rev. 3 (2014) 2. doi:10.1186/s40038-014-0002-2.

[18] X. Deckers, S. Haga, N. Tilley, B. Merci, Smoke control in case of fire in a large car park: CFD simulations of full-scale configurations, Fire Saf. J. 57 (2013) 22–34. doi:10.1016/j.firesaf.2012.02.005.

[19] X. Deckers, S. Haga, B. Sette, B. Merci, Smoke control in case of fire in a large car park : Full-scale experiments, Fire Saf. J. 57 (2013) 11–21. doi:10.1016/j.firesaf.2012.10.017.

[20] C.-H. Hwang, a. Lock, M. Bundy, E. Johnsson, Studies on Fire Characteristics in Over- and Underventilated Full-scale Compartments, J. Fire Sci. 28 (2010) 459–486. doi:10.1177/0734904110363106.

[21] L.H. Hu, L.F. Chen, W. Tang, A global model on temperature profile of buoyant ceiling gas flow in a channel with combining mass and heat loss due to ceiling extraction and longitudinal forced air flow, Int. J. Heat Mass Transf. 79 (2014) 885–892. doi:10.1016/j.ijheatmasstransfer.2014.08.045.

[22] Deckers, Haga, Tilley, Merci, Smoke control in case of fire in a large car park: CFD simulations of full-scale configurations, Fire Saf. J. 57 (2013) 22–34. doi:10.1016/j.firesaf.2012.02.005.

[23] M. Deckers, Haga, Tilley, Smoke control in case of fire in a large car park: Full-scale experiments, Fire Saf. J. 57 (2013) 22–34. doi:10.1016/j.firesaf.2012.02.005.

[24] V. Motevalli, Z.P. Yuan, Steady State Ceiling Jet Behavior under an Unconfined Ceiling with Beams, Fire Technol. 44 (2008) 97–112. doi:10.1007/s10694-007-0027-3.

[25] Hinkley, Smoke & Heat Venting, in: SFPE Handb. Fire Prot. Eng., 2nd ed., 1995.

[26] J.H. Klote, J.A. Milke, Principles of smoke management, in: Princ. Smoke Manag., 2002.

[27] J.H. Klote, The ASHRAE design manual for smoke control, Fire Saf. J. 7 (1984) 93–98. doi:10.1016/0379-7112(84)90012-2.

[28] F.D. Simulations, Guide Guide for the Verification and Validation of Computational Fluid Dynamics

Simulations, 1998 (2002).

[29] A. Mukhtar, N. Khai Ching, M. Zamri Yusoff, Optimal Design of Opening Ventilation Shaft by Kriging Metamodel Assisted Multi-objective Genetic Algorithm, Int. J. Model. Optim. 7 (2017) 92–97. doi:10.7763/IJMO.2017.V7.565.

[30] A.M. Doust, M. Rahimi, M. Feyzi, An Optimization Study by Response Surface Methodology (RSM) on Viscosity Reduction of Residue Fuel Oil Exposed Ultrasonic Waves and Solvent Injection, Iran. J. Chem. Eng. 13 (2016) 3–19.

Extended Abstract of the 4th International Conference on Mathematical Applications in Engineering (ICMAE2017), 08—09th August 2017

Simulations of dark solitons in discrete binary media with cubic-quintic nonlinearity

Lukhman Abdul Taib[1], Muhammad Salihi Abdul Hadi[2], and Bakhram A. Umarov[3]

[1]Department of Computational and Theoretical Sciences, Faculty of Science, International Islamic University Malaysia, 25200 Kuantan, Pahang Darul Makmur, MALAYSIA.

[2]Department of Computational and Theoretical Sciences, Faculty of Science, International Islamic University Malaysia.

[3]Department of Physics, Faculty of Science, International Islamic University Malaysia.

[1]*lukhman.taib@gmail.com*, [2]*salihi@iium.edu.my*, [3]*bakhram@iium.edu.my*

Introduction. The study of localized modes in discrete system has been a central attention for nearly three decades, due to its significance in different branches of science. In most of the studies, the evolution of localized modes is frequently described by the discrete nonlinear Schrödinger equation (DNLSE). Perhaps the study of DNLSE is initiated first by experimental exploration in fabricated AlGaAs waveguide arrays reported in [1], followed by the mathematical model in [2].

Strongly localized vectorial bright and dark modes (SLM's), where the modes constituted by two different excitations interacted at particular lattice site or component with different frequencies, copropagate in cubic nonlinear waveguide have been shown to exist [3, 4]. In [4], it has been demonstrated that the existence of dark soliton requires modulational stability of the background. However, the existence of strongly localized dark states in the presence of cubic and quintic nonlinearity have not been explored. Motivated by the result of modulational instability in binary discrete media with cubic-quintic (CQ) nonlinearity reported in [5], this paper aim to present the existence of dark SLM's.

The Mathematical Model. Binary discrete media with cubic-quintic nonlinearity is represented by two-component CQDNLSE:

$$\begin{aligned} i\frac{dA_n}{dz} &= -c_a\left(A_{n+1}+A_{n-1}\right)-\lambda\left(\left|A_n\right|^2+\beta\left|B_n\right|^2\right)A_n-\gamma\left(\left|A_n\right|^4+2\alpha\left|A_n\right|^2\left|B_n\right|^2+\alpha\left|B_n\right|^4\right)A_n, \\ i\frac{dB_n}{dz} &= -c_b\left(B_{n+1}+B_{n-1}\right)-\lambda\left(\left|B_n\right|^2+\beta\left|A_n\right|^2\right)B_n-\gamma\left(\left|B_n\right|^4+2\alpha\left|B_n\right|^2\left|A_n\right|^2+\alpha\left|A_n\right|^4\right)B_n, \end{aligned} \tag{1}$$

where $A_n(z), B_n(z)$ are complex-valued wave functions at lattice site n; z denotes propagation coordination in nonlinear waveguide arrays or time in Bose-Einstein condensates; c_a, c_b denote the coupling constants between two adjacent sites; λ, γ are the cubic and quintic nonlinear term respectively; and β, α are the cubic and quintic cross-phase modulation coefficients. Here, the cubic and quintic self-phase modulation coefficients are rescaled to one.

The Existence and Stability of Dark SLM's. The existence of dark SLM's can be verified by setting the ansätze $A_n = \alpha_n \exp(ik_a z)$ and $B_n = \beta_n \exp(ik_b z)$, then substituting them into Eqs. (1) to obtain the stationary equations

$$\begin{aligned} -k_a\alpha_n + c_a\left(\alpha_{n+1}+\alpha_{n-1}\right) + \lambda\left(\alpha_n^2+\beta\beta_n^2\right)\alpha_n + \gamma\left(\alpha_n^4+2\alpha\alpha_n^2\beta_n^2+\alpha\beta_n^4\right)\alpha_n = 0, \\ -k_b\beta_n + c_b\left(\beta_{n+1}+\beta_{n-1}\right) + \lambda\left(\beta_n^2+\beta\alpha_n^2\right)\beta_n + \gamma\left(\beta_n^4+2\alpha\beta_n^2\alpha_n^2+\alpha\alpha_n^4\right)\beta_n = 0. \end{aligned} \tag{2}$$

Numerical stability analysis was performed by linearization using the ansätze

$$A_n = \left[\alpha_n + \delta\left(c_n e^{-i\omega z} + d_n e^{i\omega^* z}\right)\right]e^{ik_a z}, \quad B_n = \left[\beta_n + \delta\left(f_n e^{-i\omega z} + g_n e^{i\omega^* z}\right)\right]e^{ik_b z},$$

where the ω's are the linearization eigenvalues and $\delta \ll 1$. Again, substituting the ansätze into Eqs. (1) yields the (linearization) eigenvalue problem at $O(\delta)$:

$$\omega\begin{pmatrix} c_n \\ d_n^* \\ f_n \\ g_n^* \end{pmatrix} = \begin{pmatrix} \frac{\partial F_{a,i}}{\partial A_j} & \frac{\partial F_{a,i}}{\partial A_j^*} & \frac{\partial F_{a,i}}{\partial B_j} & \frac{\partial F_{a,i}}{\partial B_j^*} \\ -\frac{\partial F_{a,i}^*}{\partial A_j} & -\frac{\partial F_{a,i}^*}{\partial A_j^*} & -\frac{\partial F_{a,i}^*}{\partial B_j} & -\frac{\partial F_{a,i}^*}{\partial B_j^*} \\ \frac{\partial F_{b,i}}{\partial A_j} & \frac{\partial F_{b,i}}{\partial A_j^*} & \frac{\partial F_{b,i}}{\partial B_j} & \frac{\partial F_{b,i}}{\partial B_j^*} \\ -\frac{\partial F_{b,i}^*}{\partial A_j} & -\frac{\partial F_{b,i}^*}{\partial A_j^*} & -\frac{\partial F_{b,i}^*}{\partial B_j} & -\frac{\partial F_{b,i}^*}{\partial B_j^*} \end{pmatrix}\begin{pmatrix} c_n \\ d_n^* \\ f_n \\ g_n^* \end{pmatrix}$$

Where

$$\begin{aligned} F_{a,i} &= -k_a\alpha_i + c_a\left(\alpha_{i+1}+\alpha_{i-1}\right) + \lambda\left(\alpha_i^3+\beta\beta_i^2\alpha_i\right) + \gamma\left(\alpha_i^5+2\alpha\alpha_i^3\beta_i^2+\alpha\beta_i^4\alpha_i\right), \\ F_{b,i} &= -k_b\beta_i + c_b\left(\beta_{i+1}+\beta_{i-1}\right) + \lambda\left(\beta_i^3+\beta\alpha_i^2\beta_i\right) + \gamma\left(\beta_i^5+2\alpha\beta_i^3\alpha_i^2+\alpha\alpha_i^4\beta_i\right). \end{aligned}$$

Topologies of dark SLM's considered in this paper are the odd and even kink-like modes (Fig. 1).

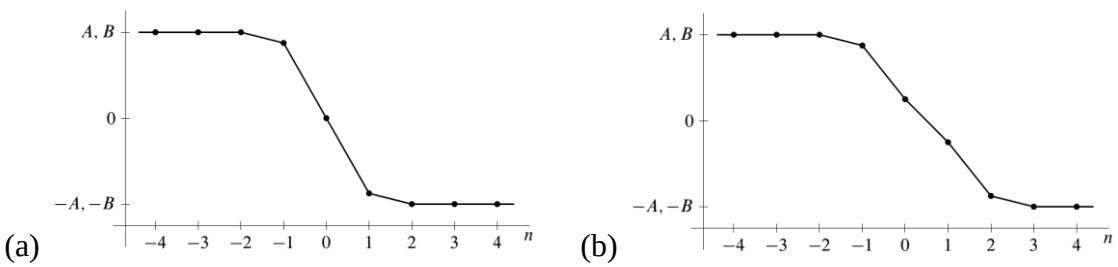

Fig. 1: Schematic representation of different kinds of dark modes. (a) odd kink-like SLM's; (b) even kink-like SLM's.

Summary

In this paper, we have shown the existence of dark SLM's in binary discrete media with cubic-quintic nonlinearity. The stability of the solutions corresponds to the results on modulational stability gains obtained in [5]: for similar amplitudes and equal strength of the inter-component coupling, quintic nonlinearity yields stronger effect than cubic's.

References

[1] H. S. Eisenberg, Y. Silberberg, R. Morandotti, A. R. Boyd and J. S. Aitchison, Phys. Rev. Lett. 81 (1998) 3383.

[2] H. S. Eisenberg, Y. Silberberg, R. Morandotti and J. S. Aitchison, Phys. Rev. Lett. 85 (2000) 1863.

[3] S. Darmanyan, A. Kobyakov, E. Schmidt and F. Lederer, Phys. Rev. E 57 (1998) 3520.

[4] A. Kobyakov, S. Darmanyan, F. Lederer and E. Schmidt, Opt. Quan. Elec. 30 (1988) 795.

[5] B. B. Baizakov, A. Bouketir, A. Messikh and B. A. Umarov, Phys. Rev. E 79 (2009) 046605.

Extended Abstract of the 4th International Conference on Mathematical Applications in Engineering (ICMAE2017), 08—09th August 2017

Artificial Neural Network versus Linear Models Forecasting Doha Stock Market

Adil Yousif[1] and **Faiz A. M. Elfaki**[2]

[1,2]Department of Mathematics, Statistics and Physics, College of Arts and Science, Qatar University, P.O. Box 2713, Doha, Qatar

[1]aeyousif@qu.edu.qa, [2]felfaki@qu.edu.qa

Introduction. Stock markets were created due to the evolution of trade in different fields. In the 13th century emerged the stock market in France when the King of France hired Brokers. During the same time period, traders were meeting in Belgium when "Van der Bürsen" family opened their hotel for traders to Exchange and over time this hotel became a famous symbol of the capital market. As a result, the term "Bürsen" began to be used for the stock market. The stock market is instrumental in measuring the strength or weakness of a country's economy. Moreover, the economic development in countries such as Britain, Denmark and the Netherlands was accompanied by a rise in trading in stock markets. In fact, the largest Exchange in the world is located in New York and is called the" Wall Street".

In Arab countries, in the 18th century, Egyptians took the initiative in setting up a stock market which is one of the oldest stock markets in the world. In gulf region, the oldest stock market was established in Kuwait in 1962. Over the course of the next few decades, other Gulf countries also progressed economically resulting in the establishment of stock markets in countries like the United Arab Emirates, Oman and Qatar.

In the state of Qatar, the stock market was established in 1995 under law no 14. After two years, in 1997, trade started with 17 listed companies and five brokerage firms. Work began with manually managing the trading floor. In August 1998, it shifted to the central registration system. In another two years, the state of Qatar became the first country in the Gulf area to have the linkage through the internet for companies. Then all manual trading systems were cancelled and trading became electronic. In 2002, it established its website on the Internet. Also in this year the Qatar Exchange allowed investors to sell shares on the same day. After one year, the market moved to a new building. By 2005, it allowed non-Qataris to invest in shares with a rate not exceeding 25% of the shares traded in the market. Then in 2006, both of the regular and irregular markets became integrated. In 2007, Qatar Exchange joined the membership of the World Federation of Exchanges (WFE). By 2009, Qatar witnessed a massive transformation into a world-class stock market when it signed a strategic partnership agreement with NYSE Euronext.

The aim of this study was to determine the volatility of Doha Stock Market and develop forecasting models. Linear time series models were used and compared to a nonlinear artificial neural network one namely Multilayer Perceptron Technique. It aims to create models using daily and monthly data collected from Qatar Exchange for the period of January 2007- March 2014. The models generated are for the general index of Qatar Stock Exchange as well as for the several sectors. The study has made use of various time series techniques to

study and analyze the data trend in order to produce appropriate results. Quadratic trend model, double exponential smoothing model and ARIMA were applied.

Neural Network. Accurate prediction of stock market returns is a very challenging task because of the highly nonlinear nature of the financial time series, [1]. It has been widely accepted by many studies that non-linearity exists in the financial markets and that neural networks can be effectively used to uncover this relationship. Unfortunately, many of these studies fail to consider alternative forecasting techniques, the relevance of input variables, or the performance of the models when using different trading strategies, [2]. During the last few years, a number of neural network models and hybrid models have been proposed for obtaining accurate prediction results, in an attempt to outperform the traditional linear and nonlinear approaches.

This paper evaluates the effectiveness of neural network models which are known to be dynamic and effective in stock-market predictions, [3]. Artificial Neural Networks have seen an explosion of interest over the last few years, and are being successfully applied across an extraordinary range of problem domains, in areas as diverse as finance, medicine, engineering, geology and physics. There have been many attempts to formally define neural networks. Artificial Neural Network (ANN) can offer a valid approximation of a vast class of nonlinear process [4]. They also added "the most significant advantage of the ANN models over the classes of linear models is that ANNs are universal approximates that can approximate a large class of functions with high degree of accuracy". [5] stated that ANN models control or are resistant to the limitations of traditional forecasting models, including misspecification, biased outliers and assumption of linearity.

Methodology. Two main methods were used for building a predictive model for the stock market data in the State of Qatar. Three time series models were utilized namely: trend model, Holt's Trend corrected models and Box and Jenkins Autoregressive Moving average (ARIMA) model. On the other hand the Artificial Neural Network, which is one of the none linear techniques was used.

Time Series Techniques. As the time series plot shows an increasing trend several time series models were used. The Quadratic Trend technique was used to investigate the trend of the data, which is given by;

$$Y_t = \beta_0 + \beta_1 t + \beta_2 t^2 \qquad (1)$$

On the other hand the plot shows breakthrough in the level, which indicates parameters are not constant and therefore, Holt's Trend Exponential Smoothing Technique was also used for forecasting.

$$L_t = \alpha \frac{Y_t}{S_{t-s}} + (1-\alpha)(L_{t-1} + b_{t-1}) \qquad (2)$$

Where, $b_t = \beta(L_t + L_{t-1}) + (1-\beta)b_{t-1}$

None-seasonal Autoregressive Moving Average (ARIMA) Technique was also used as a mean linear stochastic model for forecasting.

$$Z_t = \delta + \varphi_1 z_{t-1} + \varphi_2 z_{t-2} + \ldots + \varphi_p z_{t-p} + \alpha - \theta_1 \alpha_{t-1} - \theta_2 \alpha_{t-2} - \ldots - \theta_p \alpha_{t-p} \qquad (3)$$

Artificial Neural Network. The network model used in this study is a single hidden layer feed-forward one with n nodes in the hidden layer and linear neuron activation function given by;

$$y_{t+h} = \alpha_0 + \sum_{j=1}^{n} w_j g\left(\alpha_0 + \sum_{i=1}^{p} w_i \, y_{t+h}\right) + \sum_{i=1}^{p} \beta_i \, y_{t-i} + \varepsilon_{t+h} \qquad (4)$$

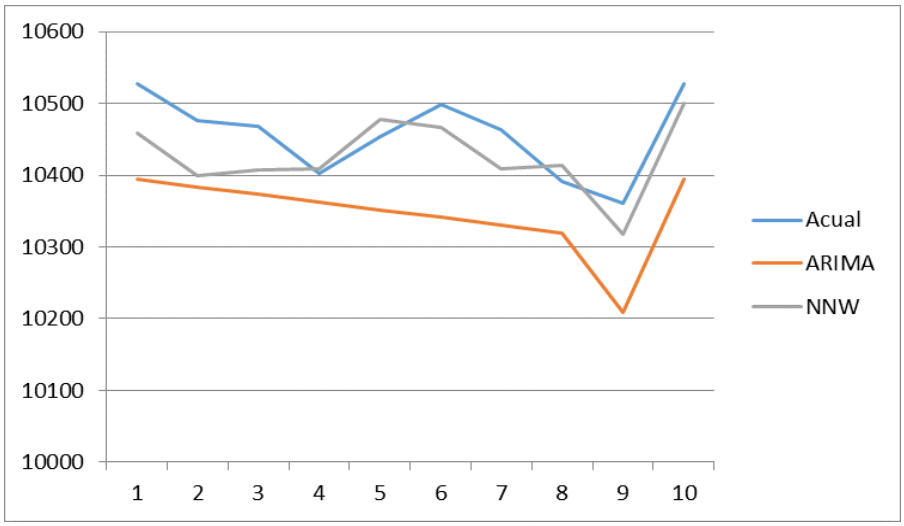

Fig 1: Compare the Acual model with NNW and AEIMA models

Conclusion. Qatar's stock market is a rapidly growing market and this is due to the tremendous economic growth in the country. As more and more companies are joining the stock market, the number of investors increases as well. Therefore, it is essential that the investors have an idea of the futurity of their investments. This can be done by Modeling the data using several techniques.

This study analyzed the general closing index for the Qatar stock market from 1st January 2007 till December 2016. Although the data that was used for modeling was from 2009 till 2016, as there was a drop in the time series and when it was investigated it was found to be due to the world's financial crisis of 2008-2009. When the Artificial Neural Network was applied it gave a better forecasting than the linear time series models as shown in Fig 1.

References

[1] Mingyue Qiu, Yu Song, and F Akage, Application of artificial neural network for the prediction of stock market returns: The case of the Japanese stock market, Elsevier. (2016); 85: 1-7.

[2] David Enke. The use of data mining and neural networks for forecasting stock market returns, Elsevier. (2005); 29 (4): 927-940.

[3] Guresen E., Kayakutlu. G., and Daim. T. U. Using artificial neural network models in stock market index prediction, Journal of Expert Systems with Applications (Elsevier). (2011); 38:10389-10397.

[4] Babikir and Mwambi. A factor -Artificial neural network model for time series forecasting: The case of South Africa, Neural Networks (IJCNN). (2014).

Extended Abstract of the 4th International Conference on Mathematical Applications in Engineering (ICMAE2017), 8-9th August 2017

Finite volume method for a Keller-Segel problem

C Messikh[a], **M. S. H. Chowdhury**[b], A Guesmia and A Berkan[b]

[a]*Department of Science University Badji Mokhtar, Faculty of sciences, Department of mathematics, Bp 12 El Hadjer Annaba, Algeria.*

[b] *Department of Science in Engineering, Faculty of Engineering International Islamic University Malaysia, Jalan Gombak, 53100 Kuala Lumpur, Malaysia. E-mail: sazzadbd@iium.edu.my*

[c]*Universit´e du 20* Aoˆut-*1955- Skikda-Alg´erie, BP 26 Route El Hadaek Skikda (21000) Laboratoire de Math´ematiques Appliqu´ees et d'Histoire et Didactique des Math´ematiques (LAMAHIS)*

Abstract

In this paper, we are interested in the numerical simulation of the mathematical model of Keller-Segel Elliptic-Parabolic problem using finite volume scheme. The finite volume scheme is applied to the elliptic-parabolic model's problem and we have shown under certain assumptions, the existence of a unique and positive approximation solution. Moreover, under adequate regularity assumption of the exact solution, the finite volume scheme is the first order accurate. A good agreement between our numerical simulation and the theoretical results has been obtained.

Introduction:

Chemotaxis is an important means for cellular communication. It is the inuence of chemical substances in the environment on the movement of mobile species. This can lead to strictly oriented movement or to partially oriented and partially tumbling movement. The movement towards a higher concentration of the chemical substance is called positive chemotaxis whereas the movement towards regions of lower chemical concentration is called negative chemotactical movement. The classical chemotaxis model the so-called Keller Segel model system defined in (1) was first introduced by Paltak [9] (1953), E. Keller and L. Segel [7]

$$\begin{aligned} u_t - \nabla\left(a\nabla u\right) + \nabla\left(\chi u \nabla v\right) &= 0 \qquad && (t,x) \in \mathbb{R}^+ \times \mathbb{R}^d \\ \alpha v_t - \Delta v + \tau v + \beta u &= 0 && x \in \mathbb{R}^d \end{aligned} \tag{1}$$

where u(t, x) denotes the density of bacteria in the position $x \in \square^d$ at time t; v the concentration of chemical signal substance, $\alpha \geq 0$ the relaxation time, the parameter X the sensitivity of cells to the chemo attractant and α, τ, β are given smooth functions. As it can be seen, when $\alpha \neq 0$ the model is called Parabolic-Parabolic while it is an Elliptic-Parabolic model when _ = 0. This model is very simple. It exhibits a profound mathematical structure and only dimension 2 is well understood, especially chemotactic collapse. It has been extensively studied in the last few years (see [5, 6, 11, 10]) for a recent survey articles).

Finite volume methods are a class of discretization schemes that have proven highly successful in approximating the solution of a wide variety of conservation law systems. They are extensively used in fluid mechanics, meteorology, electromagnetic, semi-conductor device simulation, models of biological processes and many other engineering areas governed by conservative systems that can be written in an integral control volume form. Numerical simulations for biological Keller-Segel model's problems were investigated in the following references [1, 2, 4].

The aim of this paper is to study of finite volume schemes applied to the elliptic-parabolic model's problem defined as

$$(\mathrm{P})\begin{cases} (\mathrm{P}_1)\begin{cases} u_t - \Delta u + \operatorname{div}(u\nabla v) = 0 & (t,x)\in\mathbb{R}^+\times\Omega \\ u = 0 & \partial\Omega \\ u(0,x) = u_0 & x\in\Omega \end{cases} \\ (\mathrm{P}_2)\begin{cases} -\Delta c + \tau c = 0 & x\in\Omega \\ c = g & \partial\Omega. \end{cases} \end{cases} \tag{2}$$

Finite volume method for a Elliptic-parabolic problem (P):

A finite volume scheme of the problem (P) can be de_ned by the following set of equations:

$$m(K)\frac{u_K^{n+1}-u_K^n}{k} + \sum_{\sigma\in\Xi_K} F_{K,\sigma}^{n+1} - \sum_{\sigma\in\Xi_K} F_{K,\sigma}u_{\sigma,+}^{n+1} = 0 \quad \forall K\in T,$$

$$\sum_{\sigma\in\Xi_K} F_{K,\sigma} + \tau m(K)\, v_K = 0 \quad \forall K\in T,$$

$$u_K^0 = u_0(x_K) \quad \forall K\in T,$$

$$F_{K,\sigma}^n = -\tau_{K|L}\left(u_L^n - u_K^n\right) \ \forall\sigma\in\Xi_{int} \quad \text{if } \sigma = K|L\,,$$

$$F_{K,\sigma}^n = \tau_\sigma\left(u_K^n\right) \quad \forall\sigma\in\Xi_{ext}\cap\Xi_K\,,$$

$$F_{K,\sigma} = -\tau_{K|L}\left(v_L - v_K\right) \quad \forall\sigma\in\Xi_{int} \quad \text{if } \sigma = K|L\,,$$

$$F_{K,\sigma} = -\tau_\sigma\left(g(y_\sigma) - v_K\right) \quad \forall\sigma\in\Xi_{ext} \ \text{ such that } \ \sigma\in\Xi_K.$$

In this work, we assume that the unknown's u and v are constants over each control volume K of the mesh T.

ACKNOWLEDGEMENT
The authors would like to acknowledge the financial supports received from the International Islamic University Malaysia, Ministry of higher education Malaysia through the research grant FRGS-14-143-0384.

References:

[1] Cliford S. Patlak. Random walk with persistence and external bias. The bulletin of mathematical biophysics, 15(3):311{338, 1953.
[2]. Evelyn F Keller and Lee A Segel. Initiation of slime mold aggregation viewed as an instability. J. Theor. Biol., 26:399 {415}, 1970.
[3] Miguel A Herrero and J J L Vel_azquez. A blow up mechanism for a chemotaxis model. Annali della Scuola Normale Superiore di Pisa. Classe di Scienze. Serie IV, 24(4):633{683, 1997.
[4] T Hillen and K Painter. Global existence for a parabolic chemotaxis model with prevention of overcrowding. Advances in Applied Mathematics, 26(4):280 { 301}, 2001.

[5] Michael Winkler. Aggregation vs. global di_usive behavior in the higher-dimensional keller segel model. Journal of Di_erential Equations, 248(12):2889{2905}, 2010.
[6] Michael Winkler. Absence of collapse in a parabolic chemotaxis system with signal-dependent sensitivity. Mathematische Nachrichten, 283:1664{1673}, 2010.
[7] Marianne Bessemoulin-Chatard and Ansgar J • ungel. A _nite volume scheme for a keller segel model with additional cross-di_usion. IMA Journal of Numerical Analysis, page drs061, 2013.
[8] Adrien Blanchet, Vincent Calvez, and Jos_e A Carrillo. Convergence of the mass-transport steepest descent scheme for the subcritical patlak{keller{segel model. SIAM Journal on Numerical Analysis, 46(2):691{721, 2008.
[9] Ibrahim Fatkullin. A study of blow-ups in the keller{segel model of chemotaxis. Nonlinearity, 26(1):81, 2012.

Numerical simulations:
In this section we present the results of numerical simulations.

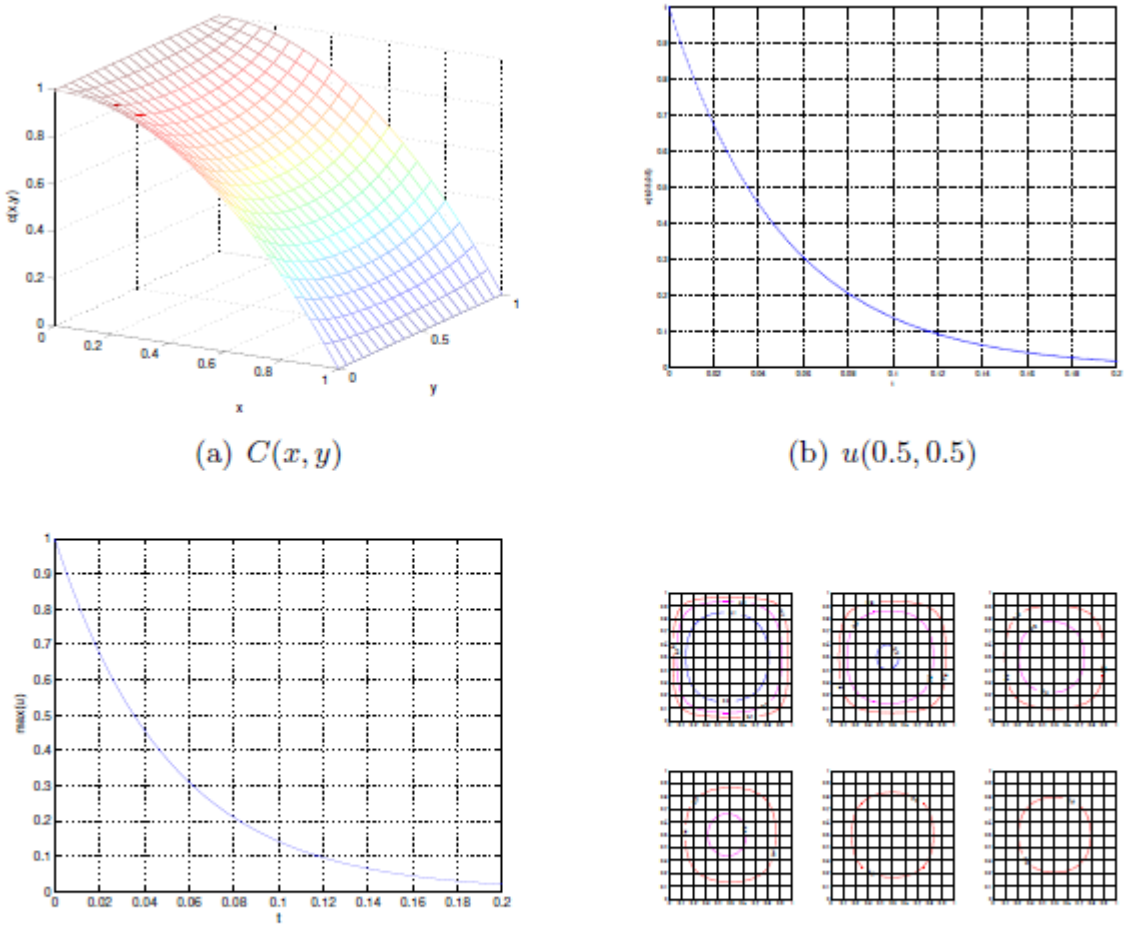

(a) $C(x, y)$ (b) $u(0.5, 0.5)$

(c) Max of u (d) Countour plot

Figure 1. Numerical solution for the Example 1

The effect of convective boundary condition on MHD mixed convection boundary layer flow over an exponentially stretching vertical sheet

Siti Suzilliana Putri Mohamed Isa[1, 2*], Norihan Md. Arifin[1, 3], Roslinda Nazar[4], Norfifah Bachok[1, 3], and Fadzilah Md Ali[1, 3]

[1]Institute for Mathematical Research, Universiti Putra Malaysia
43400 UPM Serdang, Selangor Darul Ehsan, MALAYSIA.

[2]Pusat Asasi Sains Pertanian, Universiti Putra Malaysia
43400 UPM Serdang, Selangor Darul Ehsan, MALAYSIA.

[3]Department of Mathematics, Universiti Putra Malaysia.

[4]School of Mathematical Sciences, Universiti Kebangsaan Malaysia.

[1]ctsuzilliana@upm.edu.my, [2]norihana@upm.edu.my, [3]rmn@ukm.my, [4]norfifah@upm.edu.my, [5]fadzilahma@upm.edu.my

Introduction. The present work focuses on magnetohydrodynamics mixed convection heat transfer of an electrically conducting fluid over an exponentially stretching continuous surface with an exponential temperature distribution. The system is maintained using applied convective boundary conditions, exponential magnetic field, viscous dissipation, buoyancy force, and internal heat generation. In addition, this research work explored the assisting and opposing flow conditions on the heat transfer characteristics.

Mathematical Formulation and Methods. The flow and heat transfer problems are governed by the following equations:

$$\frac{\partial u}{\partial x}+\frac{\partial v}{\partial y}=0 \tag{1}$$

$$u\frac{\partial u}{\partial x}+v\frac{\partial u}{\partial y}=\upsilon\frac{\partial^2 u}{\partial y^2}+g\beta\left(T-T_\infty\right)-\frac{\sigma B^2\left(x\right)}{\rho}u \tag{2}$$

$$u\frac{\partial T}{\partial x}+v\frac{\partial T}{\partial y}=\alpha\frac{\partial^2 T}{\partial y^2}+\frac{\sigma}{\rho c_p}B^2\left(x\right)u^2+\frac{\mu}{\rho c_p}\left(\frac{\partial T}{\partial y}\right)^2+\frac{Q}{\rho c_p}\left(T-T_\infty\right) \tag{3}$$

where u and v are the components of velocity in the x and y directions, respectively, $\upsilon = \mu/\rho$ is the kinematic viscosity, μ is the viscosity, ρ is the fluid density, g is acceleration due to gravity, β is the thermal expansion coefficient, σ is the electrical conductivity, α is the thermal diffusivity, T is the temperature of the fluid, c_p is the specific heat of the fluid at a constant pressure, and $Q>0$ is the internal heat generation coefficient. In Equation (2), we consider the special form of magnetic field, $B\left(x\right) = B_0 e^{(x/2L)}$.

The appropriate boundary conditions are as follows:

$$u = U_w(x) = U_0 e^{(x/L)}, \qquad v = 0, \qquad -k\frac{\partial T}{\partial y} = h_0\left(T_0 - T\right) \qquad \text{at } y = 0 \tag{4}$$
$$u \to 0 \qquad T \to T_\infty \qquad \text{as } y \to \infty$$

where k is the thermal conductivity of the fluid and h_0 is the convective heat transfer coefficient.

The new similarity variables that were introduced are as follows:

$$\eta = \frac{y}{L}\left(\frac{\mathrm{Re}}{2}\right)^{\frac{1}{2}} e^{\left(\frac{x}{2L}\right)}, \qquad \psi(x,y) = \sqrt{2\,\mathrm{Re}}\,\upsilon e^{(x/2L)} f(\eta),$$
$$T(x,y) = T_\infty + \left(T_0 - T_\infty\right) e^{ax/2L}\theta(\eta) \tag{5}$$

where ψ is the stream function which is defined as $u = \partial\psi/\partial y$ and $v = -\partial\psi/\partial x$, and a as the similarity variable for temperature $T(x,y)$ is a parameter of the temperature distribution in the stretching surface.

The governing nonlinear partial differential equations (Eqs. 1-3) and the boundary conditions (Eq. 4) are converted into ordinary differential equations by a similarity transformation (Eq. 5). The converted equations are then solved numerically using the shooting method. The results related to skin friction coefficient, local Nusselt number, velocity and temperature profiles are presented for several sets of values of the parameters. The parameters used in this problem are $X = x/L$ (dimensionless coordinate along the plate); $Ha = \sqrt{\sigma B_0{}^2 L^2/\rho\upsilon}$ (Hartmann number); $\mathrm{Re} = U_0 L/\upsilon$ (Reynolds number); $\lambda = Gr/\mathrm{Re}^2$ (constant mixed convection parameter), $Gr = \left[g\beta\left(T_0 - T_\infty\right)L\right]/U_0{}^2$ (Grashof number); $\mathrm{Pr} = \upsilon/\alpha$ (Prandtl number); $Bi = h_0 y/\eta k$ (Biot number); and $A^* = QL^2/\left(\mu c_p \mathrm{Re}\right)$ (dimensionless heat generation parameter). The effect of the magnetic field in this problem is considered as a ratio of the Hartmann number to the Reynolds number.

Results. Numerical computations have been performed for the velocity profile $f'(\eta)$, the temperature profile $\theta(\eta)$, the skin friction coefficient $f''(0)$ and the local Nusselt number $-\theta'(0)$ for various values of physical parameters, such as mixed convection parameter λ, parameter of the temperature distribution in the stretching surface a, Hartmann number Ha^2/Re, Biot number Bi, Eckert number Ec, dimensionless heat generation parameter A^* and dimensionless coordinate along the plate X. To examine the accuracy of the numerical method, we compare our results with those obtained by Magyari and Keller [1], Al-Odat et al. [2], and Pal [3] in Table 1. In this table, the comparison is made for the nonmagnetic case $Ha^2/\mathrm{Re} = 0$, non-buoyant flow $\lambda = 0$, and when $Bi = Ec = X = A^* = 0$. This table also shows the comparison of the values of $-\theta'(0)$ for different values of Pr and a. From this table, it can be observed that the present results are in very good agreement with the previous results, which proves our theoretical study and numerical computation.

Table 1: Comparison of local Nusselt number $-\theta'(0)$ calculated by (...) Magyari and Keller [1], <...> Al-odat et al. [2], {...} Pal [3] and * * present method.

a	***Pr***					
	0.5	**1**	**3**	**5**	**8**	**10**
−1.5	(−0.20405) <−0.19191> {−0.20405} *−0.20405*	(−0.37741) <−0.36152> {−0.37741} *−0.37741*	(−0.92386) <−0.90309> {−0.92386} *−0.92386*	(−1.35324) <−1.34143> {−1.35324} *−1.35324*	(−1.88850) <−1.82858> {−1.88849} *−1.88849*	(−2.20000) <−2.13693> {−2.20003} *−2.20003*
−0.5	(0.17582) <0.18187> {0.17582} *0.17582*	(0.29988) <0.32697> {0.29988} *0.29988*	(0.63411) <0.67215> {0.63411} *0.63411*	(0.87043) <0.84156> {0.87043} *0.87043*	(1.15032) <1.08391> {1.15032} *1.15032*	(1.30861) <1.25074> {1.30861} *1.30861*
0.0	(0.33049) <0.31006> {0.33049} *0.33049*	(0.54964) <0.53104> {0.54964} *0.54964*	(1.12219) <1.08522> {1.12209} *1.12209*	(1.52124) <1.47558> {1.52124} *1.52124*	(1.99185) <1.92633> {1.99184} *1.99184*	(2.25743) <2.18847> {2.25742} *2.25742*
1.0	(0.59434) <0.57771> {0.59434} *0.59434*	(0.95478) <0.91903> {0.95478} *0.95478*	(1.86908) <1.81039> {1.86907} *1.86907*	(2.50014) <2.28864> {2.50013} *2.50013*	(3.24213) <3.00587> {3.24212} *3.24212*	(3.66038) <3.18620> {3.66037} *3.66037*
3.0	(1.00841) <0.97665> {1.00841} *1.00841*	(1.56029) <1.46569> {1.56030} *1.56030*	(2.93854) <2.89007> {2.93853} *2.93853*	(3.88656) <3.78072> {3.88656} *3.88656*	(5.00047) <4.86245> {5.00046} *5.00046*	(5.62820) <5.58576> {5.62820} *5.62820*

Conclusion. From the numerical findings, multiple solutions are occurred for the opposing and assisting flow situations. It is observed that the three solution profiles exist for both skin friction coefficient and local Nusselt number when the flow is assisting, i.e. with the large assisting flow parameter. Moreover, two solution profiles exist for the small values of opposing and assisting flow parameters.

References

[1] E. Magyari, B. Keller, Heat and mass transfer in the boundary layers on an exponentially stretching continuous surface, J. Phys. D: Appl. Phys. 32 (1999) 577–585.

[2] M.Q. Al-Odat, R.A. Damseh, T.A. Al-Azab, Thermal boundary layer on an exponentially stretching continuous surface in the presence of magnetic field effect, Int. J. Appl. Mech. Eng. 11 (2006) 289–299.

[3] D. Pal, Mixed convection heat transfer in the boundary layers on an exponentially stretching surface with magnetic field, Appl. Maths. Comput. 217 (2010) 2356–2369.

Extended Abstract of the 4th International Conference on Mathematical Applications in Engineering (ICMAE2017), 08—09th August 2017

Numerical Simulation of the Effects of Simultaneous Internal and External Mass Transfer Resistances on the Performance of the Immobilized Spherical Catalyst Pellet for Simple Michaelis-Menten Kinetics.

Ahmad T. Jameel[1*] and Asif Hoda[2]

[1]Biotechnology Engineering Department, Kulliyyah (Faculty) of Engineering, International Islamic University Malaysia, Gombak, 50728 Kuala Lumpur. Malaysia

[2] Mechanical Engineering Department, Jubail University College, Jubail, Saudi Arabia.

[1] atjameel@iium.edu.my, [2] hodaa@ucj.edu.sa,

Introduction. Immobilized biocatalysts have many advantages in large scale processing such as retention of enzyme or cell, enhanced stability and increased half-life of the enzyme [1] The efficiency of immobilized biocatalyst particles expressed by effectiveness factor play important role in the design and optimization of bioreactors. The effectiveness factor can be calculated once concentration profile within the catalyst pellet is obtained by solving the diffusion-reaction model. Complex rate kinetics such as given by Michaelis-Menten equation which represents host of biological reactions requires numerical solutions even for the simplest diffusion-reaction model. The diffusion-reaction model becomes even more involved in the presence of external mass transfer resistance which assumes significance as particle size increases. Different attempts at numerically solving nonlinear reaction-diffusion equation with and without external mass transfer effects have been reported in literature [1-4]. In this paper, we present a new approach based on finite difference method for the numerical simulation of nonlinear reaction-diffusion process in a spherical biocatalyst pellet with external film mass transfer resistance.

Mathematical Model. In order to study the effect of internal and external mass transfer resistances and intrinsic reaction kinetics on the behavior of immobilized enzyme in a porous spherical pellet, we developed a comprehensive mathematical model described as under. We consider an isothermal spherical pellet with uniformly distributed enzyme that does not deactivate during the process. The reaction of substrate at the active sites of enzyme is presumed to follows simple Micahelis-Menten kinetics. Diffusion of substrate and products can be described using Fick's Law. The system is at steady-state. The substrate partition coefficient is unity - that is no discontinuity of concentration at the solid-liquid interface.

The steady state differential mass balance for the substrate results into,

$$D_{Se}\left(\frac{d^2C_S}{dr^2}+\frac{2}{\gamma}\frac{dC_S}{dr}\right)-\frac{V_m C_S}{K_M+C_S}=0 \qquad (1)$$

In equations (1), V_m is the maximum rate of enzyme reaction, C_S is the substrate concentrations, K_M is intrinsic Michaelis constant, r is the radial location in the pellet, and D_{Se} is the effective mass diffusivity for the substrate.

If the resistance to mass transfer through the liquid film surrounding the catalyst pellet is

significant, there exists a concentration gradient for the substrate from C_{Sb} in the bulk liquid to C_{Ss} at the pellet surface. Assuming linear gradient in the boundary layer (film theory), the boundary conditions at the particle surface can be expressed as:

$$\text{BC 1: At } r = R, \quad \frac{dC_S}{dr}\Big|_{r=R} = \frac{K_L}{D_{Se}}(C_{SL} - C_{Ss}) \tag{2}$$

where K_L is the external mass transfer coefficient. At the centre of particle, the substrate mass flux is zero.

$$\text{BC 2: At } r = 0, \quad \frac{dC_S}{dr} = 0 \tag{3}$$

Equations (1)-(3) can be expressed in dimensionless form by defining following dimensionless variables and parameters.

$$\xi = \frac{C_S}{K_M}, \quad \zeta = \frac{r}{R}, \quad \beta = \frac{C_{Sb}}{K_M}, \quad r = \frac{C_{Ss}}{C_{Sb}}, \quad \phi_m = \frac{R}{3}\sqrt{\frac{V_M}{D_{Se}K_M}}, \quad B_i \text{ (Biot no.)} = \frac{RK_L}{D_{Se}} \tag{4}$$

where B_i is the Biot no. and ϕ_m is the Thiele modulus.

Eqs. 1-3 in dimensionless form become:

$$\frac{d^2\xi}{d\zeta^2} + \frac{2}{\zeta}\frac{d\xi}{d\zeta} - 9\phi_m^2\frac{\xi}{1+\xi} = 0 \tag{5}$$

$$\text{BC 1: At } \zeta = 1, \quad \frac{d\xi}{d\zeta} = \beta B_i(1-\gamma) \tag{6}$$

$$\text{BC 2: At } \zeta = 0, \quad \frac{d\xi}{d\zeta} = 0 \tag{7}$$

An overall effectiveness factor, η_o in dimensionless form can be expressed as

$$\eta_o = \frac{3(1+\beta)}{\beta}\int_0^1 \left(\frac{\xi}{1+\xi}\right)\zeta^2 d\zeta \tag{8}$$

Under steady-state condition, the rate of substrate transport into the catalyst pellet equals the rate of substrate conversion within the pellet, which in turn is proportional to the internal effectiveness factor (η_i) times the substrate reaction rate evaluated at $C_S = C_{Ss}$ [4]. This results into the following relationship in dimensionless form to calculate the unknown parameter, γ used in Eq. 6.

$$\gamma = 1 - \frac{9\phi_S^2}{B_{iS}\beta}\int_0^1 \left(\frac{\xi}{1+\xi}\right)\zeta^2 d\zeta \tag{9}$$

Finite difference method was employed for the solution of Eqs. 5-7 in conjunction with Eq. 10 to obtain the concentration profile in the particle, ξ(ζ). Thereafter, overall effectiveness factor was calculated using Eq. (8).

Results and Discussion. Figures 1 shows the variation in the overall effectiveness factor (η_0) with the Thiele modulus and the dimensionless substrate concentration outside the catalyst pellet (β) for simple irreversible Michaelis-Menten kinetics with negligible external film resistance. As depicted, effectiveness factor tend to one with decreasing Thiele modulus and

increasing substarte concentration. The Theiele modulus can be minimized by decreasing the particle size R and V_m. V_m will depend on the amount of immobilized enzyme per unit mass of support. For an optimum value of V_m, a lower bound on the particle size can be determined in order to minimize internal mass transfer resistance consistent with a reasonable hydrodynamic pressure drop in the fixed bed reactor as also observed by Jeison et al. (2003) [2].

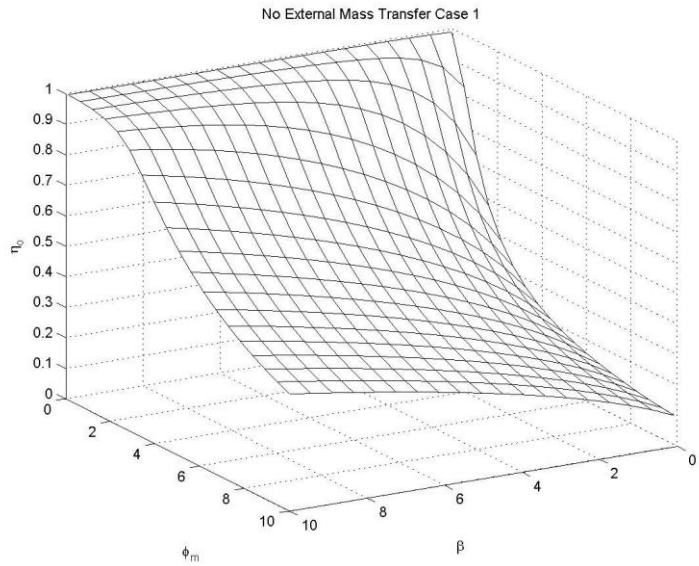

Figure 1: Effect of Thiele modulus and substrate concentration, β on the effectiveness factor with simple Michaelis-Menten kinetics and without external mass transfer resistance.

Figs. 2(a) and 2(b) show the effect of Thiele modulus and the substrate concentration β on the overall effectiveness factor for Biot numbers 1 and 50 respectively, in the presence of external film mass transfer resistance. It is obvious from Figs. 2 that the effectiveness factor significantly improves at large Biot number especially for higher Thiele modulus (large size particles). Thus it is clear from these plots that the external mass transfer resistance cannot be ignored as pellet size increases. A comparison with Fig. 1 also support the fact that external film resistance decreases the effectiveness factor, hence the efficiency of the catalyst particle.

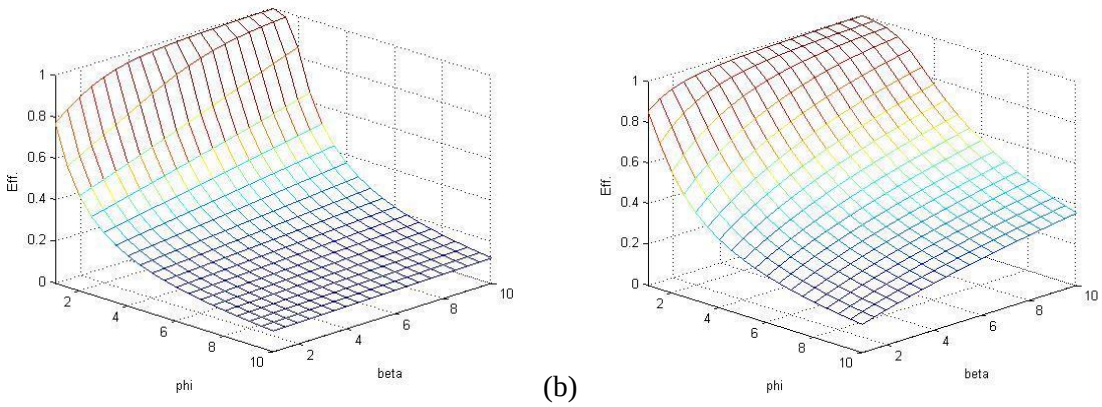

Figure 2: Effect of Thiele modulus and substrate concentration on the effectiveness factor for different Biot numbers corresponding to different liquid film mass transfer coefficient. (a) B_i =1, (b) B_i =50

References

[1] Doran, P.M., Bioprocess Engineering Principles, Academic Press, London, 2013.

[2] Jeison D., Ruiz G., Acevedo F., Illanes A. Simulation of the effect of intrinsic reaction kinetics and particle size on the behaviour of immobilised enzymes under internal diffusional restrictions and steady state operations. Process Biochemistry 2003; 39:393-399.

[3] Al-Muftah A.E., Abu-Reesh I.M. Effect of simultaneous internal and external mass transfer and product inhibition on immobilized enzyme-catalyzed reactor. Biochemical Engineering Journal 2005; 27:167-178.

[4] Bortone N., Fidaleo M., Moresi M., Internal and external mass transfer limitations on the ativity of immobilised acid urease derivatives differing in enzyme loading. Biochemical engineering Journal 2014; 82:22-33.

Extended Abstract of the 4th International Conference on Mathematical Applications in Engineering (ICMAE2017), 08—09th August 2017

Using One-way ANOVA in Completely Randomized Experiments

Zaharah Wahid[1], Ahmad Izwan Latiff[2], and Kartini Ahmad[1]

[1]Department of Science in Engineering, Faculty of Engineering
International Islamic University Malaysia
Jalan Gombak ,53100, Kuala Lumpur, MALAYSIA.

[2]Department of Biotechnology in Engineering, Faculty of Engineering
International Islamic University Malaysia.
Jalan Gombak ,53100, Kuala Lumpur, MALAYSIA.

[1]zaharahwahid@iium.edu.my, [2]izwan@iium.edu.my, [1]kartiniahmad@iium.edu.my

Introduction. An analysis of variance, often abbreviated as ANOVA is a statistical technique to compare three or more means. It is referred to a one-way ANOVA when the number of independent variable (or factor) is only one in the test. Hypothesis testing is used to evaluate the possible differences among the means. The null hypothesis for this test is that the means are all alike using the *F* distribution. The alternative hypothesis is that at least one of the means is different from the rest. With the *F*-test, all the means are compared simultaneously. Even though one is comparing three or more means in the use of the *F*-test, variances are used in the test instead of mean [1].

As discussed by [1,4] the primary assumption in applying ANOVA is that the response is normally distributed. The variance of the response is divided into the variance that can be attributed to the investigated characteristic or factor and the variance that can be attributed to the randomness in the response.

The analysis of variance was originally invented by Ronald Fisher in the 1920's and has its root in agriculture sector. It has been further developed and has been applied in various fields [2,3,4]. The basic idea remains the same.

Completely Randomized Experiments. If there is only one factor, the experimental design is referred to as a completely randomized design. In this study the factor being investigated is the location where the leachate is collected. The location is subdivided into four groups or levels. The response variable of interest is chemical oxygen demand (COD). It is measured for different levels of the factor. The order of conducting the experimental trials can affect the result. The order is selected randomly or randomly assign by allocating each trial a number and using random numbers to choose the order. The experiments were replicated three times.

Results and Discussion. The design matrix in Table 3.1 is the combinations of factor and levels that make up the experiment. The ANOVA Table 3.2 showed that there is very strong evidence that the location influences the response (chemical oxygen demand). Since p-value ($p \leq 0.000$) is less than $\alpha = 0.05$, the result is statistically significant at the 5% level. The null hypothesis is rejected. There is a difference between the mean chemical oxygen demand. The *F*-test statistic shown in Table 3.2 is 92.09 with, $df_1 = 3$ and $df_2 = 32$ degrees of freedom. Using the critical value approach with $\alpha = 0.05$, the null hypothesis is also rejected when F-

-statistic exceeds the critical value of 3.32. Again, we have sufficient evidence to suggest that at least one of the four means is different from one of the others. Next, further investigation was conducted to determine which means are different from the others.

Table 3.1: Mean Chemical Oxygen Demand in Four Locations

Location	Sample	R_1 (mg/L)	R_2 (mg/L)	R_3 (mg/L)	Average(mg/L)
1	1	256	239	230	241.667
1	2	135	158	124	139.000
1	3	135	141	129	135.000
2	1	202	224	218	214.667
2	2	233	199	141	191.000
2	3	186	181	200	189.000
3	1	591	589	581	587.000
3	2	519	504	486	503.000
3	3	628	574	632	611.333
4	1	260	285	222	255.667
4	2	399	386	375	386.667
4	3	235	231	185	217.000

In this study, Turkey's multiple comparisons at 95% confidence intervals were performed to decide which levels have significantly different. As displayed in Fig. 3.1, the second confidence interval includes zero, while the third and fourth interval does not include zero. This suggests that there is no evidence of any difference in COD between location 1 and 2. However, there is evidence of difference between locations 2, 3, and 4.

Table 3.2: One-way ANOVA of COD

Source	DF	SS	MS	F	P
Location	3	883469	294490	92.09	0.000
Error	32	102334	3198		
Total	35	985803			

S = 56.55 R-Sq = 89.62% R-Sq(adj) = 88.65%

Figure 3.1: Individual 95% Confidence Interval for Mean (COD)

```
Tukey 95% Simultaneous Confidence Intervals
All Pairwise Comparisons among Levels of location
Individual confidence level = 98.92%
location = 1 subtracted from:

location   Lower  Center   Upper  --------+---------+---------+---------+-
2         -45.86   26.33   98.53                  (--*--)
3         323.03  395.22  467.42                                (--*--)
4          42.36  114.56  186.75                     (--*-)
                                  --------+---------+---------+---------+-
                                       -250         0       250       500
location = 2 subtracted from:

location   Lower  Center   Upper  --------+---------+---------+---------+-
```

```
3          296.69   368.89   441.08                                (--*--)
4           16.03    88.22   160.42                      (--*-)
                                     --------+---------+---------+---------+-
                                         -250         0       250       500
location = 3 subtracted from:

location     Lower    Center     Upper  --------+---------+---------+---------+-
4          -352.86  -280.67  -208.47       (--*--)
                                     --------+---------+---------+---------+-
                                          -250         0       250       500
```

The adequacy of the model for COD was assesed by graphing the residuals, as shown in Fig. 3.1. The structureless residuals verified that the normality assumptions, constant variance and randomly scattered points are valid and therefore the model is adequate.

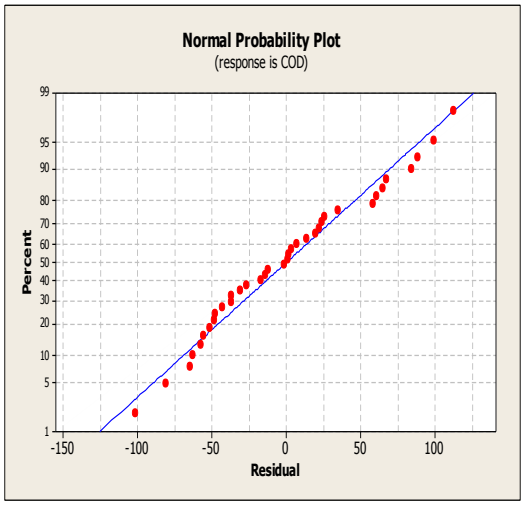

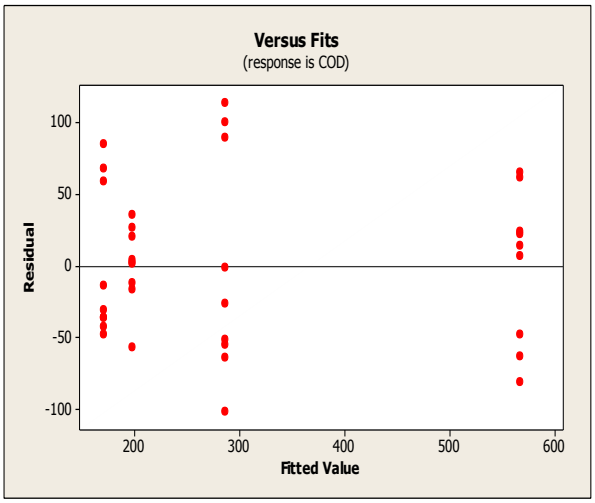

Conclusions. The experiments have provided evidence that the location influences the COD value. Determine the effect of location has statistically significant effect on the value of COD. Thus, using the above procedure one can discover which means have significantly different means, a common problem facing researchers could be answered.

References

[1] D.C. Montgomery: Design and Analysis of Experiments, 7th Edition. John Wiley & Sons, Inc.,(2009)..

[2] G. Daniel and C. Veronica Maria de Araujo: Mathematic and Statistical Methods in Food Science And Technology, 1st Edition. John Wiley & Sons, Ltd.(2014).

[3] Ellendersen, L. S. N.Granato, D., Guergoletto, K. B. and Wosiacki, G. Development and sensory profile of a probiotic beverage from apple fermented with Lactobacillus casei. Engineering in Life Sciences, 12 (2012) 475–485.

[4] R. H. Myers, D. C. Montgomery, and C. M Anderson-Cook: Response Surface Methodology: process and product optimization using designed experiments, 3rd edition. John Wiley & Sons, Inc., New York. (2009).

Extended Abstract of the 4th International Conference on Mathematical Applications in Engineering (ICMAE2017), 08—09th August 2017

Electric Quadrupole E2– Transitions of Isotopes Yb

Moh'd Kh. M. Abu El Sheikh[1], Abdurahim Okhunov[2], Hasan Abu Kassim[1]

[1]Department of Physics, University of Malaya, 50603 Kuala Lumpur, Malaysia.

[2]Department of Science in Engineering, Kulliyyah of Engineering, International Islamic University Malaysia, P.O. Box 10, IIUM, 53100 Kuala Lumpur, Malaysia.

[1]mhsr70@gmail.com, [2]abdurahimokhun@iium.edu.my, [3]hasanak@um.edu.my

Introduction. Despite the fact that the structure of deformed nuclei and nature of low excited levels have been substantially studies over more than four decades, this still occupies a central part of today's research [1–3]. The nuclei *Yb* have been well studied. It is important to note that these are investigated in a number of ways such as radioactive decay of $^{170-174}Lu$, and different nuclear reactions. In these isotopes, many 1^+ states and $K^\pi = 0^+, 2^+$ bands have been. In the present paper, the low – lying states of positive parity of isotopes $^{170-174}Yb$ is studied. The calculation are conducted by utilizing a phenomenological model [4, 5] which accounts Coriolis mixture all of the experimentally known low–lying rotational bands states.

The Model. To analyze the properties of low–lying positive parity states in *Yb* isotopes, the phenomenological model of [5] is exploited. This model takes into account the mixing of states of the $K^\pi = 0^+$, 2^+ and 1^+ + bands. The Hamiltonian model is

$$H = H_{rot}\left(I^2\right) + H^{\sigma}_{K'K}\left(I\right) \tag{1}$$

$$H^{\sigma}_{K'K}\left(I\right) = \omega_K \delta_{K,K'} - \omega_{rot}\left(I\right)\left(j_x\right)_{K,K'} \cdot \tau\left(I,K\right)\delta_{K,K'\pm 1} \tag{2}$$

where ω_K – bandhead energy of the rotational bands, $\omega_{rot}\left(I\right)$ – an angular frequency of rotational nucleus, $\left(j_x\right)_{K,K'}$ – matrix elements which describe Coriolis mixture between rotational bands and

$$\tau\left(I,0\right) = 1, \qquad \tau\left(I,2\right) = \sqrt{1 - \frac{2}{I\left(I+1\right)}}.$$

The eigenfunction of Hamiltonian (1) is

$$\left|IMK\right\rangle = \left(\frac{2I+1}{16\pi^2}\right)^{\frac{1}{2}} \left\{\sqrt{2}\Psi^I_{gr,K} D^I_{M,K}\left(\theta\right) + \sum_{K'} \frac{\Psi^I_{K',K}}{\sqrt{1+\delta_{K',0}}}\left[D^I_{M,K}\left(\theta\right) b^+_{K'} + \left(-1\right)^{I+K'} D^I_{M,-K'}\left(\theta\right) b^+_{-K'}\right]\right\} \tag{3}$$

where $\Psi^I_{K',K}$ is the amplitude of mature of basis states.

Electric Quadrupole *E2*– transitions. We shall calculate the reduced probability for *E2*–transitions, using the wave function obtained by describing the energy of states. The expression for the reduced probability of *E2*– transitions from the $I_i K_i$ states to the ground state band and intraband transitions of ground state band within the framework our model as follows:

$$B\left(E2; I_i K_i \to I_f 0_1\right) = \left\{ \left(\frac{5}{16\pi}\right)^{\frac{1}{2}} eQ_0 \left[\left[\Psi^{I_f}_{0_1,0_1} \Psi^{I_i}_{0_1,K_i} C^{I_f 0}_{I_i 0;20} + \sum_n \Psi^{I_f}_{K_n,0_1} \Psi^{I_i}_{K_n,K_i} C^{I_f K_n}_{I_i K_n;20} \right] \right.\right.$$
$$+\sqrt{2}\left[\Psi^{I_f}_{0_1,0_1} \sum_n \frac{(-1)^{K_n} \cdot m_{K_n} \Psi^{I_i}_{K_n,K_i}}{\sqrt{1+\delta_{K_n,0}}} C^{I_f K_n}_{I_i K_n;20} \right. \tag{4}$$
$$\left.\left. + \Psi^{I_f}_{0_1,K_i} \sum_n \frac{\cdot m_{K_n} \Psi^{I_i}_{K_n,0_1}}{\sqrt{1+\delta_{K_n,0}}} C^{I_f K_n}_{I_i 0;2K_n} \right] \right\}^2$$

Here $m_{K_n} =< gr \,|\, \hat{m}(E2) \,|\, K_n^+ >$ is a matrix elements between interior wave functions of the ground (0_1^+) and $K_n^+ = 0_\ell^+, 2_m^+, 1_\nu^+$ bands, whose values are defined from experimental data, $Q_0 -$ is the internal quadrupole moment of the nucleus; and $C^{I_f K_n}_{I_i K_n;2(K_i+K_f)} -$ are Clebsch–Gordan coefficients.

In the adiabatic approximation, the following equations are valid for $B\left(E2\right)$ factors from the $I = 2$ states to the K_n^+ rotational band:

$$B^{adiabatic}\left(E2; 2K_n^+ \to 0^+ 0_1^+\right) = \left(2 - \delta_{K_n,0}\right) \left| m_{K_n} C^{00}_{2K_n;2-K_n} \right|^2 \tag{5}$$

which allows to calculate the empirical values of the parameters m_{K_n} from the experimental data.

The $K^\pi = 0_2^+, 0_3^+$ and $K^\pi = 2_1^+$ state bands are located close to each ather in $^{170,172}Yb$ isotopes, which leads to a strong mixing of states even when spin is $I = 2$. In this case the adiabatic approximation Eq. 5 becomes inapplicable to determine m_{K_n}. Therefore, to describing the experimental data for $B\left(E2\right)$ in $^{170,172}Yb$ isotopes, the value of m_0 and m_2 parameters are varied slightly.

The empirical values of parameters m_{K_n} have been defined by Eq. 5, using the experimental data of the reduced probabilities of *E2*– transitions $B(E2; 2K_n \to 0^+ 0_1^+)$. Table 1 provides theoretical values of the reduced matrix elements of *E2*–transitions for ^{172}Yb, wich are compared with experemental data and values taken by other models [6–8].

We note that our calculations were performed sequentially, i.e., first describes the energy state and then corresponding their wave functions are determined. Further, using these wave functions are calculated probabilities *E2*– transitions. From Table 1, one can see that, the

results of calculation in the framework of our model for the majority cases provide a good agreement with experimental data.

The magnitude and sign of the parameters $m_{1_1} = m_{1_\nu}$ were determined from the best agrement of the ratios $R_{IK} = E2; I_i K_i^+ \to I + 10_1^+ / E2; 2K_n^+ \to 0^+ 0_1^+ \left(E2; I_i K_i^+ \to I - 10_1^+ \right)$ from odd states of the $K^\pi = 2_l^+$ and $K^\pi = 1_\nu^+$ (states with the negative signature $\tau = +1$).

The adiabatic values of the ratio of reduced probability of *E2*– transitions $R_{IK}^{adiabatic}$ is defined by the formula:

$$R_{IK}^{adiabatic} = \frac{I_\gamma \left(IK \to I_1 0_1 \right)}{I_\gamma \left(IK \to I_2 0_1 \right)} \left(\frac{E_\gamma \left(IK \to I_2 0_1 \right)}{E_\gamma \left(IK \to I_1 0_1 \right)} \right)^5 \tag{6}$$

Table 1: Reduced Matrix Elements of *E2* – transitions in ^{172}Yb

$I_i K_i \to I_f K_f$	Exp.	RVM2	IBA-1	Theory	$I_i K_i \to I_f K_f$	Exp.	RVM2	IBA-1	Theory
$22_1 \to 00_1$	$0.20^{+0.010}_{-0.040}$	0.21	0.20[a)]	0.208	$00_2 \to 20_1$	$0.166^{+0.018}_{-0.018}$	0.16	0.27	0.01
$22_1 \to 20_1$	$0.250^{+0.016}_{-0.018}$	0.25	0.31	0.255	$20_2 \to 00_1$	$0.090^{+0.010}_{-0.040}$	0.16	0.26	0.082
$22_1 \to 40_1$	$0.063^{+0.009}_{-0.004}$	0.062	0.10	0.066	$20_2 \to 20_1$	$0.162^{+0.071}_{-0.008}$	0.19	0.31	0.108
$42_1 \to 20_1$	$0.22^{+0.07}_{-0.05}$	0.20	0.13	0.11	$20_2 \to 40_1$	$0.27^{+0.02}_{-0.08}$	0.26	0.45	0.19
$42_1 \to 40_1$	$0.46^{+0.08}_{-0.13}$	0.38	0.45	0.27	$40_2 \to 40_1$	–	–	–	0.13
$32_1 \to 20_1$	$0.32(11)$	–	–	0.328					
$32_1 \to 40_1$	$0.35(6)$	–	–	0.226					

Summary. From Table 1, one can see that, the results of calculation in the framework of our model for the majority cases provide a good agreement with experimental data. The experimental values of ratios R_{I0_2} for $E2-$ transitions from the $K^\pi = 0_2^+$ states are different from the adiabatic theory of a several dozen times. It's connected with strong mixing of 0_2^+ and 2_1^+ bands. Then arises the question, why the value of rations $R_{I2_1^+}$ for the transitions from the 2_1^+ bands is not too much different from the adiabatic theory compared R_{I0_2}. This is because the matrix element $m_{2_1} =< 0_1^+ \mid \hat{m}(E2) \mid 2_1^+ >$ is 10 times greater than $m_{0_1} =< 0_1^+ \mid \hat{m}(E2) \mid 0_2^+ >$.

References

[1] A. Bohr and B.R. Mottelson. Nuclear Structure Vol. 1.2 (Benjamin, New York, 1997).

[2] V.G. Soloviev. Theory of difficult atomic nuclei (M. Nauk, 1974).

[3] D.G. Burke, V.G.Soloviev, A.V.Sushkov and N.Yu.Shirikova Nucl. Phys. A 656 (1999) 287.

[4] Ph.N. Usmanov, I.N. Mikhailov. Phys. Part. Nucl. Lett. 28 (1997)348 [Fiz.Elem.Chastits At. Yadra 28 (1997) 887].

[5] Ph.N. Usmanov, A.A. Okhunov, U.S. Salikhbaev and A.I. Vdovin. Phys. Part. Nucl. Lett. 7(3) (2010) 185 [Pisma Fiz.Elem.Chastits At. Yadra 3(159) (2010) 306].

[6] C. Fahlander, B. Varnestig, F. Backlin et al., Nucl. Phys. A147 (1992) 157.

[7] A. Faessler, W. Greiner and R.K. Sheline. Nucl. Phys. 70 (1965) 33.

[8] A. Arima and F. Iachello. Adv. Nucl. Phys. 13 (1984) 139.

Extended Abstract of the 4th International Conference on Mathematical Applications in Engineering (ICMAE2017), 08—09th August 2017

Periodic Ground States for λ-model on a Cayley Tree

Farrukh Mukhamedov[1], Chin Hee Pah[2], Muzaffar Rahmatullaev[3], and **Hakim Jamil[4]**

[1]Department of Mathematics, College of Science, The United Arab Emirates University
P. O. Box, 15551, Al Ain, Abu Dhabi, UAE.

[2]Department of Computational & Theoretical Sciences, Faculty of Science,
P. O. Box, 141, 25710, Kuantan, Pahang, MALAYSIA.

[3]Institute for Mathematics, National University of Uzbekistan,
29, Do'rmon Yo'li str., 100125, Tashkent, UZBEKISTAN.

[4]Department of Computational & Theoretical Sciences, Faculty of Science,
P. O. Box, 141, 25710, Kuantan, Pahang, MALAYSIA.

[1]far75m@gmail.com, [2]pahchinhee@iium.edu.my, [3]mrahmatullaev@rambler.ru, [4]m.hakimjamil@yahoo.com.my

Introduction. Each Gibbs measure is associated with a single phase of physical system [1]. The existence of two or more Gibbs measure means that phase transitions exist. One of the fundamental problem is to describe the extreme Gibbs measures corresponding to a given Hamiltonian. As is known, the phase diagram of Gibbs measures for a Hamiltonian is close to the phase diagram of isolated (stable) ground states of the Hamiltonian. At low temperatures, a periodic ground state correspond to a periodic Gibbs measure, see [1]. For the Potts model with competing interactions on the Cayley tree of order two, periodic ground states were studied in [2,3](see also [4]). On the other hand, it is natural to consider a model which is more general than the Potts one, therefore, in [5] it was proposed to study so-called λ-model on the Cayley tree (see also [4,5]). In that model, many possible interactions (nearest-neighbor) are taken into account. Furthermore, in [6] we have described ground states of the λ-model on Cayley tree of order two. This model is general than Potts model, and exhibits interesting structure of ground states. In the present paper, we continue an investigation of the λ-model on the Cayley Tree of order two, and study periodic ground states associated with normal subgroups of index 2.

Preliminaries. Let $\tau^k = (V, L)$ be a Cayley tree of order k, i.e., an infinite tree such that exactly $k+1$ edges are incident to each vertex. Here V is the set of vertices and L is the set of edges of τ^k. Let G_k denote the free product of $k+1$ cyclic groups $\{e, a_i\}$ of order 2 with generators $a_1, a_2, ..., a_{k+1}$, i.e., let $a_i^2 = e$. There exists one-to-one correspondence between the set V of vertices of the Cayley tree of order k and the group G_k, see[4,7]. For the group G_k (or the corresponding Cayley tree), we consider the left (right) shifts. for $g \in G_k$, we put $T_g(h) = gh (T_g(h) = hg)$ for all $h \in G^k$. The group of all left (right) shifts on G_k is isomorphic to group G_k. Each transformation S on the group G_k induces a transformation S on the vertex set V of the Cayley tree τ^k. In the sequel, we identify V with G_k.

Theorem 2.1. *The group of left (right) shifts on the right (left) representation of the Cayley tree is the group of translations.*

By the group translations, we mean the automorphism group of the Cayley tree regard as graph. Recall that a mapping ψ on the vertex set of a graph G is called an automorphism of G if ψ preserves the adjacency relation, i.e., the image $\psi(u)$ and $\psi(v)$ of vertices u and v are adjacent if and only if u and v are adjacent. For an arbitrary vertex $x_0 \in V$, we put

$$W_n = \{x \in V \mid d(x^0, x) = n\},\ V_n = \bigcup_{m=0}^{n} W_n,\ L_n = \{l = < x, y > \in V \mid x, y \in V_n\}.$$

where $d(x, y)$ is the distance between x and y in the Cayley tree, i.e., the number of edges of the path between x and y. For each $x \in G_k$, let $S(x)$ denote the set of immediate successor of x, i.e., if $x \in W_n$ then $S(x) = \{y \in W_{n+1} : d(x, y) = 1\}$. For each $x \in G_k$, let $S_1(x)$ denote the set of all neighbors of x, i.e., $S_1(x) = \{y \in G_k :< x, y > \in L\}$. The set $S_1(x) \setminus S(x)$ is a singleton. Let $x_{\downarrow}$ denote the (unique) element of this set. Assume that spin takes its values in the set $\Phi = \{1, 2, ..., q\}$. By configuration σ on V we mean a function taking $\sigma : x \in V \to \sigma(x) \in \Phi$. The set of all configurations coincides with the set $\Omega = \Phi^V$.

Consider the quotient group $G_k \setminus G_k^* = \{H_1, ..., H_r\}$, where G_k^* is normal subgroup of index r with $r \geq 1$. Recall that a configuration is $\sigma(x)$ said to be G_k^**-periodic* if $\sigma(x) = \sigma_i$ for all $x \in G_k$ with $x \in h_i$. A G_k-periodic configuration is said to be *translation invariant.*
The Hamiltonian of the λ-model [7,8] has form,

$$H(\sigma) = \sum_{<x,y> \in L} \lambda(\sigma(x), \sigma(y)).$$

In what follows, we restricted ourselves to the case $k = 2$ and $\Phi = \{1, 2, 3\}$, and for the sake of simplicity, we consider the following function:

$$\lambda(i, j) = \begin{cases} \bar{a} & ,if \quad |i - j| = 2, \\ \bar{b} & ,if \quad |i - j| = 1, \\ \bar{c} & ,if \quad i = j. \end{cases}$$

where $\bar{a}, \bar{b}, \bar{c} \in \square$ for some given numbers.

Summary. For a pair of configurations σ and φ coinciding almost everywhere, i.e., except finitely many points, we consider the relative Hamiltonian $H(\sigma, \varphi)$ determining the energy differences of the configuration σ and φ:

$$H(\sigma, \varphi) = \sum_{\substack{<x,y> \\ x,y \in V}} (\lambda(\sigma(x), \sigma(y)) - \lambda(\varphi(x), \varphi(y)))$$

Let M be the set of unit balls with vertices in V, i.e., $M = \{x, S_1(x), \forall x \in V\}$. We call the restriction of configuration σ to the ball $b \in M$ a bounded configuration σ_b. We define the energy of the configuration σ_b on b as follows:

$$U(\sigma_b) = \frac{1}{2} \sum_{\substack{<x,y> \\ x,y \in V}} (\lambda(\sigma(x), \sigma(y)))$$

The relative Hamiltonian has the form $H(\sigma, \varphi) = \sum_{b \in M} (U(\sigma_b) - U(\varphi_b))$. The inclusion

$$U(\sigma_b) \in \left\{ \frac{\alpha + \beta + \gamma}{2}, \forall \alpha, \beta, \gamma \in \{\bar{a}, \bar{b}, \bar{c}\} \right\}$$

holds for every configuration φ_b on $b (b \in M)$. Configuration φ is called ground state of the relative Hamiltonian H if

$$U(\sigma_b) = \min \left\{ \frac{\alpha + \beta + \gamma}{2}, \forall \alpha, \beta, \gamma \in \{\bar{a}, \bar{b}, \bar{c}\} \right\}$$

for any $b \in M$. If a ground state is a periodic configuration, then we call it periodic ground state. Let $k = 2$ and $|A| = 1$. Then for the λ-model the following statements hold:

(i) Let $|\sigma_1 - \sigma_2| = 0$, then H_0-periodic ground state exists if and only if $\{(\bar{a}, \bar{b}, \bar{c}) \in \mathbb{R}^3 \mid \bar{c} \le \bar{b} \le \bar{a}\} \bigcup \{(\bar{a}, \bar{b}, \bar{c}) \in \mathbb{R}^3 \mid \bar{c} \le \bar{a} \le \bar{b}\}$.

(ii) Let $|\sigma_1 - \sigma_2| = 1$, then H_0-periodic ground state exists if and only if $\{(\bar{a}, \bar{b}, \bar{c}) \in \mathbb{R}^3 \mid \bar{c} = \bar{b} \le \bar{a}\}$.

(iii) Let $|\sigma_1 - \sigma_2| = 2$, then H_0-periodic ground state exists if and only if $\{(\bar{a}, \bar{b}, \bar{c}) \in \mathbb{R}^3 \mid \bar{a} = \bar{c} \le \bar{b}\}$.

References

[1] Ya. G. Sinai, Theory of Phase Transitions: Rigorous Results, Pergamon Press, Oxford (1982).

[2] G. I. Botirov, U. A. Rozikov, Potts Model with Competing Interaction on the Cayley Tree: The Contour Method, Theo. Math. Phys 153 (2007), 1423.

[3] N. N. Ganikhodjaev, F. M. Mukhamedov, J. F. F. Mendes, On the Three State Potts Model with Competing Interactionjs on Bethe Lattice, Jour. Stat. Mech. (2006), P08012.

[4] U. A. Rozikov, Gibbs Measures on Cayley Trees, World Scientific, Hackensack, 2013.

[5] F. M. Mukhamedov, On a Factor Associated with the unordered phase of the λ-model on a Cayley Tree. Rep. Math. Phys, 52 (2004), 1-18.

[6] F. M. Mukhamedov, C. H. Pah, H. Jamil, On Ground states and Phase Transitions of λ-model on a Cayley Tree, Journal of Physics: Conference Series, 819 (2017), 1.

[7] N. N. Ganikhodjaev, Group Representation and Automorphisms of the Cayley Tree, Dokl. Akad. nauk Resp. Uzbekistan, 4 (1993) 3 [in Russian].

Extended Abstract of the 4th International Conference on Mathematical Applications in Engineering (ICMAE2017), 08—09th August 2017

MULTIPLICATIVE LYAPUNOV FUNCTION FOR VOLTERRA QSO

Farrukh Mukhamedov[1], and **Ahmad Fadillah Embong**[2]

[1]Department of Mathematical Sciences & College of Science,
The United Emirates University Al Ain, Abu Dhabi, 15551, UAE

[2]Department of Computational and Theoretical Sciences , Faculty of Science
International Islamic University Malaysia, Kuantan, Pahang, Malaysia

[1]farrukh.m@uaeu.ac.ae, [2]ahmadfadillah.90@gmail.com,

Introduction. An original work on quadratic stochastic operators (in short QSOs) was done by Bernstein [1] where such kind of operators appeared from the problems of population genetics (see also [2]). These operator appear to have tremendous applications especially in modelling in many different fields such as biology (population and disease dynamics), physics (non-equilibrium statistical mechanics), economics and mathematics (replicator dynamics and games).

A quadratic stochastic operator is usually used to present the time evolution of species in biology, which arises as follows. Consider evolution of species in biology as given in the following situation. Let $I = \{1,2,\dots,n\}$ be the n type of species (or traits) in a population and we denote $x^{(0)} = \left(x_1^{(0)},\dots,x_n^{(0)}\right)$ to be the probability distribution of the species in an early state of that population. By $P_{ij,k}$ we mean the probability of an individual in the ith species and j^{th}species to cross-fertilize and produce an individual from k^{th} species (trait). Given$x^{(0)} = \left(x_1^{(0)},\cdots,x_n^{(0)}\right)$, we can find the probability distribution of the first generation, $x^{(1)} = \left(x_1^{(1)},\dots,x_n^{(1)}\right)$ by using a total probability, i.e.,

$$\boldsymbol{x_k^{(1)} = \sum_{i,j=1}^{n} P_{ij,k} x_i x_j \qquad k \in \{1,\dots,n\}}$$

This relation defines an operator which is denoted by V and it is called *quadratic stochastic operator (QSO)*. The most well-known class in the theory QSO is Volterra one, namely

$$\boldsymbol{P_{ij,k} = 0 \ \text{ if } k \notin \{i,j\}} \tag{1}$$

The condition (5) biologically means that each individual can inherit only the species of the parents. The dynamics of Volterra QSO was somehow studied successfully in [3]. However, not all QSOs are of Volterra-type, therefore dynamics of non-Volterra QSO remains open. This is not an easy task. In [4,5], there have given along self-contained exposition of the

recent achievements and open problems in the theory of the QSO. The main problem in the nonlinear operator theory is to study the behavior of nonlinear operators.
In the present paper, we are going to investigate infinite dimensional Volterra QSO. Here we construct multiplicative Lyapunov functions for such kind of operators, which allow to explore limiting set of the associated operators.

Preliminaries. In this paper we are going to consider the set of absolutely summable sequences i.e.,

$$\boldsymbol{\ell_1} = \{\boldsymbol{x} = \{\boldsymbol{x_k}\}_{k=1}^{n}; \|\boldsymbol{x}\|_1 = \sum_{k=1}^{\infty} < \infty\} \tag{2}$$

Denote

$$\boldsymbol{S} = \{\boldsymbol{x} \in \boldsymbol{\ell_1}; \boldsymbol{x_k} \geq \mathbf{0} \text{ for all } \boldsymbol{k} \in \mathbb{N}; \|\boldsymbol{x}\|_1 = \mathbf{1}\} \tag{3}$$

Let V be a mapping defined on the simplex by

$$\boldsymbol{V}(\boldsymbol{x})_k = \sum_{i,j \in \mathbb{N}} \boldsymbol{P}_{ij,k} \boldsymbol{x}_i \boldsymbol{x}_j \quad \boldsymbol{k} \in \mathbb{N} \tag{4}$$

where, $P_{ij,k}$ are hereditary coefficients which satisfy

$$\boldsymbol{P}_{ij,k} \geq \mathbf{0}, \qquad \boldsymbol{P}_{ij,k} = \boldsymbol{P}_{ji,k}, \qquad \sum_{k=1}^{\infty} \boldsymbol{P}_{ij,k} = \mathbf{1} \qquad \boldsymbol{i,j,k} \in \mathbb{N} \tag{5}$$

One can check that V maps S into itself. The operator V is called *quadratic stochastic operator(QSO)*.

We recall a QSO $V : S \to S$ is called Volterra if and only if

$$\boldsymbol{P}_{ij,k} = \mathbf{0} \text{ if } \boldsymbol{k} \notin \{\boldsymbol{i,j}\} \tag{6}$$

Taking into account (4), one easily can check that (6) is equivalent to the following canonical form of $\boldsymbol{V}$

$$V(x)_k = x_k \left(1 + \sum_{i=1}^{\infty} a_{ki} x_i\right) \text{ for all } k \in \mathbb{N}.$$

Here and henceforth, we use $V^{(n)}(x_0)$ to denote the iterations of the given QSO V and $x \in S$. Recall, a continuous function $\varphi: S \to \mathbb{R}$ is called a *Lyapunov function* for V if the limit $\lim_{n\to\infty} \varphi\left(V^{(n)}(x)\right)$ exists for any initial point $x \in S$. The following section is the main results in this paper.

Lyapunov Function and Limiting Point. In this section we are going to construct multiplicative Lyapunov function for Volterra QSO given by (6). Denote

$$\mathbb{P}^{m-1} = \left\{x \in S^{m-1}; \sum_{i=1}^{m} a_{ki}x_i \geq 0; \text{ for every } k \in \{1, \dots, m\}\right\}$$

Analogously, we define such infinite dimensional case i.e.,

$$\mathbb{P} = \left\{x \in S; \sum_{i=1}^{\infty} a_{ki}x_i \geq 0; \text{ for every } k \in \mathbb{N}\right\}$$

Theorem 1. Let V be infinite dimensional Volterra QSO such that $\mathbb{P}$ is non-empty. The functional

$$\varphi_p(x) = \prod_{k=1}^{\infty} x_k^{p_k} \tag{7}$$

is a Lyapunov function to V if there exist finitely many $p_k > 0$ i.e., there exist m such that

$$\boldsymbol{p = (p_1, p_2, \dots, p_m, 0, \dots) \in \mathbb{P};\ p_i \geq 0 \text{ for } 1 \leq i \leq m} \tag{8}$$

From the last theorem, it seem hard to choose $p \in \mathbb{P}$ that satisfied condition (**8**) due to infiniteness. Now, we want to provide some conditions on skew-symmetric matrix A so that the existence of Lyapunov function in the form of **(7)** is always true.

Theorem 2. Let V be infinite dimensional Volterra QSO associated with skew-symmetric matrix $A = (a_{ki})$. Assume there exist m such that

$a_{ij} \geq 0$ for $i \geq n+1, j = 1, \dots, m$

Let $x \in riS$, then for any $p \in \mathbb{P}^{m-1}$, the following functional

$$\varphi_p(x) = \prod_{k=1}^{m} x_k^{p_k}$$

is a Lyapunov function for V.

Using the previous Lyapunov function, it allows us to study their limiting point.

Theorem 3. Let V be Volterra QSO that satisfies conditions in Theorem 2 and we assume

$$lim_{n\to\infty} V^{(n)}(x)_k = x_k^* \text{ for every } k \in \mathbb{N}$$

If either

i. there exist some k_0 such that

$$\sum_{i=1}^{m} a_{k_0 i} p_i > 0$$

Or

ii. there exist some k_0 such that

$$a_{k_0 i_0} > 0\,,\ p_{i_0} > 0 \text{ where } k_0 > n+1, i_0 = 1, \dots, n$$

then, $x^* \in \partial S$ where ∂S is boundaries of the simplex S.

Using the same argument on Theorem 3, one has the following result.

Corollary 4. Let V be Volterra QSO that satisfies the conditions given in Theorem 3. Then one has limiting point w.r.t point-wise convergence on the boundaries of the simplex S.

References

[1] S. Bernstein, Uch. Zap. n.-i. kaf. Ukrainy 1, 83–115 (1924).

[2] Y. I. Lyubich, D. Vulis, A. Karpov, and E. Akin, Biomathematics(Berlin) (1992).

[3] R. Ganikhodzhaev, Russian Academy of Sciences. Sbornik Mathematics 76, p. 489 (1993).

[4] R. Ganikhodzhaev, F. Mukhamedov, and U. Rozikov, Infinite Dimensional Analysis, Quantum Probability and Related Topics 14, 279–335 (2011).

[5] F. Mukhamedov and N. Ganikhodjaev, Quantum quadratic operators and processes, Vol. 2133 (Springer, 2015).

Extended Abstract of the 4th International Conference on Mathematical Applications in Engineering (ICMAE2017),
8 - 9th August 2017

Ergodicity of power series-map on the simplex of group algebra of a finite group

U. Bekbaev, M. Aidil

Department of Science in Engineering, KOE, International Islamic University of Malaysia 50728 Kuala Lumpur, Malaysia[1],

Department of Mathematics, FS,Universiy Putra Malaysia, 43400, Serdang, Selangor, Malaysia[2].

Introduction and preliminaries. The convergence problems of the sequences $\{p^{[n]}(x)\}_{n\in N}$ (regularity of the map p at x) and $\{q^{(n)}(x)\}_{n\in N}$(ergodicity of the map p at x) , where $p : S \to S$ is a given map, S is a simplex in a finite dimensional real vector space, $x \in S$, $p^{[1]}(x) = p(x)$, $p^{[n+1]}(x) = p(p^{[n]}(x))$, $q^{(n)}(x) = \frac{1}{n}\sum_{i=1}^{n} p^{[i]}(x)$ for $n \in N$, are important problems in applications of Mathematics in other areas of Science (see, for example,[1],[2]). We study these problems when S is the natural simplex in the group algebra of a finite group over the real numbers and p is a power series. The polynomial case of $p(t)$ has been considered in [3] and [4].

First let us prove some common results to use in the future. Let $\{p^{[n]}(t) = \sum_{k=0}^{\infty} a_k^{[n]} t^k\}_{n\in N}$ be any sequence of power series for which $\sum_{k=0}^{\infty} |a_k^{[n]}| < \infty$ and $\lim_{n\to\infty} a^{[n]} = 0$,
where $a^{[n]} = \sup\{|a_k^{[n]}| : k \in N\}$. It should be noted that the sequence of series $\{q^{(n)}(t)\}_{n\in N} = \{\sum_{k=1}^{\infty} b_k^{(n)} t^k\}_{n\in N}$ also holds the same property i.e. $\lim_{n\to\infty} b^{(n)} = 0$, where $b^{(n)} = \sup\{|b_k^{(n)}| : k \in N\}$ and $q^{(n)}(t) = \frac{1}{n}\sum_{i=1}^{n} p^{[i]}(t)$. Let $p_0^{[n]}(t)$ stand for $p^{[n]}(t) - a_0^{[n]}$.

Assume that A is a finite dimensional mono associative algebra over R i.e. every subalgebra of A generated by one element is an associative algebra. In future the vector space A will be considered only with respect to Euclidian topology.

Lemma 1. *If $x \in A$ is such an element that $\lim_{n\to\infty} x^n = 0$ then $\lim_{n\to\infty} p_0^{[n]}(x) = 0$ as well.*

Lemma 2. *If $x \in A$ and $\lim_{n\to\infty} x^n = x_0$ then $\lim_{n\to\infty} p^{[n]}(x)$ exists if and only if $\lim_{n\to\infty}[a_0^{[n]}e + (p^{[n]}(1) - a_0^{[n]})x_0]$ exists, where e stands for the identity element of A. Moreover when it is the case then*

$$\lim_{n\to\infty} p^{[n]}(x) = \lim_{n\to\infty}[a_0^{[n]}e + (p^{[n]}(1) - a_0^{[n]})x_0]$$

Now we will consider any finite group G and its group algebra $A = R[G]$ over the field of real numbers [5]. For any $x \in R[G]$ the number x_g stands for the coefficient at g in the linear expansion of x with respect to the basis $\{g : g \in G\}$.

Let $L : R[G] \to R$ be map defined by $L(x) = \sum_{g\in G} x_g$ for any $x = \sum_{g\in G} x_g g \in R[G]$ and

$$S = \{x \in R[G] : L(x) = 1, x_g \geq 0 \text{ for any } \quad g \in G\}$$

It is clear that S is a compact set and moreover it is closed with respect to the multiplication as far as $L(xy) = L(x)L(y)$ for any $x, y \in R[G]$.

Let $\mathrm{Supp}(x) = \{g : x_g \neq 0\}$ and c stand for $\frac{1}{|G|}\sum_{g\in G} g \in \overset{\circ}{S}$, where

$$\overset{\circ}{S} = \{x \in S : x_g > 0 \text{ for any } \quad g \in G\}$$

It is evident that $cS = Sc = \{c\}$.

Proposition 1. *If $y, z \in R[G]$ any two elements with nonnegative components then*

1. *$Supp(y + z) = Supp(y) \cup Supp(z)$*
2. *$Supp(yz) = Supp(y)Supp(z)$, where $Supp(y)Supp(z)$ stands for $\{gh : y \in Supp(y), h \in Supp(z)\}$. In*

particular, $|Supp(yz)| \geq max\{|Supp(y)|, |Supp(z)|\}$*, and, if* $y_e \neq 0$,$z_e \neq 0$ *then* $Supp(y) \cup Supp(z) \subset Supp(yz)$

Further x will stand for a fixed element of S,

$$n_x = \min\{k \in N : (x^k)_e \neq 0\} = \min\{k \in N : e \in \mathrm{Supp}(x^k)\},$$

and let

$$G_x = \langle \mathrm{Supp}(x^{n_x}) \rangle$$

be the subgroup of G generated by $\mathrm{Supp}(x^{n_x})$, $c_x = \frac{1}{|G_x|} \sum_{g \in G_x} g$ and

$$m_x = \min\{k \in N : x^k \in R[G_x]\} = \min\{k \in N : \mathrm{Supp}(x^k) \subset G_x\}.$$

It is clear that m_x divides n_x whenever $x \in S$.

Let $S(x)$ stand for the set of all limits of all converging subsequences of $\{x^m\}_{m \in N}$.

Theorem 1. *For any* $x \in S$ *the equalities*

$$xc_x = c_x x,$$

$$S(x) = \{c_x x^r : 0 \leq r < m_x\}$$

are valid. In particular, $|S(x)| = 1$ *i.e.* $S(x) = \{c_x\}$ *if and only if* $x \in R[G_x]$.

Lemma 3. *For any* $x \in S$ *either both limits* $\lim_{n\to\infty} p^{[n]}(x)$, $\lim_{n\to\infty} p^{[n]}(xc_x)$ *do not exist or both of them exist and* $\lim_{n\to\infty} p^{[n]}(x) = \lim_{n\to\infty} p^{[n]}(xc_x)$

Theorem 2. *If* $x \in S$, $c_x \neq e$ *and* $n_{xc_x} = n_x$ *then the limit* $\lim_{n\to\infty} p^{[n]}(x)$ *exists if and only if* $\lim_{n\to\infty} a_0^{[n]}$, $\lim_{n\to\infty} \sum_{k=0}^{\infty} a_{km_x+r}^{[n]}$ *exist for all* $0 \leq r < m_x$. *If* $x \in S$, $c_x = e$ *and* $n_{xc_x} = n_x$ *then the limit* $\lim_{n\to\infty} p^{[n]}(x)$ *exists if and only if* $\lim_{n\to\infty} \sum_{k=0}^{\infty} a_{km_x+r}^{[n]}$ *exists for all* $0 \leq r < m_x$. *When it is the case then*

$$\lim_{n\to\infty} p^{[n]}(x) = c_x \sum_{r=0}^{m_x-1} x^r \lim_{n\to\infty} \sum_{k=0}^{\infty} a_{km_x+r}^{[n]} + (e - c_x) \lim_{n\to\infty} a_0^{[n]}$$

Lemma 4. *If* $a_1, a_2, a_3, ...$ *is a sequence of nonnegative real numbers such that* $a_1 + a_2 + a_3 + ... = 1$ *then for any* $k \geq 2$ *and* $2 \leq i \leq k$ *the following inequality*

$$\sum_{j_1+j_2+...+j_i=k} a_{j_1} a_{j_2} ... a_{j_i} \leq (1 - a_k)a$$

is valid, where $a = \sup\{a_1, a_2, a_3, ...\}$ *and the expression* $\sum_{j_1+j_2+...+j_i=k}$ *stands for the summation taken over all* $(j_1, j_2, ..., j_i)$ *with natural entries for which* $j_1 + j_2 + ... + j_i = k$. *In particular*

$$\sum_{j_1+j_2+...+j_i=k} a_{j_1} a_{j_2} ... a_{j_i} \leq a$$

for any $k \geq 1$ *and* $1 \leq i \leq k$.

Ergodicity of power series-map. Let now $p(t) = \sum_{k=0}^{\infty} a_k t^k = a_0 + a_1 t + a_2 t^2 + ...$ be any power series, where $0 \leq a_i < 1$, and $p(1) = a_0 + a_1 + a_2 + ... = 1$. Consider its iterations $p^{[n+1]}(t) = p(p^{[n]}(t))$, where $n \in N$, $p^{([1]}(t) = p(t)$. It is clear that coefficients of power series

$$p^{[n]}(t) = \sum_{k=0}^{\infty} a_k^{[n]} t^k$$

are nonnegative and $p^{[n]}(1) = \sum_{k=0}^{\infty} a_k^{[n]} = 1$. The following result is about the behavior of $a_0^{[n]}$ and $a^{[n]} = Sup\{a_k^{[n]} : k \in N\}$.

Theorem 3. *The sequence* $\{a_0^{[n]}\}_{n \in N}$ *is a monotone increasing sequence,* $\{a^{[n]}\}$ *is monotone decreasing sequence and* $\lim_{n\to\infty} a^{[n]} = 0$

Theorem 2 motivates investigation of the following problem. Let $p(t) = \sum_{i=0}^{\infty} a_i t^i$, where $0 \leq a_i < 1$ whenever $i \in N \cup \{0\}$ and $p(1) = 1$, be a power series, m be a fixed natural number. When does

$$\lim_{n\to\infty} \sum_{k=0}^{\infty} a_{km+r}^{[n]}$$

exist for all $0 \leq r < m$? Obviously it is equivalent to the question: When does $\lim_{n\to\infty} p^{[n]}(\bar{t})$ exist, where $\bar{t} = t \mathrm{mod}(t^m - 1)$? Let $\mathrm{Supp}(p(t)) = \mathrm{Supp}(\sum_{i=0}^{\infty} a_i t^i) = \{t^i : a_i \neq 0\ , i \in N \cup \{0\}\}$.

In future it is assumed that $p(t) = t^r p_0(t)$, where $r \geq 0$, $\mathrm{Supp} p_0(t) = \{t^{q_i} : i < l\}$, where $2 \leq l \leq \infty$ and $0 = q_0 < q_1 < q_2 < ....$ It is not difficult to see that

$$p^{[n]}(t) = t^{r^n} p_0^{(n)}(t) \quad \text{and} \quad p_0^{(n+1)}(t) = p_0^{(n)}(t)^r p_0(t^{r^n} p_0^{(n)}(t))$$

, which, due to Proposition 1, implies that

1. $\mathrm{Supp}(p_0^{(n)}(t)) \subset \langle\{t^{q_i} : i < l\}\rangle$, where $\langle\{t^{q_i} : i < l\}\rangle$ stands for the semigroup generated by $\{t^{q_i} : i < l\}$.
2. $t^{q_i}\mathrm{Supp}(p_0^{(n)}(t)) \subset \mathrm{Supp}(p_0^{(n+1)}(t))$ for any $i < l$

The second property implies, as far as $\mathrm{Supp}(p_0^{(n)}(t)) \subset \mathrm{Supp}(p_0^{(n+1)}(t))$, that the sets $\mathrm{Supp}(p_0^{(n)}(\bar{t}))$ are the same sets for all big enough $n \in N$. Let us denote it by $G_{p_0(t)}$. Moreover $\bar{t}^{q_i} G_{p_0(t)} \subset G_{p_0(t)}$ and $\{\bar{t}^{q_i} : i < l\} \subset G_{p_0(t)}$. Therefore taking into account the first property one can conclude that $G_{p_0(t)}$ is the subgroup of $\{\bar{t}^0, \bar{t}^1, ..., \bar{t}^{m-1}\}$ generated by $\{\bar{t}^{q_i} : i < l\}$. Assume that it is as a cyclic group generated by $\bar{t}^q$, where $0 \leq q < m$.

It is clear that the sequence $\{r^k \mathrm{mod} m\}_{k\in N}$ is a repeating sequence i.e. there are $d \in N$ and different numbers $m_0, m_1, ..., m_{d-1}$ between 0 and $m-1$ for which $r^{kd+i} = m_i \mathrm{mod}\, m$ whenever $i \in \{0, 1, ..., d-1\}$ and k is big enough.

Theorem 4. *1. If $\cap_{i=0}^{d-1} \bar{t}^{m_i} G_{p_0(t)} = \emptyset$ then $\lim_{n\to\infty} p^{(n)}(\bar{t})$ does not exist.*
2. If $\cap_{i=0}^{d-1} \bar{t}^{m_i} G_{p_0(t)} \neq \emptyset$ then $\bar{t}^{m_i} G_{p_0(t)} = \bar{t}^{m_j} G_{p_0(t)}$ whenever $i, j \in \{0, 1, ..., d-1\}$, the limit $\lim_{n\to\infty} p^{[n]}(\bar{t})$ exists and

$$\lim_{n\to\infty} p^{[n]}(\bar{t}) = \bar{t}^{m_0} c_{p_0(t)} + (e - c_{p_0(t)})a$$

, where $c_{p_0(t)} = \frac{1}{|G_{p_0(t)}|} \sum_{g\in G_{p_0(t)}} g$ and $a = \lim_{n\to\infty} a_0^{[n]}$

Theorem 5. *The above considered map $p : S \to S$ is ergodic on S.*

References

[1]. H. Kesten, Quadratic transformations: a model for population growth. I,II. Adv. Appl. Probab. **2**(1970), 1-82; 179-228.

[2]. Yu.I. Lyubich, Mathematical structures in population genetics, Springer-Verlag, Berlin, 1992.

[3]. U. Bekbaev,Regularity and ergodicity properties of polynomial maps induced by the multiplication of group algebra of a finite group. Proceedings of The second International Conference on Research and Education in Mathematics (ICREM 2),pp.134-144,May 25-27, 2005.

[4]. U. Bekbaev, Mohamat Aidil M. J.,Regularity and ergodicity properties of polynomial maps induced by the multiplication of group algebra of a finite group (Nonzero constant case). Proceedings of The second International Conference on Research and Education in Mathematics (ICREM 2), pp.144-153,May 25-27, 2005.

[5]. S.Lang, Algebra, Columbia University,Addison-Wesley,1972.

Extended Abstract of the 4th International Conference on Mathematical Applications in Engineering (ICMAE2017), 08—09th August 2017

Uniform Convergence of the Eigenfunction Expansions Associated with the Polyharmonic Operator on Closed Domain

Abdumalik Rakhimov[1] and Siti Nor Aini Mohd Aslam[2]

[1]Department of Science, Kulliyyah of Engineering, International Islamic University Malaysia.
53100 Jalan Gombak, Kuala Lumpur, MALAYSIA.

[2]Institute for Mathematical Research, Universiti Putra Malaysia.

[1]abdumalik@iium.edu.my, [2]aini_lily@yahoo.com

Introduction. In [1] Il'in studied uniform convergence of the spectral expansions E_λ associated with the Laplace operator in the Sobolev classes $W_p^a(\Omega)$ and found sufficient conditions of uniform convergence for the Riesz means $E_\lambda^s f$ as $a+s \geq \frac{N-1}{2}$, $pa > N$. Later, Alimov in [2] established the uniform convergence of the Riesz means for the functions from the Nikol'skii classes $H_p^a(\Omega)$. The convergence of the spectral decompositions of the Laplace operator on closed domain firstly investigated by Il'in (see in [1]) and then Moiseev [3] proved uniformly convergence of the eigenfunction expansions of the functions from $W_p^{\left(\frac{N}{2}+1\right)}(\Omega)$ on closed domain $\overline{\Omega}$. Furthermore, in [4] Eskin considered the $2m$ order elliptic differential operator with the Lopatinsky boundary condition and proved uniformly convergent of the spectral expansions of the functions from $W_p^{\left(\frac{N}{2}+1\right)}(\Omega)$, $\varepsilon > 0$ on closed domain $\overline{\Omega}$. The uniform convergence of the eigenfunction expansions of the Laplace operator in closed domain was considered by Rakhimov [5], where he showed that the conditions $a+s > \frac{N-1}{2}$, $pa = N$ secure the uniform convergence of the expansions in closed domain for the continuous functions from the Nikolskii classes $H_p^a(\Omega)$. Uniform convergence of the Riesz means of eigenfunction expansions of countinuous function in case of Laplace operator studied in [6] and for the general elliptic operator in [7]. The problems of the uniformly the Riesz summability on a closed domain for the Schredinger operator with the singular potential studied in [8] and [9].

The spaces of the functions. Let $\Omega \subset R^2$ be a domain with smooth boundary $\partial\Omega$. Let define the classes of the functions (see in [10]). We say that a function $f(x,y) \in L_p(\Omega)$ belongs to the $H_p^a(\Omega)$, if for any $h=(h,k) \in R^2$ and for all integers α, β satisfying $\alpha+\beta=l$:

$$\left|\partial_x^\alpha \partial_y^\beta f(x+h,y+k) - 2\partial_x^\alpha \partial_y^\beta f(x,y) + \partial_x^\alpha \partial_y^\beta f(x-h,y-k)\right|_{L_p(\Omega_{\sqrt{h^2+k^2}})} \le C\left(h^2+k^2\right)^{\frac{\sigma}{2}}.$$

where a is written as $a=l+\sigma$, $l-$positive integer and $0<\sigma\le 1$. Using the notation $\Delta_{h,k}^2 f(x,y) = f(x+h,y+k) - 2f(x,y) + f(x-h,y-k)$, a norm in $H_p^\alpha(\Omega)$ is defined by

$$\|f\|_{p,\alpha} = \|f\|_{L_p(\Omega)} + \sum_{\alpha+\beta=l} \sup_{h,k} \left(h^2+k^2\right)^{-\frac{\sigma}{2}} \left\|\Delta_{h,k}^2 \partial_x^\alpha \partial_y^\beta f(x,y)\right\|_{L_p(\Omega_{\sqrt{h^2+k^2}})}.$$

The closure of the space $C_0^\infty(\Omega)$ in the norm of $H_p^a(\Omega)$ denoted by $\dot{H}_p^a(\Omega)$.

Let $a \ge 0$ an integer and a function $\gamma(t)$ defined and continuous for $1 \le t \le \infty$, positive and vanishing in $t \to \infty$. Consider an operator

$$I_{r,\gamma} f = F^{-1}\left[(1+|\omega|^2)^{\frac{-a}{2}} \cdot \gamma\left(\sqrt{1+|\omega|^2}\right) \cdot Ff\right]$$

Then the generalized Besov spaces $B_{p,\theta}^{r,\gamma}(R^N)$ defined as

$$B_{p,\theta}^{r,\gamma}(R^N) = I_{r,\gamma} B_{p,\theta}^0(R^N).$$

Here F and F^{-1} direct and inverse Fourier transformations in $J'(R^N)$.

Now we define the generalized Sobolev spaces in the finite domain Ω. Unless whole space R^N in the finite domain the definition not involving the Fourier transformation. For any square integrable in the domain Ω function u and for any positive number r by $\omega(u,r)$ we denote the second order modulus of continuity in the metric of the space $L_2(\Omega)$

$$\omega(u,r) = \sup_{|h|<r} \|u(x+h) - 2u(x) + u(x+h)\|_{L_2(\Omega_h)}$$

where $\Omega_h = \{y \in \Omega: \mathrm{dist}(y, \partial\,\Omega) < h\}$.

Let $a>0$, $a=\mu+\varepsilon$, where $\mu \ge 0$ integer number and $0<\varepsilon\le 1$. Let $\beta(\delta) = ln\delta$, $1 \le \delta < \infty$. Then by $W_2^{\alpha,\beta}(\Omega)$ we denote the space of functions from $L_2(\Omega)$ with the finite norm

$$\|u\|_{a,\beta} = \|u\|_0 + \sum_{|\alpha|=\mu} \sup_{0<r<1} \frac{\omega(D^\alpha u, r)}{\delta^\varepsilon \beta\left(\frac{1}{r}\right)}$$

here α is multiindex, i.e. $\mathbf{N}$ - dimensional vector with non negative integer components $\alpha = (\alpha_1, \alpha_2, \ldots\ldots, \alpha_N)$ and $|\alpha| = \alpha_1 + \alpha_2 + \cdots + \alpha_N$ called length of multiindex. Then $D^\alpha = \frac{\partial^{|\alpha|}}{\partial x_1^{\alpha_1} \ldots \partial x_N^{\alpha_N}}$ denote the generalized partial derivative.

Eigenfunction expansions associated with the polyharmonic operator. Let consider the biharmonic operator Δ^2 with the domain $D_{\Delta^2} = \{ u \in C^4\Omega) : u|_{\partial\Omega} = \Delta u|_{\partial\Omega} = 0 \}$. Denote by $\{u_{nm}(x, y)\}$ eigenfunctions and by $\{\lambda_{nm}\}$ the set of eigenvalues of the biharmonic operator.

Let $E_\lambda^s f$ be the Riesz means of the eigenfunction expansions associated with the operator above

$$E_\lambda^s f(x, y) = \sum_{\lambda_{nm} < \lambda} (1 - \frac{\lambda_{nm}}{\lambda})^s \, f_{nm} \, u_{nm}(x, y), \qquad s \geq 0,$$

where f_{nm} is the Fourier coefficients of the function f :

$$f_{nm} = \iint_\Omega f(x, y) \, u_{nm}(x, y) \, dx \, dy, \qquad n, m = 1,2,\ldots$$

For the eigenfunctions $\mathrm{u_{nm}(x,y)}$ and eigenvalues λ_{nm} of biharmonic operator with the domain of definition D_{Δ^2} we have (Anvarjon, Siti Nor Aini and Siti Fatimah):

$$\sum_{|\sqrt[4]{\lambda_{nm}} - \lambda| \leq 1} \sum u_{nm}^2(x, y) = O\left(\lambda \ln^2 \lambda\right), \qquad \lambda > 1, \tag{1}$$

uniformly for all $(x, y) \in \overline{\Omega} = \Omega \cup \partial\Omega$.

From this, it follows that if $a + s > \frac{1}{2}, pa > 2, p \geq 1,$ then the Riesz means $E_\lambda^s f(x, y)$ uniformly convergence for the functions from Nikolskii classes $\boldsymbol{H_p^a}$ in closed domain. An estimation (1) for the polyharmonic operator obtained by Anvarjon, Siti Nor Aini and Gafurjan Ibragimov.

Summary. In this paper the uniform convergence of eigenfunction expansions of the distributions from the generalized Sobolev spaces.

References

[1] V.A. II'in, On the uniform convergence of expansions in eigenfunctions for summation in the order of the eigenvalues, Dokl. Akad. Nauk SSSR 114:4 (1957) 698– 701.

[2] Sh.A. Alimov and V.A Ilin, Spectral decompositions corresponding to an arbitrary nonnegative selfadjoint extension of Laplace's operator, Dokl. AN SSSR 193 (1970) 9–12.

[3] E.I. Moiseev, The uniform convergence of certain expansions within a closed domain, Dokl. Akad. Nauk SSSR 233:6 (1977) 1042-45.

[4] G. Eskin, Asymptotics near the boundary of spectral functions of elliptic self-adjoint boundary problems,

Isr. J.Math. 22:3-4 (1975) 214-46.

[5] A.A. Rakhimov, About uniform convergence of the spectral decomposition for the functions from Nikolskii classes in closed domain, VINITI 1564-B87 (1987) 17.

[6] A.A. Rakhimov, On uniform convergence of spectral resolutions of a continuous function in a closed domain. Izv. Akad. Nauk UzSSR, Ser. Fiz.-Mat. Nauk, 6 (1987), 17-22.

[7] Sh.A. Alimov , A.A. Rakhimov, On the uniformly convergence of spectral expansions in a closed domain. Dokl. Acad Nauk UzSSR, 10 (1986), 5-7.

[8] A.A. Rakhimov, Kamran Zakariya, On an Estimation of Eigenfunctions of Schrödinger's operator on a closed domain, MathDigest, UPM, Malaysia, June edition, 2010, p. 1-4.

[9] A.A. Rakhimov, Kamran Zakariya and Nazir Alikhan, Uniform convergence spectral expansions connected with Schrodinger's operator of continuous function on a closed domain. J. The Nucleus, 2010, V.47, No 4, p.261-265.

[10] H. Triebel, Interpolation Theory - Function Spaces - Differential Operators (Wiley, Jan 6, 1999 - Science), 1- 532.

Extended Abstract of the 4th International Conference on Mathematical Applications in Engineering (ICMAE2017), 8-9th August 2017

Instabilities in Non-isothermal Falling Thin Film Flows

Ahmad T. Jameel[2*], Mohammad A. Hamza[1], Asif Hoda[3], Tariq M. Rahman[1], and Waqar Asrar[1]

[1]Department of Mechanical Engineering, [2] Department of Biotechnology Engineering
Faculty of Engineering, International Islamic University Malaysia, P.O. Box 10
Gombak, 50728 Kuala Lumpur. Malaysia

[3]Department of Mechanical Engineering, Jubail University College, P.O. Box 10074
Jubail Industrial City 31961, Saudi Arabia.

[1]atjameel@iium.edu.my, [2]mahamza2000@gmail.com, [3]hodaa@ucj.edu.sa,*
[4]tariq.ridwan@gmail.com, [5]waqar@iium.edu.my

Introduction. The stability and dynamics of thin liquid films subjected to van der Waals attraction, thermocapillarity and evaporative instabilities at the free surface, is studied using numerical simulations. For a Newtonian liquid, flow in thin liquid film on a solid support and bounded by a passive gas is represented by Navier-Stokes equation, equation of continuity and appropriate boundary conditions. The external effects are generally incorporated in the body force term of the Navier-Stokes equation. These governing equations can then be simplified using so called long-wave approximation to arrive at a nonlinear partial differential equation, henceforth called equation of evolution (EOE), which describes the time evolution of the interfacial instability caused by internal and/or external effects [1-3].

The comprehensive characterization of the nonlinear dynamics and surface morphology of thin-film requires efficient numerical method for the solution of the equation of evolution (EOE). Our thin-film flow configuration has been numerically simulated using a fully explicit finite difference formulation as well as an implicit finite difference scheme. The explicit finite difference scheme seems to replicate the solution from spectral method as well as implicit scheme to a high degree of conformity for most of the cases investigated. Thus explicit scheme presented here is a relatively simple numerical scheme with much less computational expense compared to Fourier spectral and implicit Crank Nicholson schemes for the full scale simulation of the various thin film models. However, the detailed numerical simulation of the thin film problem is being investigated.

The Thin Film Model. Consider a thin viscous Newtonian liquid film supported on a uniformly heated rigid plane inclined at angle β to the horizontal and bounded above by its vapour. Film is thick enough that a continuum theory of the liquid is applicable. The film is laterally unbounded and with constant material properties. Mean film thickness is h_0. The layer is evaporating so that at the vapour-liquid interface there is mass loss, momentum transfer and energy consumption. Plate has a fixed constant temperature T_H. Liquid temperature, T_F on the free surface is controlled by losses to the passive gas above. The surface tension, σo depends on temperature, so that the thermocapiliary effects are present. The flow in the thin film can be represented using a two-dimensional Cartesian co-ordinate system (x, z), by the Navier-Stokes, energy and continuity equations together with the shear stress, normal stress conditions and the constitutive equation at the free surface. Following the derivations in Joo et al. (1991), an equation of evolution (in space and time) for the film

thickness *h(x,t)* can be obtained as [1-4],

$$h_t + \frac{E}{h+K} + Gh^2 h_x \sin\theta + \left[\frac{2}{15}G^2 h^6 h_x \sin^2\theta + \frac{KM}{P}\frac{h^2 h_x}{(h+K)^2} + \frac{E^2}{D}\frac{h^3 h_x}{(h+K)^3} - \frac{1}{3}Gh^3 h_x \cos\theta + \frac{A}{h}h_x + Sh^3 h_{xxx}\right]_x + \frac{5}{24}GE\left(\frac{h^4}{h+K}\right)_x \sin\theta + EP\left(\frac{h}{h+K}\right)^3\left[\frac{E}{3(h+K)} + \frac{G}{120}(7h-15K)hh_x \sin\theta\right] = 0 \qquad (1)$$

The scale factors used between parameters in Eq. (1) and those used in EOE of Joo et al. (1991) are: (E, D, S) = (ε¯, ε2D, ε-2¯). Joo et. al. (1991) have employed ε=0.2 and¯=0.1 throughout their simulations [3].
Eq. (1) can be solved for the film thickness *h(x,t)* using a space periodic initial condition,

$$h(0,x) = 1 - \varepsilon\cos kx\,; \qquad |\varepsilon| < 1 \qquad (2)$$

together with periodic boundary conditions in x-domain over a disturbance wavelength, $\lambda = 2\pi/k$, where k is a wavenumber. For a cosine wave initial condition, the boundary conditions can be expressed as [2,4],

$$\left(\frac{\partial^i h}{\partial x^i}\right)_{x=-\lambda/2} = \left(\frac{\partial^i h}{\partial x^i}\right)_{x=\lambda/2} \quad (i = 0,1,2,3);\ -\lambda/2 \le x \le \lambda/2, \qquad (3)$$

Numerical Method. To fully characterize the nonlinear dynamic behaviour of our non-isothermal thin film model, one needs to solve numerically the evolution equation (Eq. 1) for a wide range of parameter values under different thermo-physical states. Thus we need robust numerical method to solve Eq. (1) reliably and efficiently. Hamza et al. (2016) have used implicit Crank Nicholson mid-point rule in their simulations of Eq. (1) [1-4,7]. Here we have compared the results from numerical simulations using an explicit finite difference (FD) schemes with those of implicit Crank-Nicholson mid-point method employed by Hamza (2017). The explicit FD scheme is briefly described in the following paragraph.

*Explicit Finite Difference Formulation***.** A second order accurate backward difference scheme is used for temporal discretization while the periodic spatial domain is discretized using 41 equally spaced points. The spatial terms in the governing equations are calculated at the current time step where the solution is known and is used explicitly to find the film thickness profile at the next time step, employing sufficiently small time steps to ensure the stability of time integration. The spatial derivatives h_x and h_{xxx} are evaluated using second order accurate finite differencing [5-7). Our explicit discretization has been extensively validated by solving the various cases of isothermal/nonisothermal liquid layer of Joo et al. (1991) where a Fourier spectral method was used to solve the governing equations and identical results were obtained as shown in the 'results and discussion' section.

Results and Discussion. The results of the numerical solution of the equation of evolution (EOE) given in Eq. (1) in the absence of van der Waals force term (identical with EOE of Joo et al. (1991)) using our explicit code are compared with the results of implicit code of Hamza (2017) and with the numerical results of Joo et al. (1991) obtained using Fourier spectral

method in figures 1 and 2. Fig. 1 depicts the evolution of the film interface for a liquid layer under the influence of thermocapillarity and gravity for an angle of inclination 30°. Simulations from our explicit finite difference method (FDM) are almost identical with Fourier spectral method (not shown here) of Joo et al. (1991), however, implicit FDM shows slight deviation. Simulation of evaporating layers without gravitational effect is shown in Fig. 2. Figure 2 shows identical film profiles from explicit and implicit methods with slight difference in the rupture time (τ = 4.9388 (explicit) and τ= 4.8915 (implicit)).

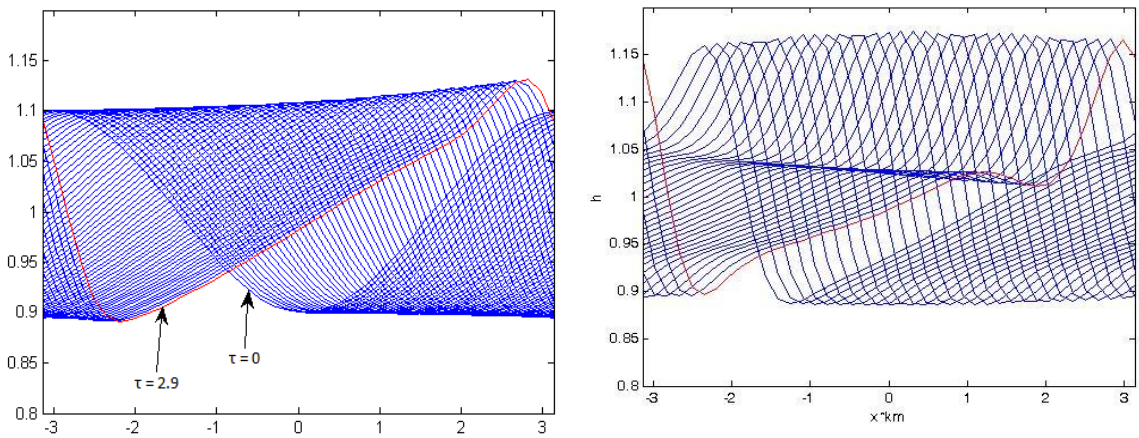

Figure 1: Evolution of the free-interface when $k = 0.7, G = 5, \theta = 30°, \frac{KM}{P} = 1, K = 0.1, S = 2.5$ ($\overline{S} = 0.1$), for $0 \leq \tau \leq 2.9$ with $\Delta\tau = 0.1$.

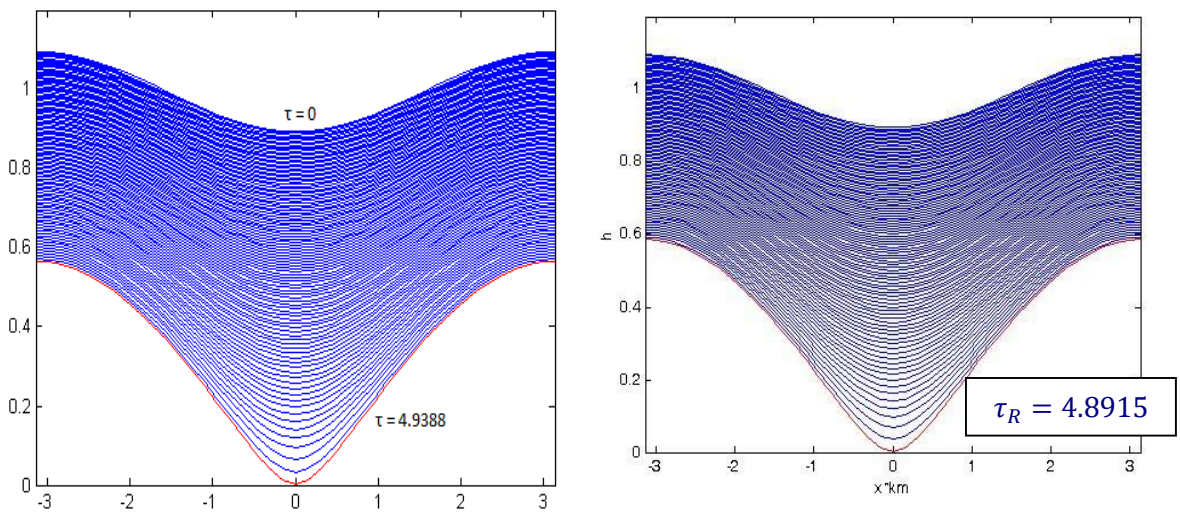

Figure 2: Growth of free-surface instability for an evaporating film shown with $\Delta\tau = 0.05$ and at $\tau_R = 4.9388\ (explicit),\ \tau_R = 4.8915\ (implicit)).\ k = 0.7, G = 0, E = 0.02\ (\overline{E} = 0.1), K = 0.1, P = 1$, and S=2.5 ($\overline{S} = 0.1$).

Summary. The results presented above show a high degree of conformity in the solutions obtained from our explicit finite difference scheme to those of Fourier spectral method as well as results obtained from implicit Crank Nicholson scheme. The fully explicit finite difference scheme seems to replicate the solution of the Fourier spectral method of Joo et al.

(1991) as well as implicit scheme of Hamza et al. (2017) to a high degree of accuracy for most of the cases investigated so far. Thus it is proved beyond doubt that our fully explicit finite difference formulation is capable of simulating the highly nonlinear thin film model to a high degree of accuracy with remarkable ease of implementation and at much less computational expense compared to more computationally intensive methods of Fourier spectral and implicit Crank Nicholson schemes.

References

[1] M.A. Hamza, A.T. Jameel, W. Asrar, and A. Hoda, International Conference on Mechanical, Automotive and Aerospace Engineering 2016. IOP Conf. Series: Materials Science and Engineering 184 (2017) 012065. doi:10.1088/1757-899X/184/1/012065.

[2] M.A. Hamza, The Numerical Simulation of Non-isothermal Thin Liquid Film Flow On Inclined Plane, MS dissertation, International Islamic University Malaysia, Kuala Lumpur (2017).

[3] S.W. Joo, S.H. Davis, and S.G. Bankoff, J. Fluid Mech. 230 (1991) 117-146.

[4] M.A. Ali, A.T. Jameel, and F.-R. Ahmadun, Computer and Chemical Engineering 29 (2005) 2144-2154. doi:10.1016/j.compchemeng.2005.07.003.

[5] T.M. Rahman, FYP Report, Kulliyyah of Engineering, International Islamic University Malaysia, Kuala Lumpur (2014).

[6] B. Fornberg, SIAM Rev. 40 (1998) 685-691.

[7] K.A. Hoffmann and S.T. Chiang, Computational Fluid Dynamics: vol. 1, 4th ed. Engineering Education System, Wichita, USA (2004).